bioRxiv preprint doi: https://doi.org/10.1101/2020.09.21.306217; this version posted September 21, 2020. The copyright holder for this preprint (which was not certified by peer review) is the author/funder, who has granted bioRxiv a license to display the preprint in perpetuity. It is made available under aCC-BY-NC-ND 4.0 International license.

Acute neonatal oxytocin impacts hippocampal network development and restores adult social memory deficits in a mouse model of autism spectrum disorder.

Alessandra Bertoni[1], Fabienne Schaller[1], Roman Tyzio[1], Stephane Gaillard[2], Francesca Santini[4], Marion Xolin[1], Diabé Diabira[1], Radhika Vaidyanathan[3], Valery Matarazzo[1], Igor Medina[1], Elizabeth Hammock[3], Jinwei Zhang[5], Bice Chini[4], Jean-Luc Gaiarsa[1], Françoise Muscatelli[1#]

[1] Institute of Neurobiology of Méditerranée (INMED), Institut National de la Santé et de la Recherche Médicale (INSERM) UMR 1249, Aix- Marseille Université, Marseille, France.
[2] Phenotype-expertise, Marseille, France.

[3] Florida State University, Tallahassee, FL, USA.

[4]Institute of Neuroscience, National Research Council (CNR), Department of Medical Biotechnology and Translational Medicine, Università degli Studi di Milano Milan, and Humanitas Clinical and Research Center, Rozzano, Italy.

[5]Institute of Biomedical and Clinical Sciences, College of Medicine and Health, University of Exeter, Hatherly Laboratories, Exeter, EX4 4PS, UK.

#: corresponding author

Email: francoise.muscatelli@inserm.fr.

Institut de Neurobiologie de la Méditerranée (INMED)

INSERM-Aix Marseille Université

Campus Scientifique de Luminy, 13273 Marseille, France

Keywords: Magel2, Schaaf-Yang Syndrome, Prader-Willi Syndrome, neurodevelopmental disorder, GABA-shift, Excitation/Inhibition balance, Somatostatin, Parvalbumin.

Number of pages: 34

Number of words (introduction, results, discussion): 5520

Number of figures: 9 figures and 8 supplementary figures

Supplementary data: Statistical file

bioRxiv preprint doi: https://doi.org/10.1101/2020.09.21.306217; this version posted September 21, 2020. The copyright holder for this preprint (which was not certified by peer review) is the author/funder, who has granted bioRxiv a license to display the preprint in perpetuity. It is made available under aCC-BY-NC-ND 4.0 International license.

Abstract

Several studies on rodent models with an Autism Spectrum Disorders-like (ASD) phenotype, notably *Magel2*-deficient mice, have shown a rescue of deficits in adult social behavior after neonatal administration of oxytocin. However, the neurobiological alterations responsible for the social deficits and the mechanism by which oxytocin-administration in infancy has a rescue effect in adulthood remain unclear.

Here we show that *Magel2*-deficient adult mice exhibit a deficit in social memory that is corrected by neonatal oxytocin administration. We studied hippocampal regions known to be associated with social memory engrams involving the OT-system. At critical stages of development, we characterized cellular, physiological and biochemical alterations of these hippocampal regions in *Magel2*-deficient mice, alterations present in several ASD models. Overall we demonstrate a strong impact of oxytocin-administration at key stages of postnatal hippocampal neurodevelopment, shedding light on the role for oxytocin in treating neurodevelopmental disorders characterized by deficits in social memory.

bioRxiv preprint doi: https://doi.org/10.1101/2020.09.21.306217; this version posted September 21, 2020. The copyright holder for this preprint (which was not certified by peer review) is the author/funder, who has granted bioRxiv a license to display the preprint in perpetuity. It is made available under aCC-BY-NC-ND 4.0 International license.

INTRODUCTION

Oxytocin (OT) and its signaling pathway, the OT-system, are disrupted in several animal models of neurodevelopmental disorders characterized with autism-like phenotypes (1, 2). Indeed, knock-out mouse models of *Ot* (3, 4), *oxytocin receptor* (*Oxtr*) (5-7), or *ADP-ribosyl cyclase* (*Cd38*) (8, 9) genes show changes in social behavior. In addition, several rodent models of autism spectrum disorders (ASD) endophenotypes due either to the inactivation of genes such as *Fmr1*, *Cntnap2*, *Magel2*, *Oprm1*, or to environmental valproic acid exposure (VPA), exhibit a disruption of the brain OT-system (1). Many of these models have in common at least two constant phenotypes (10). First, pups isolated from the dam and littermates present a decrease in the number of ultrasonic vocalizations (USVs), the earliest behavioral test that can be performed in mice to measure social deficits. A second robust phenotype is a social recognition memory deficit in adulthood.

OT is thought to regulate aspects of social recognition, social novelty and social memory via interactions with OT-receptors (OXTR) in a number of key brain regions (11). With regard to social memory, a critical role has been ascribed to hippocampal OXTR expression in the anterior dentate gyrus (aDG) hilar and anterior CA2/CA3distal regions (aCA2/CA3d) (12-15). In the aCA2/CA3d region, OXTRs are expressed in glutamatergic pyramidal neurons (which are also CCK positive) and in GABAergic interneurons, which account for over 90% of OXTR positive cells in the hippocampus (16). Notably, both types of neuron are necessary for the formation of stronger synapses that mediate LTP and social memory (12, 13).

Although most studies of OT-dependent social behaviors have been conducted in adulthood, compelling data support key roles for OT in shaping various behaviors and social traits in infancy (17-21). Genetic mutations and stressful early-life social environments can impair social behaviors via changes in the OT-system (22, 23). On the other way, OT-dependent systems may be particularly vulnerable around the neonatal period where OXTR expression is dynamic, with a strong expression in the first 2 weeks postnatal followed by a decreased expression thereafter (24, 25), and involved in critical functions such as the excitatory-to-inhibitory developmental GABA switch (26-28), a delay in which has been implicated as a driver of several rodent ASD models (27, 29). It has also been demonstrated that, in mouse pups, sensory experience influences OT production and OT shapes neuronal circuits by modulating spontaneous and evoked activity in the cortex (25, 30, 31). Thus, the modulation of GABAergic activity throughout life appears to be an important key factor in the function of OT. In addition, OT acts also on glutamatergic neurons (32) and drives dendritic and synaptic refinement in immature hippocampal glutamatergic neurons (33). Collectively, these studies confirm a role

bioRxiv preprint doi: https://doi.org/10.1101/2020.09.21.306217; this version posted September 21, 2020. The copyright holder for this preprint (which was not certified by peer review) is the author/funder, who has granted bioRxiv a license to display the preprint in perpetuity. It is made available under aCC-BY-NC-ND 4.0 International license.

for the OT-system in early postnatal development of diverse brain regions involved in sensory processing, the limbic system, and the generation of motor output related to social behaviors. *MAGEL2* is an imprinted gene that is paternally expressed and is involved in Prader-Willi (34) and Schaaf-Yang syndromes (35) (PWS and SYS, respectively). Both of these genetic neurodevelopmental disorders present feeding difficulties and hypotonia in infancy, followed by alterations in social behavior and deficits in cognition that persist over the lifespan (36). *Magel2* knock-out mouse models are pertinent models for both syndromes (36), mimicking a disturbance in early feeding (poor sucking activity (37)), and alterations to social behavior and learning abilities in adulthood (38, 39). *Magel2* mRNA is highly expressed in the developing hypothalamus until adulthood and *Magel2*$^{tm1.1Mus}$ knock-out neonates display a deficiency of several hypothalamic neuropeptides, particularly OT (37). Daily administration of OT during the first week of life restores normal sucking activity of *Magel2* KO mice and normalizes social behavior and learning abilities beyond treatment into adulthood (38). Comparable effects have also been reported in other genetic rodent models of ASD, such as the VPA-induced rat model (40), the *Cntnap2* and *Fmr1* KO mouse (41, 42), and maternal separation (43). Furthermore, OT-treatment of human infants with PWS significantly improves early feeding and "social skills" in early infancy (44), confirming the translational relevance of this system. However, the developmental alterations responsible for social behavior deficits in these models, and the mechanism by which OT-treatment exerts its long-lasting beneficial effects, remain mysterious. Here, we aimed to clarify the physiological and cellular mechanisms underlying the loss of social memory in *Magel2*$^{tm1.1Mus}$-deficient mice and those responsible for the long-term rescue effects of OT.

RESULTS

To overcome the phenotypic heterogeneity of the heterozygous +m/-p *Magel2* $^{tm1.1Mus}$ mouse, due to the stochastic expression of the maternal *Magel2* allele when the paternal allele is deleted (45), *Magel2* $^{tm1.1Mus}$ homozygous (-/-) mice were used ("*Magel2* KO" hereafter). In the following experiments WT and *Magel2* KO pups were naïve or treated for four days (Postnatal day P0, P2, P4 and P6) with one subcutaneous administration of physiological saline ("vehicle") or oxytocin (2 µg, "OT-treatment" or "+OT") per day.

Deficits in isolation-induced vocalizations in *Magel2* KO pups and social memory in *Magel2* KO adults are differentially rescued by neonatal OT-treatment.

Mice at suckling age elicit USVs, when separated from their dam and littermates. We found a significant reduction of the number of separation-induced USVs in P8 male and female *Magel2* KO compared to wild-type (WT) pups (Figure 1A-B), demonstrating altered social behavior in

bioRxiv preprint doi: https://doi.org/10.1101/2020.09.21.306217; this version posted September 21, 2020. The copyright holder for this preprint (which was not certified by peer review) is the author/funder, who has granted bioRxiv a license to display the preprint in perpetuity. It is made available under aCC-BY-NC-ND 4.0 International license.

early infancy. We confirmed that vehicle or OT-treatment had no effect on vocalization in WT pups and did not significantly increase the number of USVs recorded in mutant animals (Figure 1C). Thus, OT-treatment did not exert immediately measurable effects on neonatal social behaviors in *Magel2* KO pups.

At adulthood, we focused on social behavior using the three-chamber test in order to assess social exploration (sociability), the preference for social novelty (social discrimination) and social memory (short-term social memory) (46) (Figure 2A). *Magel2* KO males showed levels of sociability and social discrimination similar to WT males but exhibited a significant deficit in social memory (Figure 2B, Figure 2-figure supplement 1). As previously reported (47), we observed a failure of the three-chamber test in revealing sociability in the cohort of female mice (Figure 2-figure supplement 2); a result reproduced in second cohort of WT females (data not shown). As a consequence, we restricted all following studies to male mice.

First, the effects of neonatal vehicle and OT-treatment were assessed in WT male pups at adulthood in the three-chamber test. We found that neither treatment had any measurable effect on sociability, social discrimination or social memory: the amount of time spent sniffing in different compartments was similar to that recorded in untreated WT males (Figures 2 B-C). Furthermore, no significant effects of neonatal OT-treatment were detected on adult performance of novel object recognition (Figure2-Supplement 3A), open field (Figure 2-Supplement 3B) or elevated plus maze tests (Figure2-Supplement 3C). Thus, neonatal OT-treatment has no significant adverse or beneficial long-lasting effects on widely used assays of social behavior, object recognition, anxiety-like or motor behaviors in WT animals but a reduction in the distance moved in the open-field in females.

Unsurprisingly, *Magel2* KO-vehicle males presented with a social memory deficit similar to untreated *Magel2* KO males (Figure 2D-B). However, this was rescued by neonatal OT-treatment (Figure 2D). Sociability and social discrimination indices were not affected by *Magel2* deletion or OT-treatment (Figure 2-Supplement 1).

Thus, the loss of *Magel2* causes a deficit in USV calls in pups and a deficit in social memory in male *Magel2* KO adults. While the USV deficit was not affected by post-natal OT-treatment, the deficit in social memory was rescued by a neonatal OT-treatment. Due to the robust effect observed on social memory, we focused our subsequent investigations on the hippocampal region, previously shown to be specifically involved in OT-mediated effects on social memory (12, 13).

aDG and aCA2/CA3d regions are activated by the social memory test in WT and *Magel2* KO mice.

Cells in the aCA2/CA3d and aDG regions have been previously shown to express OXTRs and are involved in social memory (12, 13). We therefore asked whether these cells could be

bioRxiv preprint doi: https://doi.org/10.1101/2020.09.21.306217; this version posted September 21, 2020. The copyright holder for this preprint (which was not certified by peer review) is the author/funder, who has granted bioRxiv a license to display the preprint in perpetuity. It is made available under aCC-BY-NC-ND 4.0 International license.

activated by the social memory test. WT and *Magel2* KO mice were sacrificed 90 min after the end of three-chamber test (+SI, for Social Interactions) and their brains examined for cFos immunolabeling, a marker of neuronal activity (Figure 3A). We found a significant increase (83%) in the number of cFos+ cells in the *stratum pyramidale* of aCA2/CA3d in tested WT (WT+SI) compared with untested WT (WT-SI) mice; in *Magel2* KO+SI mice we observed a 25% significant increase of cFos+ cells compared with WT+SI. In the aDG, a significant increase of ~60% of cFos+ cells compared with WT-SI was observed in both WT+SI and *Magel2* KO+SI, mainly in the hilus and *stratum granulare*. Thus, the activation of c-Fos is significant in both regions following social memory test in both genotypes (WT+SI and *Magel2* KO+SI mice) with an increase of cFos activated cells observed in the aCA2/CA3d region in *Magel2* KO+SI. Overall, these data confirm a strong activation of neurons in aCA2/CA3d regions in WT and *Magel2* KO mice following social interactions.

Expression profile of *Magel2* and *Oxtr* in the aDG and aCA2/CA3d regions

Magel2 is known to be highly expressed in hypothalamus, while its expression in hippocampal regions is less well characterized. We investigated the developmental expression of *Magel2* and *Oxtr* transcripts in the anterior hippocampus using RNAscope technique at two different time points (P7 and P21), taking in account the dynamic expression of OXTRs. At P7 (Figure 4A), we detected *Oxtr* and *Magel2* mRNAs in the aCA2/CA3d region with *Magel2* more expressed in the deep layer of the *stratum pyramidale*, a fainter expression is also detected all over the layer. At this stage, *Oxtr* transcripts were more concentrated in the CA2 region, compared to *Magel2*. At P21 (Figure 4), the level of *Magel2* transcripts was reduced but still present in the deep layer of aCA2/CA3d region and *Oxtr* transcripts were also strongly expressed in pyramidal cells. Expression of *Magel2* and *Oxtr* was also detected in few cells of the *stratum oriens* and *stratum radiatum* where co-expression can be observed. In the DG, an expression of *Oxtr* and *Magel2* is detected in the hilus, some cells presenting a co-localization of both transcripts.

In adulthood, based on the *in-situ* hybridization maps of Allen Brain Atlas, we could confirm expression of *Magel2* in the CA3 deep layer of the stratum *pyramidale* (not shown). Then, we consulted the public Allen brain RNAseq data from cortex and hippocampal samples (*http://celltypes.brain-map.org/rnaseq/mouse/cortex-and-hippocampus*) to define the cell types expressing *Magel2* and *Oxtr*. *Oxtr* transcripts are expressed in GABAergic interneurons mainly in SST and also in parvalbumin (PV) and Calbindin expressing interneurons. Expression is also detected in glutamatergic neurons of a CA2-CA3 region co-expressing CCK. *Magel2* is faintly detected in the glutamatergic neurons only. Finally, from RNAseq data extracted from the atlas of cell types from Linnarsson Lab.

bioRxiv preprint doi: https://doi.org/10.1101/2020.09.21.306217; this version posted September 21, 2020. The copyright holder for this preprint (which was not certified by peer review) is the author/funder, who has granted bioRxiv a license to display the preprint in perpetuity. It is made available under aCC-BY-NC-ND 4.0 International license.

(http://mousebrain.org/genesearch.html) co-expression of *Oxtr* and *Magel2* is detected in the CA3 excitatory neurons of adult mice and also in several interneuron sub-populations expressing SST or SST and PV such as the axo-axonic long-range projections interneurons and the basket bistratified cells. These sub-populations of interneurons represent a small number of cells that have a wide and diverse spectrum of actions. These data suggest that the lack of *Magel2* can alter the Oxtr expressing excitatory neurons in the aCA2/CA3d region and also the SST or PV interneurons.

The quantity of OT-binding sites is increased in the aCA2/CA3d and aDG regions of *Magel2* KO adult mice and normalized in the aDG following an OT-treatment

We then looked at the distribution of OT-binding sites in *Magel2 KO*-vehicle or *Magel2 KO*+OT compared with WT-vehicle hippocampi by autoradiography (Figure 5). We observed a significant increase of OT-binding sites in the aCA2/CA3 (100%, Figure 5A-B) and aDG (80%, Figure 5C-D) regions but not in the ventral CA1/CA2/CA3 region (Figure 5E-F). In *Magel2* KO+OT we observed a normalization of the quantity of OT-binding sites in the aDG, but not in the aCA2/CA3 region where OT-binding sites level was decreased but remained elevated compared to WT (Figure 5A-B). The binding study indicate subregions specific modulation of OXTR in the hippocampus. We then asked if this subregion specific effect could be linked to specific changes in neuronal subpopulations in the same regions.

The number of SST+ neurons is increased in the aCA2/CA3d and aDG regions of *Magel2* KO adult mice and normalized following an OT-treatment.

In the anterior adult hippocampus OXTRs are expressed in pyramidal cells and in SST and/or PV interneurons of aCA2/CA3d region and in interneurons of aDG (see above, (12, 16)). In control mice following social memory test, cFos expression was detected in 23 or 30% of SST-immunopositive cells (SST+) and 22 or 28% of PV+ cells in the aCA2/CA3d or aDG regions following the social memory test, respectively (Figure 6-figure supplement 1), suggesting an involvement of those interneurons in social memory. Then we quantified the number of SST+ and PV+ cells in *Magel2* KO versus WT adult hippocampi and observed a significant higher number of SST+ cells in both aCA2/CA3d (1.6 x) and aDG (1.8 x) regions of *Magel2* KO animals (Figure 6 A-F and M-N). PV+ cells are present in the same quantity in both genotypes (Figure 6-figure supplement 2). In contrast, the number of SST+ cells was significantly decreased in both aCA2/CA3d (less 12%) and DG regions (less 17%) in OT-treated *Magel2* KO mice compared with untreated WT mice (Figure 6 G-L and O-P). An increase of SST+ neurons was observed in anterior hippocampus of adult *Magel2* KO and, conversely, OT-treatment of *Magel2* KO pups was associated with a slight decrease of SST+ neurons in adult mutant compared with WT hippocampi. PV+ cells were equally abundant in both genotypes

bioRxiv preprint doi: https://doi.org/10.1101/2020.09.21.306217; this version posted September 21, 2020. The copyright holder for this preprint (which was not certified by peer review) is the author/funder, who has granted bioRxiv a license to display the preprint in perpetuity. It is made available under aCC-BY-NC-ND 4.0 International license.

(Figure 6-figure supplement 2). This change in the quantity of SST+ cells might have consequences in the alteration of the excitation/inhibition (E/I) balance.

GABAergic and glutamatergic activities are altered in *Magel2* KO aCA3d pyramidal neurons and neonatal OT-treatment normalizes the GABAergic activity but reduces the glutamatergic activity in WT mice.

Alterations in GABA/glutamate (Excitatory/Inhibitory; E/I) balance is an electrophysiological feature frequently associated with multiple neurodevelopmental disorders. In addition, here, with an alteration of the quantity of OXTRs and of SST+ cells, we expect an alteration of the E/I ratio. Hippocampal brain slices of WT, *Magel2* KO, WT+OT and *Magel2* KO+OT juvenile (P25-P30) male mice were analyzed using whole cell patch clamp to record the activity of aCA3d pyramidal neurons (Figure 7A). Spontaneous activities analysis (Figure 7B) revealed a reduced amplitude of postsynaptic glutamatergic currents (sGlut-PSCs) in *Magel2* KO as compared to WT mice (Figure 7D), while the frequency of sGlut-PSCs was not changed (Figure 7C). The same *Magel2* KO neurons presented a significant increase in GABAergic (sGABA-PSCs) frequency (Figure 7E) while the amplitude of sGABA-PSCs was similar to that of WT (Figure 7F). Patch clamp recordings of the glutamatergic and GABAergic miniature currents (mGlut-PSCs and mGABA-PSCs, respectively) showed a significant reduction in amplitude of mGlut-PSCs, with no change in their frequency, in *Magel2* KO neurons compared to WT (Figure7- figure supplement1B-C) but no differences in frequencies and amplitudes of mGABA-PSCs (Figure7-figure supplement1D-E).

An abnormal dendritic morphology of the *Magel2* KO CA3 pyramidal neurons could be associated with the alterations of the GABAergic or glutamatergic activities. We defined the morphology of recorded CA3d neurons by adding biocytin in the recording solution and performing Neurolucida reconstruction followed by a Sholl analysis. No differences were revealed in dendritic morphology between *Magel2* KO and WT CA3 pyramidal neurons in juvenile mice (Figure7-figure supplement2).

Altogether, those results show that, in *Magel2* KO pyramidal neurons of aCA3d, there is a significant increase in the GABA/Glutamate ratio with no change in their neuronal morphology.

We next investigated the effects of OT-treatment on the GABA/Glutamate balance in WT and *Magel2* KO. Quite unexpectedly, the spontaneous glutamatergic activity was significantly reduced in WT+OT mice compared with WT: frequency was considerably reduced (x 2.7), being even lower than in OT-treated mutants (Figure 7C) and the amplitude was reduced (x1.5), being similar to the one observed in mutant mice (Figure 7D) . These findings indicate that OT-treatment reduced strongly the glutamatergic activity in WT juvenile mice without any apparent impact on the behavioral outcome measured (see above). In *Magel2* KO, OT-treatment in the first week of life decreased significantly the frequency of sGABA-PSCs

bioRxiv preprint doi: https://doi.org/10.1101/2020.09.21.306217; this version posted September 21, 2020. The copyright holder for this preprint (which was not certified by peer review) is the author/funder, who has granted bioRxiv a license to display the preprint in perpetuity. It is made available under aCC-BY-NC-ND 4.0 International license.

restoring a frequency similar to WT (Figure 7E). There was no effect of OT-treatment on the amplitude of sGABA-PSCs (Figure 7F). However, on the same pyramidal neurons, such treatment in *Magel2* KO+OT reduces significantly the frequency of sGlut-PSCs (2x) compared with the frequency recorded in WT or in the *Magel2* KO mice (Figure 7C). The amplitude of sGlut-PSCs was not changed in *Magel2* KO+OT compared with *Magel2* KO, being reduced in the untreated or OT-treated mutants compared with WT mice (Figure 7D). These results show that OT administration in the first week of life normalized the frequency of spontaneous GABAergic activity and reduced significantly the frequency of spontaneous glutamatergic activity in *Magel2* KO compared with WT untreated mice. OT-treatment in WT juvenile mice reduced strongly the gutamatergic activity (frequency and amplitude).

The excitatory-to-inhibitory developmental GABA-shift is delayed in *Magel2* KO hippocampal neurons

Because *Oxtr* and *Magel2* are expressed in aCA2/CA3d hippocampus in infancy, and because in *Oxtr* KO mice (28) as in several models (48) of autism the depolarizing to hyperpolarizing (D-to-H) developmental GABA switch is delayed, we investigated the GABA switch timing in *Magel2* KO pups. First, we performed calcium (Ca^{2+}) imaging experiments by measuring the percentage of neurons showing GABA-induced Ca^{2+} responses in developing hippocampal neuronal cultures of *Magel2* KO embryos collected at E18.5 (DIV0 for days in vitro 0) (Figure 8A-B). At DIV4, we found a significant two-fold higher proportion of *Magel2 KO* neurons increasing Ca^{2+} upon GABA stimulation compared with WT. At DIV8 and DIV11, the percentage of responsive neurons was markedly decreased and similar in both genotypes. We checked that the amplitude of Ca^{2+} responses were similar in both genotypes (Figure 8-figure supplement 1A). Noticeably, comparing the KCl-induced Ca^{2+} responses between WT and *Magel2* KO, we found no increase and even a significant reduction at DIV2, DIV4 and DIV8 in *Magel2* KO cultures (Figure 8-figure supplement 1B), suggesting that the voltage-operated calcium channels were not responsible for the significant higher proportion of *Magel2* KO neurons increasing Ca^{2+} upon GABA stimulation. All together, these results showed a developmental delay in GABA-induced Ca^{2+} responses in cultures of *Magel2* KO embryonic hippocampal neurons and suggest a developmental GABA-shift delay in *Magel2* KO hippocampal neurons.

To further examine whether the action of GABA was altered in *Magel2* KO hippocampal neurons, cell-attached recordings of single $GABA_A$ channels/receptors were performed in acute brain slices in order to measure the Driving Force of $GABA_A$ (DF_{GABA}). DF_{GABA} translates the differences in the actions of GABAergic synapses via $GABA_A$-receptors revealing a hyperpolarizing or depolarizing response of GABA, associated with mature or immature neurons, respectively. Thus, we measured the DF_{GABA} in aCA3 pyramidal cells (PCs) at

bioRxiv preprint doi: https://doi.org/10.1101/2020.09.21.306217; this version posted September 21, 2020. The copyright holder for this preprint (which was not certified by peer review) is the author/funder, who has granted bioRxiv a license to display the preprint in perpetuity. It is made available under aCC-BY-NC-ND 4.0 International license.

postnatal days 1 (P1), 7 (P7) and 15 (P15), on acute brain slices obtained from male mice (Figure 8C). At P1, both *Magel2* KO and WT mice did not show significant differences in the DF_{GABA} but a tendency to an increase of DF_{GABA} in *Magel2* KO compared with WT. Significant difference in the DF_{GABA} was observed at P7 with a 1.8 fold increase of the DF_{GABA} value in mutant neurons, whereas a similar DF_{GABA} was obtained at P15. Since *Magel2* and *Oxtr* are expressed in interneurons (Ins), in which a GABA shift has been also described (49), we also measured the DF_{GABA} in INs and observed similar values in CA3 interneurons of mutant and WT mice (Figure 8-figure supplement 1C). Noticeably, at P7, the resting membrane potential (Figure 8-figure supplement 1D), the conductance (Figure 8-figure supplement 1F) and the capacitance (Figure 8-figure supplement 1E) did not differ statistically between WT and *Magel2* pyramidal neurons. Altogether these data suggest a transient higher GABA depolarizing activity at P7 in CA3 pyramidal neurons of *Magel2* KO pups and consequently a delay in GABA-shift.

Then, at P7, we assessed the effect of the *in vivo* OT-treatment in *Magel2*-KO and WT animals compared with WT untreated pups (Figure 8D). Both *Magel2* KO+OT and WT+OT mice showed a significant decrease in the DF_{GABA} values compared with WT-vehicle. suggesting a reduction in GABA depolarizing activity following an OT administration in infancy.

Post-translational changes in cation-chloride co-transporter KCC2 in *Magel2* KO hippocampus

We then asked if the altered DF_{GABA} values could be due to alteration in the expression of the neuronal transporters of Cl^- in Magel2 KO. The neuronal level of $[Cl^-]_i$ and Cl- dependent depolarizing or hyperpolarizing strength of GABA are determined by complex mechanism involving primarily Cl^- extrusion by potassium/chloride cotransporter type 2 (KCC2) whose expression increases progressively during neuronal maturation (Rivera et al., 1999; Stein et al., 2004). In developing WT hippocampal neurons, the emerging activity of KCC2 contributes to progressive lowering of $[Cl^-]_i$ that at P7 shifts GABA action from depolarizing to hyperpolarizing. As consequence, the activation of $GABA_AR$ produces neuronal Cl^- influx.

The quantitative western blot analysis of the total KCC2 protein expression in hippocampi of P7 mice did not reveal statistically significant difference of the amount of KCC2 between WT and *Magel2* KO animals (Figure 9 A-B). The ion-transport activity of KCC2 and its stability at the cellular plasma membrane also strongly depend on posttranslational modifications of multiple phosphorylation sites (50). We therefore applied in a next step phospho-site-specific antibodies, as they were previously shown to quantitatively monitor changes in KCC2 phosphorylation (51-53). Currently, a limited number of such phospho-specific antibody is available. They are directed against the well-known KCC2's phospho-sites Ser^{940} (54) and

bioRxiv preprint doi: https://doi.org/10.1101/2020.09.21.306217; this version posted September 21, 2020. The copyright holder for this preprint (which was not certified by peer review) is the author/funder, who has granted bioRxiv a license to display the preprint in perpetuity. It is made available under aCC-BY-NC-ND 4.0 International license.

Thr^{1007} (52, 53). Western blot analysis revealed that the *Magel2* KO hippocampi (as compared to WT) were characterized by significantly decreased amount of the phosphorylated form of Ser^{940} (P-Ser^{940}). The amount of phosphorylated Thr^{1007} (P- Thr^{1007}) was not statistically different, but albeit higher in *Magel2* KO mice (Figure 9A- B). Thus, in *Magel2* KO mice there was significant decrease of P-Ser^{940} (inactivation of function lee (54)) and no change of P-Thr^{1007} whose progressive developmental de-phosphorylation is associated with increase of KCC2 activity Friedel (52). At P7, the decreased P-Ser^{940}/P-Thr^{1007} ratio in *Magel2* KO mice may thus result in predominance of KCC2 internalization over surface expression. As a consequence of the decreased amount of surface expressed molecules, the Cl^- extrusion ability of KCC2 is decreased, causing an increase of $[Cl^-]_i$ and could induce a depolarizing shift of GABA described above (Figure 8C).

DISCUSSION

Here we show that *Magel2* KO mice display two specific and constant phenotypes that are stereotypical of other models characterized by a deficit in OT-system: isolation-induced vocalizations in infancy and social memory at adulthood (10). OT administration in the first week of life rescued the latter but not the former. To understand how neonatal OT-treatment drives such long-term effect in *Magel2* KO mice, we studied the hippocampal regions that contains social memory engrams, which also involve the OT-system, and unraveled several and successive temporal changes in the aDG and aCA2/CA3d hippocampal regions that might contribute to the social memory deficit in *Magel2* KO mice. We showed that *Magel2* deficiency alters the GABAergic developmental sequence probably resulting from post-translational biochemical modifications of KCC2, modifies the activity of pyramidal neurons and presents a higher number of SST-positive interneurons and an increase in the quantity of OT-binding sites at adulthood. Interestingly nearly all those changes are rescued by administration of OT in the first days after birth.

The effect of neonatal OT-administration on *Magel2* KO mice

With regard to social behavior, the consequences of postnatal administration of OT in *Magel2* KO mice are consistent with those described previously (38). We have shown a rescue of all social deficits described in adult *Magel2* KO mice without an effect on USVs (here and (38). The “USV test” measures early communication behavior in rodent pups with an ASD-like phenotype and in particular in those with a deficit in the OT-system; however, the role of OT-system in USV calls remains unknown. We cannot explain yet why the OT-administration in the first week of life does not improve the number of USVs in *Magel2* KO pups (P8).

One surprising finding of the current study is the relatively mild behavioral phenotype of the homozygous mutant, which we expected to be more profoundly affected than heterozygous

bioRxiv preprint doi: https://doi.org/10.1101/2020.09.21.306217; this version posted September 21, 2020. The copyright holder for this preprint (which was not certified by peer review) is the author/funder, who has granted bioRxiv a license to display the preprint in perpetuity. It is made available under aCC-BY-NC-ND 4.0 International license.

animals, previously reported to exhibit a social deficit (38). This difference may reflect differences in behavioral assays used in the two studies (3-chamber test versus open field) or the fact that heterozygous mice grew up with WT littermates, whereas homozygous -/- mutants constitute a homogeneous population. Indeed, it has been shown that transgenic mice and their WT littermates can modify each other's behavior (55). The behavior of the mother can also be modified in the presence of one or two genotypes in the same litter and thus impact the behavior of her offspring differently. The modulation of the severity of the social behavior deficits based on the genotype of the *Magel2* KO pups and their environmental context open a number of interesting translational opportunities that will need to be deeply investigated.

Converging evidence suggests that the neurobiological alterations described here may be related to a deficiency in the OT-system of *Magel2* KO mice. Noticeably, Ates et al. (56) showed, *ex vivo,* that lack of *Magel2* expression is associated with significant suppression of the overall activity of oxytocin neurons, suggesting that dysregulation of the OT-system goes beyond oxytocin expression. Furthermore, given the role of *MAGEL2* in ubiquitination, actin regulation and endosomal sorting processes (57), the absence of *Magel2* expression could induce a wide range of post-translational modifications of various molecular and cellular processes in OT and OXTR expressing neurons. Considering The observed long-lasting OT effects could result from a strong impact of OT administration in key developmental hippocampal processes (as discussed below) and can also be achieved by epigenetic modifications that impact gene expression such as the *Oxtr* expression, as observed in prairie voles following a maternal OT administration (58). Transcriptomic and proteomic studies at different developmental ages would help to understand the life-long effect of an early OT-treatment in mutant and WT mice.

Hippocampal alterations in *Magel2* KO in relation with the OT-system: causes and consequences

In vitro, OXTR activation can increase KCC2 phosphorylation (on Ser^{940}) via a PKC -dependent pathway (28), allowing translocation of KCC2 to the cell membrane and post-translational modifications that collectively enhance KCC2 mediated Cl^- transport (54, 59), mechanisms which may also be relevant to control of the GABAergic developmental sequence *in vivo* (60). We therefore hypothesized that the low level of mature OT and/or the lack of *Magel2* in OXTR-positive neurons in *Magel2* KO neonates could induce a deficit in KCC2 Ser^{940} phosphorylation which, in turn, could induce a delay in GABA shift. Our findings are consistent with that hypothesis: we confirm that the GABAergic developmental sequence is transiently delayed in *Magel2* KO mice during the first week of life, with $GABA_A$-mediated responses more depolarizing in *Magel2* KO that WT pyramidal neurons at P7. We furthermore show that this

bioRxiv preprint doi: https://doi.org/10.1101/2020.09.21.306217; this version posted September 21, 2020. The copyright holder for this preprint (which was not certified by peer review) is the author/funder, who has granted bioRxiv a license to display the preprint in perpetuity. It is made available under aCC-BY-NC-ND 4.0 International license.

electrophysiological deficit corresponds well with decreased functional KCC2 at the cell membrane, caused by a deficit of Ser^{940}phosphorylation.

Although a delay in the developmental GABA-shift in *Magel2* KO pyramidal neurons were no longer detectable at P15, there are compelling reasons to suspect that transient disruption of GABAergic maturation in the immediate postnatal period could be enough to permanently alter neural circuit dynamics. Indeed, P7 is a critical milestone in the development of GABAergic neurons in the mouse neocortex and hippocampus, characterized by major changes in network dynamics (e.g. end of *in vitro* giant-depolarizing-potentials (61) and *in vivo* early sharp waves (62)), intrinsic membrane properties (e.g. input resistance) and synaptic connectivity (63). Altogether those data suggest that the absence of *Magel2* delays neuronal maturation during this critically vulnerable period of brain development, resulting in a distinct adult phenotype. Whether the delay of the GABA-shift alone is sufficient to derail neurotypical developmental trajectory remains a key question for future study: notably, similar or longer GABA-shift delays have been observed in several models of autism (64, 65) and in *Oxtr* KO mouse models (28). Recently, Kang et al. (66) showed in *Disc1* KO mouse model, that elevated depolarizing GABA signaling is a precursor for the later E/I imbalance (in favor of inhibition) and social impairment. Similarly, we showed that, in a KCC2 mutant mouse, the GABA shift delay is responsible for the E/I alteration (60).

Importantly, OT-treatment has a relative hyperpolarizing effect at P7 in *Magel2* KO and WT pups compared with WT-vehicle animals that might modify the maturation of the circuitry.

The E/I ratio and social behavior

Reductions in synaptic signal-to-noise in cortical and hippocampal pyramidal neurons, driven by a change in the ratio of dendritic excitatory and inhibitory synapses, are widely thought to contribute to reduced efficiency of signal processing in ASD, a mechanism known as the E/I ratio hypothesis (67). We confirm E/I imbalance characterized by increased GABAergic activity and lower glutamatergic activity in CA3 neurons in *Magel2* KO mice, consistent with observations made in other ASD models (68-71). Furthermore, we report that perinatal OT administration restored normal GABAergic activity in *Magerl2* KO mice without improving glutamatergic transmission. Unexpectedly, perinatal OT treatment has a significant impact on the WT neurons inducing a strong reduction of glutamatergic activity without affecting GABAergic activity. This is a significant observation, because it shows that, although the ASD-like behavior *Magel2* KO animals correlated with a change in E/I ratio, E/I imbalance in OT treated WT animals was not sufficient to drive detectable changes in social behavior or cognitive performance. We therefore conclude that E/I imbalance characterized by isolated decreased spontaneous glutamatergic transmission is unlikely to underlie the ASD traits

bioRxiv preprint doi: https://doi.org/10.1101/2020.09.21.306217; this version posted September 21, 2020. The copyright holder for this preprint (which was not certified by peer review) is the author/funder, who has granted bioRxiv a license to display the preprint in perpetuity. It is made available under aCC-BY-NC-ND 4.0 International license.

investigated here, and suggest that an upper threshold of GABAergic or glutamatergic activity, but not the E/I ratio *per se*, may be important for normal development.

Role of oxytocin receptors and somatostatin neurons.

In adult *Magel2* KO mice we observed increased OT-binding in the DG and CA2/CA3d regions of the anterior hippocampus compared to WT mice. OT administration in *Magel2* KO neonates normalized hippocampal OT binding sites in adulthood, suggesting that the increased expression of OXTR observed in *Magel2* KO hippocampus may be a consequence of the reduced OT production reported in these animals (37). This observation supports the idea that life-long OXTR expression is to some extent determined by early life OT binding, described as a “hormonal imprinting” effect (58, 72).

Since hippocampal OXTRs are mainly expressed in PV and SST interneurons, we quantified those populations and found a significant increase (1.6x to 1.8x) in the number of aDG and aCA2/CA3d SST+ neurons in mutant mice, the number of PV+ interneurons was not modified. OT-treatment normalized the number of SST-expressing neurons in *Magel2* KO pups, revealing a causal link between the administration of OT in infancy and the quantity of SST+-neurons. This result may reflect actual changes in the number of SST+ neurons, or alternatively changes in SST expression and hence more reliable detection of SST-synthesizing neurons. Interestingly, OT modulates the activity of the SST+ neurons, increasing the excitability of SST interneurons (31) but no studies report an effect of OT on SST production.

SST interneurons have recently been shown to play a role in the modulation of social behavior (73, 74) and a reduction in the number of PV or SST interneurons has been reported to be associated with social deficits or ASD. Noticeably, a link between altered social memory and an increase in SST cell number has been recently reported in LPS-treated female neonates (75). It is tempting to speculate that OXTR-transmission regulates the activity of SST hippocampal interneurons and the production/release of mature SST and impacts social memory. Further work is needed to fully characterize the role of OXTRs on SST interneurons in relation with social memory.

Conclusions

Short-term OT-treatment in infancy reduced behavioral traits associated with ASD in adulthood and permanently rescued functional and cellular hippocampal alterations that were identified in *Magel2* KO mice. However, we do not know whether the deficient OT-system observed in *Magel2* KO mice (37, 38) is the only cause of these alterations since the lack of *Magel2* expression may disrupt neuronal development and circuit formation via signaling pathways independent of OT. Another open question is whether developmental alterations in the *Magel2*

bioRxiv preprint doi: https://doi.org/10.1101/2020.09.21.306217; this version posted September 21, 2020. The copyright holder for this preprint (which was not certified by peer review) is the author/funder, who has granted bioRxiv a license to display the preprint in perpetuity. It is made available under aCC-BY-NC-ND 4.0 International license.

KO are a consequence of dysfunction in a single sequential pathway, or whether they reflect parallel interconnected circuits in the developing hippocampus. Finally, and surprisingly, postnatal OT-treatment plays a role in many key processes, suggesting a pleiotropic action of oxytocin stimulating the maturation of hippocampal circuitry involved in social memory and possibly other behavioral deficits. A significant impact of such treatment was also observed in WT animals without any effect on social behavioral as tested.

Overall, we have shown that OT-treatment in infancy has a significant impact and rescues permanent specific hippocampal alterations in *Magel2* KO mice at different developmental ages, many of these hippocampal alterations have been described in several models of neurodevelopmental disorders with ASD (see discussion). In addition, OT deficit has often been described in rodent models of ASD (see introduction). Taken together, our findings reinforce the idea that OT-treatment in early life may represent a viable therapeutic strategy for patients with SYS or PWS and possibly other neurodevelopmental disorders.

MATERIALS AND METHODS

Animals

To perform functional studies, we chose to work with the *Magel2* $^{tm1.1Mus}$ homozygous (-/-) mice, here named *Magel2* KO, in order to have a greater homogeneity in the values, allowing a better analysis of the effects of the mutation.

Magel2 $^{tm1.1Mus}$+/+ (WT) and *Magel2* $^{tm1.1Mus}$-/- (*Magel2* KO) mice were maintained on a C57BL/6J genetic background and stabulated in standard conditions, with *ad-libitum* access to food and water. Mice were handled and cared for in accordance with the Guide for the Care and Use of Laboratory Animals (N.R.C., 1996) and the European Communities Council Directive of September 22th 2010 (2010/63/EU, 74). Experimental protocols were approved by the institutional Ethical Committee guidelines for animal research with the accreditation no. B13-055-19 from the French Ministry of Agriculture. We maintain grouped-house mice (3-5 mice/cage). All efforts were made to minimize the number of animals used. *Magel2*-deficient mice were generated as previously described (37). Due to the parental imprinting of *Magel2* (paternally expressed only), to obtain heterozygote mice (+m/-p), males carrying the mutation on the maternal allele (-m/+p) were crossed with wild-type C57BL/6J females.

To obtain homozygote mice, *Magel2* KO homozygote males and females were crossed. Importantly, we checked that *Magel2* KO mothers had a similar maternal behavior as WT mothers. All mice were genotyped by PCR starting from DNA extracted from tail snips (around 3 mm), using the following couples of primers:

bioRxiv preprint doi: https://doi.org/10.1101/2020.09.21.306217; this version posted September 21, 2020. The copyright holder for this preprint (which was not certified by peer review) is the author/funder, who has granted bioRxiv a license to display the preprint in perpetuity. It is made available under aCC-BY-NC-ND 4.0 International license.

Ml2KO F Ml2KO R	5'-CCCTGGGTTGACTGACTCAT-3' 5'-TCTTCTTCCTGGTGGCTTTG-3'	to discriminate the mutant allele from the WT one
71456 F 71457 R	5'-CACTCGATCACGTATGGCTCCATCA-3' 5'-GATGGCAGGCACTGACTTACATGCTG-3'	to discriminate the heterozygous from the homozygous mice

Oxytocin Treatment

WT pups and *Magel2* KO pups were removed from their mother, placed on a heating pad, given a subcutaneous (s.c.) injection and quickly returned to the mother. The solutions injected were isotonic saline (10 µl) for the control mice and 2 µg of OT (Phoenix Pharmaceuticals Inc., cat #051-01) diluted in isotonic saline (10 µl) for the treated mice. The treatment was performed during the first week of life every other day (P0, P2, P4, P6).

Behavior

All the behavioral tests were performed by Phenotype Expertise, Inc. (France). For all tests, animals were first acclimated to the behavioral room for 30 minutes.

Ultrasonic vocalization (USVs). Early social communication was tested by analyzing isolation-induced ultrasonic vocalizations (USVs) in P8 pups of both sexes. Briefly, after 30 min of habituation to the testing room, P8 pups were isolated from the mother and gently transferred to a new cage on a heating pad (37°C). After 5 min of separation, each pup was transferred in an isolation box located inside an anechoic box (54 x 57 x 41 cm; Couldbourn instruments, PA, USA). USVs were recorded for 300 s by an ultrasonic microphone (Avisoft UltraSoundGate condenser microphone capsule CM16/CMPA, Avisoft bioacustic, Germany) sensitive to frequencies of 10-250 kHz. Recordings were done using Avisoft recorder software (version 4.2) with a sampling rate of 250 kHz in 16-bit format. Data were analyzed for the total number of calls using Avisoft SASLab software.

Elevated-Plus Maze. The EPM is used to assess anxiety state of animals. The device consists of a labyrinth of 4 arms 5 cm wide located 80 cm above the ground. Two opposite arms are open (without wall) while the other two arms are closed by side walls. The light intensity was adjusted to 20 Lux on the open arms. Mice were initially placed on the central platform and left free to explore the cross-shaped labyrinth for 5 minutes. Maze was cleaned and wiped with H_2O and with 70% ethanol between each mouse. Animal movement was video-tracked using Ethovision software 11.5 (Noldus). Time spent in open and closed arms, the number of entries in open arms, as well as the distance covered, are directly measured by the software.

Open-field. Open-field test was performed in a 40 x 40 cm square arena with an indirect illumination of 60 lux. Mouse movement was video-tracked using Ethovision software 11.5 (Noldus) for 10 minutes. Total distance traveled and time in center (exclusion of a 5 cm border

bioRxiv preprint doi: https://doi.org/10.1101/2020.09.21.306217; this version posted September 21, 2020. The copyright holder for this preprint (which was not certified by peer review) is the author/funder, who has granted bioRxiv a license to display the preprint in perpetuity. It is made available under aCC-BY-NC-ND 4.0 International license.

arena) are directly measured by the software. Grooming (time and events) and rearing were manually counted in live using manual functions of the software, by an experimented behaviorist. The open-field arena was cleaned and wiped with H_2O and with 70% ethanol between each mouse.

New object recognition. The arena used for the novel object recognition test was the same used for the open-field test. The arena was cleaned and wiped with 70% ethanol between each mouse. Two identical objects (50 ml orange corning tube) were placed in the opposite corners of the arena, 10 cm from the side walls. The tested mouse was placed at the opposite side of the arena and allowed to explore the arena for 10 min. After 1h, one object was randomly replaced with another novel object, which was of similar size but differ in the shape and color with the previous object (white and blue lego bricks). Then, the same mouse was placed in the arena and allowed to explore the two objects (a new and an "old" familiar object) for 10 min. The movement of the mice was video-tracked with Ethovision 11.5 software. Time of exploration of both objects (nose located in a 2 cm area around object) was automatically measured by the software.

Three-chamber social preference test. The test was performed as described previously (46). The three-chamber apparatus consisted of a Plexiglas box (50x25 cm) with removable floor and partitions dividing the box into three chambers with 5-cm openings between chambers. The task was carried out in four trials. The three-chambers apparatus was cleaned and wiped with 70% ethanol between each trial and each mouse.

In the first trial (habituation), a test mouse was placed in the center of the three-chamber unit, where two empty wire cages were placed in the left and right chambers to habituate the test mouse to arena. The mouse was allowed to freely explore each chamber. The mouse was video-tracked for 5 min using Ethovision software. At the end of the trial, the animal was gently directed to the central chamber with doors closed. In the second trial (social exploration), a 8-weeks old C57BL/6J mouse (S1) was placed randomly in one of the two wire cages to avoid a place preference. The second wire cage remained empty (E). Then, doors between chambers were opened and the test mouse was allowed to freely explore the arena for 10 min. At the end of the trial, animal was gently directed to the central chamber with doors closed. A second 8-weeks old C57BL/6J mouse (S2) was placed in the second wire cage for the third trial (social discrimination). Thus, the tested mouse had the choice between a familiar mouse (S1) and a new stranger mouse (S2) for 10 min. At the end of the trial, the mouse was returned to home-cage for 30 min. For the fourth trial (short-term social memory), S2 was replaced by a new stranger mouse (S3), the familiar mouse (S1) staying the same. Then tested mouse was allowed to freely explore the arena for 10 min. Time spent in each chamber and time of contact with each wire cage (with a mouse or empty) were calculated using Ethovision software. The measure of the real social contact is represented by the time spent in nose-to-nose interactions

bioRxiv preprint doi: https://doi.org/10.1101/2020.09.21.306217; this version posted September 21, 2020. The copyright holder for this preprint (which was not certified by peer review) is the author/funder, who has granted bioRxiv a license to display the preprint in perpetuity. It is made available under aCC-BY-NC-ND 4.0 International license.

with the unfamiliar or familiar mouse. This test was performed using grouped-house mice of 4 months old.

Primary hippocampal cultures

Embryonic day 18 dissociated hippocampal neurons were obtained from wild-type and *Magel2* KO timed pregnant mice as previously described (76) with slightly modifications here described. Briefly, the hippocampi of E18 embryos were dissociated by an enzymatic treatment (0.25% trypsin for 18 min at 37°C) followed by mechanic dissociation with a fire-smoothed Pasteur pipette or p1000µl/p200µl tips. For calcium imaging experiments, 200 000 cell/well (in MW 6 wells) were plated on round 26 mm glass coverslips pre-coated with poly-L-lysine containing Neurobasal medium (Life Technologies) augmented with B27 supplement (2% v/v; Life Technologies), L-glutamine (2mM), penicillin/streptomycin (100U/ml) and 25µM Glutamate. This media was replaced with glutamate-free media after 5 hours. Neurons were then maintained at 37°C in humidified atmosphere (95% air and 5% CO_2), and half of the medium was refreshed twice a week.

Calcium imaging recordings

Calcium imaging experiments were carried out as previously described (28). Briefly, hippocampal neurons were loaded with the membrane-permeable fluorescent Ca^{2+} indicator Fura-2/AM (1 µM; SigmaAldrich) for 40 min at 37°C, 5% CO_2. The cells were then placed into the recording chamber of an inverted microscope (Axiovert 100, Zeiss), washed with the extracellular recording solution, KRH buffer, and imaged through a 40x objective (Zeiss). Fura-2/AM was excited at 380 nm and at 340 nm through a Polychrom V, (TILL Photonics GmbH) controlled by the TillVisION software 4.01. Emitted light was acquired at 505nm at 1Hz, and images collected with a CCD Imago-QE camera (TILL Photonics GmbH). The fluorescence ratio F340/380 (ΔF340/380) was used to express Ca^{2+} concentrations in regions of interest (ROI) corresponding to neuronal cell bodies. 100µM GABA was administered in the recording solution and temporal changes in ΔF340/380 were followed. Increases in ΔF340/380 higher than 0.04 units were considered reliable Ca^{2+} responses. After wash with KRH buffer and recover, KCl (50mM) was administered to identify viable neurons. Responses with a ΔF340/380 smaller than 0.1 units were excluded from the analyses. From DIV8 on, 1 µM TTX (Tocris, cat #1069) was added to this extracellular recording solution.

Hippocampal slice preparation and electrophysiological recordings

Brains were removed and immersed into ice-cold (2-4°C) artificial cerebrospinal fluid (ACSF) with the following composition (in mM): 126 NaCl, 3.5 KCl, 2 $CaCl_2$, 1.3 $MgCl_2$, 1.2 NaH_2PO_4,

bioRxiv preprint doi: https://doi.org/10.1101/2020.09.21.306217; this version posted September 21, 2020. The copyright holder for this preprint (which was not certified by peer review) is the author/funder, who has granted bioRxiv a license to display the preprint in perpetuity. It is made available under aCC-BY-NC-ND 4.0 International license.

25 $NaHCO_3$ and 11 glucose, pH 7.4 equilibrated with 95% O_2 and 5% CO_2. Hippocampal slices (400 µm thick) were cut with a vibrating microtome (Leica VT 1000s, Germany) in ice cold oxygenated choline-replaced ACSF and were allowed to recover at least 90 min in ACSF at room (25°C) temperature. Slices were then transferred to a submerged recording chamber perfused with oxygenated (95% O_2 and 5% CO_2) ACSF (3 ml/min) at 34°C.

Whole-cell patch clamp recordings were performed from P20-P25 CA3 pyramidal neurons in voltage-clamp mode using an Axopatch 200B (Axon Instrument, USA). To record the spontaneous and miniature synaptic activity, the glass recording electrodes (4-7 MΩ) were filled with a solution containing (in mM): 100 KGluconate, 13 KCl, 10 HEPES, 1.1 EGTA, 0.1 $CaCl_2$, 4 MgATP and 0.3 NaGTP. The pH of the intracellular solution was adjusted to 7.2 and the osmolality to 280 mOsmol l^{-1}. The access resistance ranged between 15 to 30 MΩ. With this solution, the $GABA_A$ receptor-mediated postsynaptic current (GABAA-PSCs) reversed at -70mV. GABA-PSCs and glutamate mediated synaptic current (Glut-PSCs) were recorded at a holding potential of -45mV. At this potential GABA-PSC are outwards and Glut-PSCs are inwards. Spontaneous synaptic activity was recorded in control ACSF and miniature synaptic activity was recorded in ACSF supplemented with tetrodotoxin (TTX, 1µM). Spontaneous and miniature GABA-PSCs and Glut-PSCs were recorded with Axoscope software version 8.1 (Axon Instruments) and analyzed offline with Mini Analysis Program version 6.0 (Synaptosoft).

Single $GABA_A$ channel recordings were performed at P1, P7 and P15 visually identified hippocampal CA3 pyramidal cells in cell-attached configuration using Axopatch-200A amplifier and pCLAMP acquisition software (Axon Instruments, Union City, CA). Data were low-pass filtered at 2 kHz and acquired at 10 kHz. The glass recording electrodes (4-7 MΩ) were filled with a solution containing (in mM) for recordings of single $GABA_A$ channels: NaCl 120, KCl 5, TEA-Cl 20, 4-aminopyridine 5, $CaCl_2$ 0.1, $MgCl_2$ 10, glucose 10, Hepes-NaOH 10. The pH of pipette solutions was adjusted to 7.2 and the osmolality to 280 mOsmol l^{-1}. Analysis of currents trough single channels and current-voltage relationships were performed using Clampfit 9.2 (Axon Instruments) as described by (77).

Morphological analysis

During electrophysiological recordings, biocytin (0.5%, Sigma, USA) was added to the pipette solution for post hoc reconstruction. Images were acquired using a Leica SP5 X confocal microscope, with a 40x objective and 0,5 µm z-step. Neurons were reconstructed tree-dimensionally using Neurolucida software version 10 (MBF Bioscience) from 3D stack images. The digital reconstructions were analyzed with the software L-Measure to measure the number of primary branches and the total number of ramifications of each neuron (78). Comparisons between groups were done directly in L-Measure.

bioRxiv preprint doi: https://doi.org/10.1101/2020.09.21.306217; this version posted September 21, 2020. The copyright holder for this preprint (which was not certified by peer review) is the author/funder, who has granted bioRxiv a license to display the preprint in perpetuity. It is made available under aCC-BY-NC-ND 4.0 International license.

Immunohistochemistry and quantification

WT and mutant mice were deeply anaesthetized with intraperitoneal injection of the ketamine/xylazine mixture and transcardially perfused with 0.9% NaCl saline followed by Antigenfix (Diapath, cat #P0014). Brains were post-fixed in Antigenfix overnight at 4°C and included in agar 4%. 50 µm-thick coronal sections were sliced using a vibratom (Zeiss) and stored in PBS at 4°C. Floating slices (of the hippocampal region corresponding to slices 68 to 78 on Allan Brain Atlas) were incubated for 1 hour with blocking solution containing 0.1% (v/v) Triton X-100, 10% (v/v) normal goat serum (NGS) in PBS, at room temperature. Sections were then incubated with primary antibodies diluted in incubation solution (0.1% (v/v) Triton X-100, 3% (v/v) NGS, in PBS), overnight at 4C°. After 3 x 10 min washes in PBS, brain sections were incubated with secondary antibodies diluted in the incubation solution, for 2 hours at RT. Sections were washed 3 x 10 min in PBS and mounted in Flouromount-G (EMS, cat #17984-25). Primary antibodies used were: rabbit polyclonal anti-cFos (1:5000, Santa Cruz Biotech , cat #ab190289), goat polyclonal anti-Sst (D20) (1:500, Santa Cruz Biotech, cat #sc-7819), mouse monoclonal anti-Sst (H-11) (1:500, Santa Cruz Biotech, cat #sc-74556), goat polyclonal anti-PV (1:6000, SWANT, cat #PVG213). Fluorochrome-conjugated secondary antibodies used were: goat anti-rabbit Alexa Fluor 647 (1:500, Invitrogen, cat # A32733), goat anti-rabbit Alexa Fluor 488 (1:500, Invitrogen, cat #A-31565), goat anti-mouse Alexa Fluor 488 (1:500, Invitrogen, cat #A21121), donkey anti-goat Alexa Fluor 488 (1:500, Invitrogen, cat # A32814).

For c-Fos, PV and SST quantification, images were acquired using a fluorescence microscope (Zeiss Axioplan 2 microscope with an Apotome module), and z stacks of 8 µm were performed for each section. Counting were performed on the right and left hippocampus for 5-7 sections (cFos) or 7-9 sections (PV, SST) per animal in the hippocampal regions indicated on the figures and corresponding to slices 68 to 78 on Allen Brain Atlas.

OT binding assay

Adult WT and mutant mice were sacrificed and non-perfused mouse brain were frozen in -25°C isopenthane and stored at -80°C until cut. 14 µm thick brain slices were cut using a cryostat (Frigocut-2700, Reichert-Jung) and collected on chromallume-coated slides and stored at -80°C until use. Slides were pre-incubated for 5 minutes in a solution of 0.2% paraformaldehyde in phosphate-buffered saline (pH 7.4), and rinsed twice in 50 mM Tris HCl + 0.1% BSA buffer. Slides were then put in a humid chamber and covered with 400 µL of incubation medium (50 mM Tris HCl, 0.025% bacitracin, 5 mM MgCl2, 0,1% BSA) containing the radiolabeled I [125] OVTA (Perkin Elmer), at a concentration of 10 pM. After a 2h incubation under gentle agitation, the incubation medium is removed and slides are rinsed twice in ice-

bioRxiv preprint doi: https://doi.org/10.1101/2020.09.21.306217; this version posted September 21, 2020. The copyright holder for this preprint (which was not certified by peer review) is the author/funder, who has granted bioRxiv a license to display the preprint in perpetuity. It is made available under aCC-BY-NC-ND 4.0 International license.

cold incubation medium and a third time in ice cold distilled water. Each slide is then dried in a stream of cold air, and placed in a X-ray cassette in contact with a KODAK film for 3 days.

ROIs were chosen and analyzed through ImageJ, using Paxinos' Mouse Brain Atlas as a reference to find the brain areas of interest. To remove background noise caused by nonspecific binding, each slide was compared with its contiguous one, which had been incubated in presence of an excess of "cold" oxytocin (2 μM). Net grey intensity was quantified and then converted to nCi/mg tissue equivalent using a calibration curve. For each region, a minimum of 4 slices per brain were included in the analysis. Data plotted on graphs are the differences between the total and the nonspecific binding. Right and left hemispheres were kept separate.

Chromogenic In situ Hybridization

Fresh-frozen brains from WT mice at post-natal days (P)7, P21, and P28 were sectioned in a cryostat in the coronal plane at 20μm thickness and mounted on Superfrost Plus slides and stored at -80°C. RNA detection was performed on tissue sections using RNAscope 2.5HD Duplex Assay (Cat #322430, Advanced Cell Diagnostics (ACD), Hayward, CA). The two probes used are synthetic oligonucleotide probes complementary to the nucleotide sequence 1198 – 2221 of Oxtr (NM_001081147.1) (Oxtr-E4-C2, ACD Cat #411101-C2) and 3229 – 4220 of Magel2 (NM_013779.2) (Magel2-01, ACD Cat #535901). Briefly, slides were fixed in 4% paraformaldehyde in PBS (pH 9.5) on ice for 2 hours and dehydrated in increasing concentrations of alcohol, then stored in 100% ethanol overnight at -20°C. The slides were air dried for 10 minutes, then pretreated in target retrieval solution (ref. 322001, ACD) for 5 minutes while boiling, after which, slides were rinsed 2 times in water followed by 100% ethanol and then air dried. A hydrophobic barrier pen (ImmEdge) was used to create a barrier around selected sections. Selected sections were then incubated with protease plus (ref. 322331, ACD) for 15 minutes in a HybEZ oven (ACD) at 40°C, followed by water washes. The sections were then hybridized with the probe mixture at 40°C for 2 hr per slide. Unbound hybridization probes were removed by washing 2 times in wash buffer. After hybridization, sections were subjected to signal amplification using the HD 2.5 detection Kit following the kit protocol. Hybridization signal was detected using a mixture of fast-RED solutions A and B (60:1) for Oxtr-E4-C2 and a mixture of Fast-GREEN solutions A and B (50:1) for Magel2-01. The slides were then counterstained with Gill's hematoxylin and air-dried in a 60°C oven for 15 min. Slides were cooled and cover-slipped with Vectamount TM (Vector Laboratories, Inc. Burlingame, CA). Slides were imaged at 4x and 20x on a bright field microscope (Keyence BZ-X710, Keyence Corp., Osaka, Japan). Hippocampal sections were investigated for colocalization of Oxtr (red) with Magel2 (blue-green) transcripts.

bioRxiv preprint doi: https://doi.org/10.1101/2020.09.21.306217; this version posted September 21, 2020. The copyright holder for this preprint (which was not certified by peer review) is the author/funder, who has granted bioRxiv a license to display the preprint in perpetuity. It is made available under aCC-BY-NC-ND 4.0 International license.

Western Blot

P7 mice were sacrificed and hippocampi were dissected and rapidly frozen in liquid nitrogen and stored at -80°C until protein extraction. Hippocampi were lysed in lysis buffer (50 mM Tris/HCl, pH 7.5, 1 mM EGTA, 1 mM EDTA, 50 mM sodium fluoride, 5 mM sodium pyrophosphate, 1 mM sodium orthovanadate, 1% (w/v) Triton-100, 0.27 M sucrose, 0.1% (v/v) 2-mercaptoethanol, and protease inhibitors (complete protease inhibitor cocktail tablets, Roche, 1 tablet per 50 mL)) and protein concentrations were determined following centrifugation of the lysate at 16,000 x g at 4 °C for 20 minutes using the Bradford method with bovine serum albumin as the standard. Tissue lysates (15 µg) in SDS sample buffer (1X NuPAGE LDS sample buffer (Invitrogen), containing 1% (v/v) 2-mercaptoethanol) were subjected to electrophoresis on polyacrylamide gels and transferred to nitrocellulose membranes. The membranes were incubated for 30 min with TBS-Tween buffer (TTBS, Tris/HCl, pH 7.5, 0.15 M NaCl and 0.2% (v/v) Tween-20) containing 5% (w/v) skim milk. The membranes were then immunoblotted in 5% (w/v) skim milk in TTBS with the indicated primary antibodies overnight at 4°C. The blots were then washed six times with TTBS and incubated for 1 hour at room temperature with secondary HRP-conjugated antibodies diluted 5000-fold in 5% (w/v) skim milk in TTBS. After repeating the washing steps, the signal was detected with the enhanced chemiluminescence reagent. Immunoblots were developed using ChemiDoc™ Imaging Systems (Bio-Rad). Primary antibodies used were: anti-KCC2 phospho-Ser940 (Thermo Fisher Scientific, cat #PA5-95678), anti-KCC2 phospho-Thr1007 (Thermo Fisher Scientific, cat #PA5-95677), anti-Pan-KCC2, residues 932-1043 of human KCC2 (NeuroMab, cat #73-013), anti(neuronal)-β-Tubulin III (Sigma-Aldrich, cat #T8578). Horseradish peroxidase-coupled (HRP) secondary antibodies used for immunoblotting were from Pierce. Figures were generated using Photoshop and Illustrator (Adobe). The relative intensities of immunoblot bands were determined by densitometry with ImageJ software.

Statistical Analysis

Statistical analyses were performed using GraphPad Prism (GraphPad Software, Prism 7.0 software, Inc, La Jolla, CA, USA). All statistical tests were two-tailed and the level of significance was set at $P<0.05$. Appropriate tests were conducted depending on the experiment; tests are indicated in the figure legends or detailed in supplementary statistical file. Values are indicated as Q2 (Q1, Q3), where Q2 is the median, Q1 is the first quartile and Q3 is the third quartile when non-parametric tests were performed and scatter dot plots report Q2 (Q1,Q3) or as mean ± SEM when parametric tests were performed usually in histograms. N refers to the number of animals or primary culture preparations, while n refers to the number of brain sections or hippocampi or cells recorded.

bioRxiv preprint doi: https://doi.org/10.1101/2020.09.21.306217; this version posted September 21, 2020. The copyright holder for this preprint (which was not certified by peer review) is the author/funder, who has granted bioRxiv a license to display the preprint in perpetuity. It is made available under aCC-BY-NC-ND 4.0 International license.

Mann-Whitney (MW) non-parametric test or t-test (parametric test) were performed to compare two matched or unmatched groups. ANOVA or Kruskal-Wallis tests were performed when the different groups have been experienced in the same experimental design only; if this was not the case, MW or t-test were used. One-way ANOVA followed by Bonferroni or Dunnett's or Tukey's post-hoc tests were used to compare three or more independent groups. Two-way ANOVA followed by Bonferroni post-hoc test was performed to compare the effect of two factors on unmatched groups. *: $p< 0.05$; **: $p <0.01$; ***: $p<0.001$; ****: $p<0.0001$. All the statistical analyses (corresponding to each figure) are reported in a specific file.

Acknowledgements

The authors thank the Foundation for Prader-Willi Research (FPWR) grants, Agence Nationale pour la Recherche (ANR-14-CE13-0025-01), Thyssen Foundation (Grant 10.16.2.018MN), Prader-Willi France and Fondation Jerôme LeJeune for their financial support.

The authors thank Pr. Simon McCullan for comments and careful reading of the manuscript. Dr. A. Baude for her technical advices, Dr F. Michel for his help in microscopy and the use of image softwares,

Financial disclosures

Fabienne Schaller and Françoise Muscatelli are co-inventors on a patent to use oxytocin in the treatment of infant feeding disorder, e.g. Prader-Willi Syndrome (No. WO/2011/147889; US/2014/US9125862B2). The other authors have indicated they have no potential conflicts of interest to disclose.

bioRxiv preprint doi: https://doi.org/10.1101/2020.09.21.306217; this version posted September 21, 2020. The copyright holder for this preprint (which was not certified by peer review) is the author/funder, who has granted bioRxiv a license to display the preprint in perpetuity. It is made available under aCC-BY-NC-ND 4.0 International license.

REFERENCES

1. Wagner S, Harony-Nicolas H. Oxytocin and Animal Models for Autism Spectrum Disorder. Current topics in behavioral neurosciences. 2018;35:213-37.
2. Muscatelli F, Desarmenien MG, Matarazzo V, Grinevich V. Oxytocin Signaling in the Early Life of Mammals: Link to Neurodevelopmental Disorders Associated with ASD. Current topics in behavioral neurosciences. 2018;35:239-68.
3. Winslow JT, Hearn EF, Ferguson J, Young LJ, Matzuk MM, Insel TR. Infant vocalization, adult aggression, and fear behavior of an oxytocin null mutant mouse. Horm Behav. 2000;37(2):145-55.
4. Ferguson JN, Aldag JM, Insel TR, Young LJ. Oxytocin in the medial amygdala is essential for social recognition in the mouse. J Neurosci. 2001;21(20):8278-85.
5. Takayanagi Y, Yoshida M, Bielsky IF, Ross HE, Kawamata M, Onaka T, et al. Pervasive social deficits, but normal parturition, in oxytocin receptor-deficient mice. Proc Natl Acad Sci U S A. 2005;102(44):16096-101.
6. Sala M, Braida D, Lentini D, Busnelli M, Bulgheroni E, Capurro V, et al. Pharmacologic rescue of impaired cognitive flexibility, social deficits, increased aggression, and seizure susceptibility in oxytocin receptor null mice: a neurobehavioral model of autism. Biol Psychiatry. 2011;69(9):875-82.
7. Sala M, Braida D, Donzelli A, Martucci R, Busnelli M, Bulgheroni E, et al. Mice heterozygous for the oxytocin receptor gene (Oxtr(+/-)) show impaired social behaviour but not increased aggression or cognitive inflexibility: evidence of a selective haploinsufficiency gene effect. J Neuroendocrinol. 2013;25(2):107-18.
8. Jin D, Liu HX, Hirai H, Torashima T, Nagai T, Lopatina O, et al. CD38 is critical for social behaviour by regulating oxytocin secretion. Nature. 2007;446(7131):41-5.
9. Liu HX, Lopatina O, Higashida C, Tsuji T, Kato I, Takasawa S, et al. Locomotor activity, ultrasonic vocalization and oxytocin levels in infant CD38 knockout mice. Neurosci Lett. 2008;448(1):67-70.
10. Caldwell HK, Aulino EA, Freeman AR, Miller TV, Witchey SK. Oxytocin and behavior: Lessons from knockout mice. Developmental neurobiology. 2017;77(2):190-201.
11. Johnson ZV, Walum H, Xiao Y, Riefkohl PC, Young LJ. Oxytocin receptors modulate a social salience neural network in male prairie voles. Horm Behav. 2017;87:16-24.
12. Raam T, McAvoy KM, Besnard A, Veenema AH, Sahay A. Hippocampal oxytocin receptors are necessary for discrimination of social stimuli. Nature communications. 2017;8(1):2001.
13. Lin YT, Hsieh TY, Tsai TC, Chen CC, Huang CC, Hsu KS. Conditional Deletion of Hippocampal CA2/CA3a Oxytocin Receptors Impairs the Persistence of Long-Term Social Recognition Memory in Mice. J Neurosci. 2018;38(5):1218-31.
14. Okuyama T. Social memory engram in the hippocampus. Neurosci Res. 2018;129:17-23.
15. Cilz NI, Cymerblit-Sabba A, Young WS. Oxytocin and Vasopressin in the Rodent Hippocampus. Genes Brain Behav. 2018:e12535.
16. Young WS, Song J. Characterization of Oxytocin Receptor Expression Within Various Neuronal Populations of the Mouse Dorsal Hippocampus. Frontiers in molecular neuroscience. 2020;13:40.
17. Bosch OJ, Neumann ID. Brain vasopressin is an important regulator of maternal behavior independent of dams' trait anxiety. Proc Natl Acad Sci U S A. 2008;105(44):17139-44.
18. Eaton JL, Roache L, Nguyen KN, Cushing BS, Troyer E, Papademetriou E, et al. Organizational effects of oxytocin on serotonin innervation. Dev Psychobiol. 2012;54(1):92-7.
19. Miller TV, Caldwell HK. Oxytocin during Development: Possible Organizational Effects on Behavior. Frontiers in endocrinology. 2015;6:76.
20. Lefevre A, Sirigu A. The two fold role of oxytocin in social developmental disorders: A cause and a remedy? Neurosci Biobehav Rev. 2016;63:168-76.

bioRxiv preprint doi: https://doi.org/10.1101/2020.09.21.306217; this version posted September 21, 2020. The copyright holder for this preprint (which was not certified by peer review) is the author/funder, who has granted bioRxiv a license to display the preprint in perpetuity. It is made available under aCC-BY-NC-ND 4.0 International license.

21. Muscatelli F, Desarmenien MG, Matarazzo V, Grinevich V. Oxytocin Signaling in the Early Life of Mammals: Link to Neurodevelopmental Disorders Associated with ASD. Current topics in behavioral neurosciences. 2017.
22. Veenema AH. Toward understanding how early-life social experiences alter oxytocin- and vasopressin-regulated social behaviors. Horm Behav. 2012;61(3):304-12.
23. Perkeybile AM, Carter CS, Wroblewski KL, Puglia MH, Kenkel WM, Lillard TS, et al. Early nurture epigenetically tunes the oxytocin receptor. Psychoneuroendocrinology. 2019;99:128-36.
24. Hammock EA. Developmental perspectives on oxytocin and vasopressin. Neuropsychopharmacology : official publication of the American College of Neuropsychopharmacology. 2015;40(1):24-42.
25. Mitre M, Marlin BJ, Schiavo JK, Morina E, Norden SE, Hackett TA, et al. A Distributed Network for Social Cognition Enriched for Oxytocin Receptors. J Neurosci. 2016;36(8):2517-35.
26. Tyzio R, Cossart R, Khalilov I, Minlebaev M, Hubner CA, Represa A, et al. Maternal oxytocin triggers a transient inhibitory switch in GABA signaling in the fetal brain during delivery. Science. 2006;314(5806):1788-92.
27. Tyzio R, Nardou R, Ferrari DC, Tsintsadze T, Shahrokhi A, Eftekhari S, et al. Oxytocin-mediated GABA inhibition during delivery attenuates autism pathogenesis in rodent offspring. Science. 2014;343(6171):675-9.
28. Leonzino M, Busnelli M, Antonucci F, Verderio C, Mazzanti M, Chini B. The Timing of the Excitatory-to-Inhibitory GABA Switch Is Regulated by the Oxytocin Receptor via KCC2. Cell reports. 2016;15(1):96-103.
29. Banerjee A, Rikhye RV, Breton-Provencher V, Tang X, Li C, Li K, et al. Jointly reduced inhibition and excitation underlies circuit-wide changes in cortical processing in Rett syndrome. Proc Natl Acad Sci U S A. 2016.
30. Zheng JJ, Li SJ, Zhang XD, Miao WY, Zhang D, Yao H, et al. Oxytocin mediates early experience-dependent cross-modal plasticity in the sensory cortices. Nat Neurosci. 2014;17(3):391-9.
31. Maldonado P, Nuno-Perez, A., Kirchner, J., Hammock, E., Gjorgjieva, J. and Lohmann, C. . Oxytocin shapes spontaneous activity patterns in the developing visual cortex by activating somatostatin interneurons. bioRxiv. 2020.
32. Tirko NN, Eyring KW, Carcea I, Mitre M, Chao MV, Froemke RC, et al. Oxytocin Transforms Firing Mode of CA2 Hippocampal Neurons. Neuron. 2018;100(3):593-608 e3.
33. Ripamonti S, Ambrozkiewicz MC, Guzzi F, Gravati M, Biella G, Bormuth I, et al. Transient oxytocin signaling primes the development and function of excitatory hippocampal neurons. eLife. 2017;6.
34. Boccaccio I, Glatt-Deeley H, Watrin F, Roeckel N, Lalande M, Muscatelli F. The human MAGEL2 gene and its mouse homologue are paternally expressed and mapped to the Prader-Willi region. Hum Mol Genet. 1999;8(13):2497-505.
35. Schaaf CP, Gonzalez-Garay ML, Xia F, Potocki L, Gripp KW, Zhang B, et al. Truncating mutations of MAGEL2 cause Prader-Willi phenotypes and autism. Nat Genet. 2013.
36. Fountain MD, Schaaf CP. Prader-Willi Syndrome and Schaaf-Yang Syndrome: Neurodevelopmental Diseases Intersecting at the MAGEL2 Gene. Diseases. 2016;4(1).
37. Schaller F, Watrin F, Sturny R, Massacrier A, Szepetowski P, Muscatelli F. A single postnatal injection of oxytocin rescues the lethal feeding behaviour in mouse newborns deficient for the imprinted Magel2 gene. Hum Mol Genet. 2010;19(24):4895-905.
38. Meziane H, Schaller F, Bauer S, Villard C, Matarazzo V, Riet F, et al. An Early Postnatal Oxytocin Treatment Prevents Social and Learning Deficits in Adult Mice Deficient for Magel2, a Gene Involved in Prader-Willi Syndrome and Autism. Biol Psychiatry. 2015;78(2):85-94.
39. Fountain MD, Aten E, Cho MT, Juusola J, Walkiewicz MA, Ray JW, et al. The phenotypic spectrum of Schaaf-Yang syndrome: 18 new affected individuals from 14 families. Genet Med. 2017;19(1):45-52.

bioRxiv preprint doi: https://doi.org/10.1101/2020.09.21.306217; this version posted September 21, 2020. The copyright holder for this preprint (which was not certified by peer review) is the author/funder, who has granted bioRxiv a license to display the preprint in perpetuity. It is made available under aCC-BY-NC-ND 4.0 International license.

40. Dai YC, Zhang HF, Schon M, Bockers TM, Han SP, Han JS, et al. Neonatal Oxytocin Treatment Ameliorates Autistic-Like Behaviors and Oxytocin Deficiency in Valproic Acid-Induced Rat Model of Autism. Frontiers in cellular neuroscience. 2018;12:355.
41. Penagarikano O, Lazaro MT, Lu XH, Gordon A, Dong H, Lam HA, et al. Exogenous and evoked oxytocin restores social behavior in the Cntnap2 mouse model of autism. Science translational medicine. 2015;7(271):271ra8.
42. Francis SM, Sagar A, Levin-Decanini T, Liu W, Carter CS, Jacob S. Oxytocin and vasopressin systems in genetic syndromes and neurodevelopmental disorders. Brain Res. 2014.
43. Mansouri M, Pouretemad H, Roghani M, Wegener G, Ardalan M. Autistic-Like Behaviours and Associated Brain Structural Plasticity are Modulated by Oxytocin in Maternally Separated Rats. Behav Brain Res. 2020:112756.
44. Tauber M, Boulanouar K, Diene G, Cabal-Berthoumieu S, Ehlinger V, Fichaux-Bourin P, et al. The Use of Oxytocin to Improve Feeding and Social Skills in Infants With Prader-Willi Syndrome. Pediatrics. 2017.
45. Matarazzo V, Muscatelli F. Natural breaking of the maternal silence at the mouse and human imprinted Prader-Willi locus: A whisper with functional consequences. Rare diseases. 2013;1:e27228.
46. Zhang JB, Chen L, Lv ZM, Niu XY, Shao CC, Zhang C, et al. Oxytocin is implicated in social memory deficits induced by early sensory deprivation in mice. Molecular brain. 2016;9(1):98.
47. Karlsson SA, Haziri K, Hansson E, Kettunen P, Westberg L. Effects of sex and gonadectomy on social investigation and social recognition in mice. BMC neuroscience. 2015;16:83.
48. Ben-Ari Y. Is birth a critical period in the pathogenesis of autism spectrum disorders? Nat Rev Neurosci. 2015;16(8):498-505.
49. Tyzio R, Minlebaev M, Rheims S, Ivanov A, Jorquera I, Holmes GL, et al. Postnatal changes in somatic gamma-aminobutyric acid signalling in the rat hippocampus. Eur J Neurosci. 2008;27(10):2515-28.
50. Zhang J, Cordshagen A, Medina I, Nothwang HG, Wisniewski JR, Winklhofer M, et al. Staurosporine and NEM mainly impair WNK-SPAK/OSR1 mediated phosphorylation of KCC2 and NKCC1. PLoS One. 2020;15(5):e0232967.
51. Kahle KT, Merner ND, Friedel P, Silayeva L, Liang B, Khanna A, et al. Genetically encoded impairment of neuronal KCC2 cotransporter function in human idiopathic generalized epilepsy. EMBO Rep. 2014;15(7):766-74.
52. Friedel P, Kahle KT, Zhang J, Hertz N, Pisella LI, Buhler E, et al. WNK1-regulated inhibitory phosphorylation of the KCC2 cotransporter maintains the depolarizing action of GABA in immature neurons. Sci Signal. 2015;8(383):ra65.
53. de Los Heros P, Alessi DR, Gourlay R, Campbell DG, Deak M, Macartney TJ, et al. The WNK-regulated SPAK/OSR1 kinases directly phosphorylate and inhibit the K+-Cl- co-transporters. Biochem J. 2014;458(3):559-73.
54. Lee HH, Deeb TZ, Walker JA, Davies PA, Moss SJ. NMDA receptor activity downregulates KCC2 resulting in depolarizing GABAA receptor-mediated currents. Nat Neurosci. 2011;14(6):736-43.
55. Kalbassi S, Bachmann SO, Cross E, Roberton VH, Baudouin SJ. Male and Female Mice Lacking Neuroligin-3 Modify the Behavior of Their Wild-Type Littermates. eNeuro. 2017;4(4).
56. Ates T, Oncul M, Dilsiz P, Topcu IC, Civas CC, Alp MI, et al. Inactivation of Magel2 suppresses oxytocin neurons through synaptic excitation-inhibition imbalance. Neurobiol Dis. 2019;121:58-64.
57. Tacer KF, Potts PR. Cellular and disease functions of the Prader-Willi Syndrome gene MAGEL2. Biochem J. 2017;474(13):2177-90.
58. Kenkel WM, Perkeybile AM, Yee JR, Pournajafi-Nazarloo H, Lillard TS, Ferguson EF, et al. Behavioral and epigenetic consequences of oxytocin treatment at birth. Sci Adv. 2019;5(5):eaav2244.
59. Kahle KT, Deeb TZ, Puskarjov M, Silayeva L, Liang B, Kaila K, et al. Modulation of neuronal activity by phosphorylation of the K-Cl cotransporter KCC2. Trends Neurosci. 2013;36(12):726-37.
60. Pisella LI, Gaiarsa JL, Diabira D, Zhang J, Khalilov I, Duan J, et al. Impaired regulation of KCC2 phosphorylation leads to neuronal network dysfunction and neurodevelopmental pathology. Sci Signal. 2019;12(603).

bioRxiv preprint doi: https://doi.org/10.1101/2020.09.21.306217; this version posted September 21, 2020. The copyright holder for this preprint (which was not certified by peer review) is the author/funder, who has granted bioRxiv a license to display the preprint in perpetuity. It is made available under aCC-BY-NC-ND 4.0 International license.

61. Ben-Ari Y, Spitzer NC. Nature and nurture in brain development. Trends Neurosci. 2004;27(7):361.
62. Leinekugel X, Khazipov R, Cannon R, Hirase H, Ben-Ari Y, Buzsaki G. Correlated bursts of activity in the neonatal hippocampus in vivo. Science. 2002;296(5575):2049-52.
63. Shi Y, Grieco SF, Holmes TC, Xu X. Development of Local Circuit Connections to Hilar Mossy Cells in the Mouse Dentate Gyrus. eNeuro. 2019;6(2).
64. He Q, Nomura T, Xu J, Contractor A. The Developmental Switch in GABA Polarity Is Delayed in Fragile X Mice. Journal of Neuroscience. 2014;34(2):446-50.
65. Ben-Ari Y. The GABA excitatory/inhibitory developmental sequence: a personal journey. Neuroscience. 2014;279:187-219.
66. Kang E, Song J, Lin Y, Park J, Lee JH, Hussani Q, et al. Interplay between a Mental Disorder Risk Gene and Developmental Polarity Switch of GABA Action Leads to Excitation-Inhibition Imbalance. Cell reports. 2019;28(6):1419-28 e3.
67. Sohal VS, Rubenstein JLR. Excitation-inhibition balance as a framework for investigating mechanisms in neuropsychiatric disorders. Mol Psychiatry. 2019;24(9):1248-57.
68. Harrington AJ, Raissi A, Rajkovich K, Berto S, Kumar J, Molinaro G, et al. MEF2C regulates cortical inhibitory and excitatory synapses and behaviors relevant to neurodevelopmental disorders. eLife. 2016;5.
69. Tabuchi K, Blundell J, Etherton MR, Hammer RE, Liu X, Powell CM, et al. A neuroligin-3 mutation implicated in autism increases inhibitory synaptic transmission in mice. Science. 2007;318(5847):71-6.
70. Unichenko P, Yang JW, Kirischuk S, Kolbaev S, Kilb W, Hammer M, et al. Autism Related Neuroligin-4 Knockout Impairs Intracortical Processing but not Sensory Inputs in Mouse Barrel Cortex. Cerebral cortex. 2017:1-14.
71. Wood L, Shepherd GM. Synaptic circuit abnormalities of motor-frontal layer 2/3 pyramidal neurons in a mutant mouse model of Rett syndrome. Neurobiol Dis. 2010;38(2):281-7.
72. Carter CS. Developmental consequences of oxytocin. Physiol Behav. 2003;79(3):383-97.
73. Perez SM, Boley A, Lodge DJ. Region specific knockdown of Parvalbumin or Somatostatin produces neuronal and behavioral deficits consistent with those observed in schizophrenia. Translational psychiatry. 2019;9(1):264.
74. Scheggia D, Manago F, Maltese F, Bruni S, Nigro M, Dautan D, et al. Somatostatin interneurons in the prefrontal cortex control affective state discrimination in mice. Nat Neurosci. 2020;23(1):47-60.
75. Smith C, Kingsbury, M., Dziabis, J., Hanamsagar, R., Malacon, K. Tran,J., Norris, A., Gulino, M. and Bilbo, S. Neonatal immune challenge induces female-specific changes in social behavior and somatostatin cell number, independent of microglial inflammatory signaling bioRxiv. 2020.
76. Kaech S, Banker G. Culturing hippocampal neurons. Nature protocols. 2006;1(5):2406-15.
77. Tyzio R, Ivanov A, Bernard C, Holmes GL, Ben-Ari Y, Khazipov R. Membrane potential of CA3 hippocampal pyramidal cells during postnatal development. J Neurophysiol. 2003;90(5):2964-72.
78. Scorcioni R, Polavaram S, Ascoli GA. L-Measure: a web-accessible tool for the analysis, comparison and search of digital reconstructions of neuronal morphologies. Nature protocols. 2008;3(5):866-76.

bioRxiv preprint doi: https://doi.org/10.1101/2020.09.21.306217; this version posted September 21, 2020. The copyright holder for this preprint (which was not certified by peer review) is the author/funder, who has granted bioRxiv a license to display the preprint in perpetuity. It is made available under aCC-BY-NC-ND 4.0 International license.

LEGENDS

Figure 1: Ultrasonic vocalization calls (USVs) in male and female *Magel2* KO pups (P8) versus WT pups and having been OT-treated or vehicle-treated in neonates.

(**A**) Paradigm of the USVs recordings. Number of total calls, measured during 5 min isolation after pup separation, is indicated in the histograms (B-D). (**B**) Comparison of the number of calls recorded in male (N=14) and female (N=9) *Magel2* KO and WT pups (males N=9; females N=11). (**C**) Effect of the OT-treatment in WT (males N=11; females N=12; in pink) and in *Magel2* KO pups (males N=24; females N=21; in green) versus vehicle-treated WT (males N=11; females N=13; in blue) and vehicle-treated *Magel2* KO (males N=18; females N=13; in orange). Histograms indicate the median (Q2) and quartiles (Q1,Q3) with scattered plots that show individual data points. (B) Mann-Whitney test, (C) One-way ANOVA + Dunnett's *post hoc* test. *P<0.05, **P<0.01
Statistical analysis is reported in Table 1.

Figure 2: Social behavior in three-chamber test of male *Magel2* KO adult versus WT adults and having been OT-treated or vehicle-treated in neonates.

(**A**) Paradigm of the three-chamber test. Sniffing time between mice is measured in each test. (**B**) WT males (N=9) show normal behavior in all the steps of the test; *Magel2* KO males (N=9) show a significant impairment in short term social memory. (**C**) WT mice were treated in the first week of life with vehicle or OT and then tested at four months. WT mice treated with vehicle (N=18) or treated with OT (N=10) have similar profiles with significant differences in each step of the test. (**D**) *Magel2* KO mice were treated in the first week of life with vehicle or OT and then tested at four months. *Magel2* KO-vehicle (N=19) mice show a significant difference in the social exploration and social discrimination, but, in short term social memory, they do not show a higher sniffing time with the novel mouse. OT-treated *Magel2* KO (N=19) mice present significant differences in each step of the step. Data represented in histograms report the interaction time (time of sniffing in seconds) as mean ± SEM. Mann-WhitneyTest. *P<0.05, **P<0.01, ***P<0.001.
Statistical analysis is reported in Table 2.

Figure 2-figure supplement 1. Social-index values comparing *Magel2* KO versus WT male mice or *Magel2* KO+OT versus *Magel2* KO-vehicle male.

These indexes report for the social exploration: the sniffing time with S1/ sniffing time with S1 + time in empty room x 100; for the discrimination: the sniffing time with S2/ sniffing time with S1 + sniffing time with S2 time x 100 and for short term memory: the sniffing time with S3/ sniffing time with S1 + sniffing time with S3 time x 100. They are measured in (**A**) *Magel2* KO versus WT mice and (**B**) *Magel2* KO+OT versus Magel2 KO-vehicle. It appears clearly that social exploration and social discrimination are similar between WT and *Magel2* KO (A) and between *Magel2* KO-vehicle and *Magel2* KO+OT (B). Only short memory index is decreased in *Magel2* KO compared with WT and increased in *Magel2* KO+OT compared with *Magel2* KO-vehicle. Data in histograms report social indexes calculated for each individual as mean ± SEM. Mann-Whitney test, *P<0.05.
Statistical analysis is reported in Table S2-1.

Figure 2-figure supplement 2. Social behavior in three-chamber test of female *Magel2* KO adults versus WT adults.

bioRxiv preprint doi: https://doi.org/10.1101/2020.09.21.306217; this version posted September 21, 2020. The copyright holder for this preprint (which was not certified by peer review) is the author/funder, who has granted bioRxiv a license to display the preprint in perpetuity. It is made available under aCC-BY-NC-ND 4.0 International license.

(**A**) Paradigm of the three-chamber test. Sniffing time between mice is measured in each test. (**B**) WT (N=11) females do present differences in social exploration but do not present significant differences in social discrimination and short-term social memory, suggesting that the three-chamber test is not relevant to assess the social behavior in females. Similarly, *Magel2* KO (N=9) females do not present significant differences in all three steps of the paradigm. Data in histograms report interaction time (time of sniffing in seconds) as mean ± SEM. Mann-Whitney test, *P<0.05.
Statistical analysis is reported in Table S2-2.

Figure 2-figure supplement 3. Behavioral tests in male and female WT mice having been OT-treated or vehicle-treated in neonates.

Behavioral analysis of male and female OT-treated versus vehicle-treated WT mice. (**A**) Novel object recognition (NOR) test allows to assess the non-social memory. Training simply involves visual exploration of two identical objects, while after one hour the test session involves replacing one of the previously explored objects with a novel object. Because mice have an innate preference for novelty, a mouse that remembers the familiar object (same object) will spend more time exploring the novel object (new object) conducting to a discrimination index significantly different from 50%. A similar discrimination index is observed in vehicle or OT-treated WT males and females. (**B**) Open field (OF) test measures locomotor activity and vertical activity (rearing) and anxiety-related behavior (time in zones and grooming): no significant differences have been detected in all those activities between OT-treated and vehicle-treated WT mice but WT+OT females present an approximately 15% reduction in the moved distance and a tendency to increase rearing. (**C**) Elevated Plus Maze (EPM) test allows to measure anxiety (time spent in open arms and number of entries in open arms) and shows a similar behavior with a tendency to spend more time and enter more often in open arms in WT+OT males, suggesting an anxiolytic effect of OT. Data in histograms report mean ± SEM. Mann-Whitney test, * P<0.05.
Statistical analysis is reported in Table S2-3.

Figure 3: cFos activity in aCA2/CA3d and aDG regions of *Magel2* KO and WT male mice following the social memory task in the three-chamber test.

(**A**) Paradigm of the three-chamber test (+SI) followed 90 min later by dissection of the brains and immunohistochemistery experiments. Control mice (-SI) were not tested in the three-chamber test. (**B-C**) cFos-immunolabeling on coronal brain sections in the aCA2/CA3d and aDG regions as indicated in (**B**) of WT-SI, WT+SI and *Magel2* KO+SI mice (**C**). (**D-E**) Quantification of cFos+ cells/section in WT-SI (n=18, N=3), WT+SI (n=24, N=4) and *Magel2* KO+SI (n=24, N=4) in the aCA2/CA3d region (**D**) and in the aDG region (**E**). N: number of animals, n: number of sections/hippocampus. Scale bar: 500µm (B); 100µm (C).
Data represented in box and whisker-plots report the number of cFos + cells by sections (6 sections/ hippocampus) with the median (Q2) and quartiles (Q1, Q3) for the genotype and treatment. One-way ANOVA + Dunnett's *post hoc* test, ***P<0.001.
Statistical analysis is reported in Table 3.

Figure 4: **Expression of *Magel2* and *Oxytocin receptor* (Oxtr) transcripts in hippocampus of wild-type male mice at P7 and P21.**

(**A**) Representative image obtained by RNAscope technology showing the respective localization of *Magel2* (blue) and *Oxtr* (pink) transcripts in dentate gyrus (DG) and aCA2/CA3d

bioRxiv preprint doi: https://doi.org/10.1101/2020.09.21.306217; this version posted September 21, 2020. The copyright holder for this preprint (which was not certified by peer review) is the author/funder, who has granted bioRxiv a license to display the preprint in perpetuity. It is made available under aCC-BY-NC-ND 4.0 International license.

region of hippocampus. (**B**) Heatmap of mouse cortex and hippocampus transcriptomic data in Allen Cell types Database (2015 - Allen Institute) indicating the expression of *Magel2, Oxtr, Avpr1a, Gad1, Slc17A7, Cck, Sst, Pvalb, Calb1* and *Vip* transcripts. *Magel2* and *Oxtr* are expressed in glutamatergic (*Slc17A7+)* neurons of the CA3 region. *Oxtr* transcripts are also present in GABAergic (Gad1+) interneurons expressing *Sst, Pvalb, Calb1*. (**C**) Representative image obtained by RNAscope technique showing the respective localization of *Sst* (blue) and *Oxtr* (pink) transcripts in the aCA2/CA3 region from hippocampal slices of WT male pups at P10. Arrows indicate colocalization of both transcripts in the same cell. Scale bar: 100µm.

Figure 5: Quantification of OT binding sites by brain autoradiography in *Magel2* KO male mice treated with OT or vehicle versus WT-vehicle male mice.

(**A-C-E**) Representative sections of autoradiographic labeling of OT binding sites displayed in grayscale, showing the regions of interest (ROI) selected for analysis: (**A**) anterior CA2/CA3 (aCA2/CA3), (**C**) dentate gyrus (aDG) and (**E**) ventral CA1/CA2/CA3 (vCA1/CA2/CA3) regions of hippocampus. (**B-D-F**) Quantification of OT binding sites expressed as nCi/mg of tissue equivalent in (**B**) anterior CA2/CA3, (**D**) dentate gyrus and (**F**) ventral CA1/CA2/CA3 regions of hippocampus. Histograms report median (Q2) and quartiles (Q1, Q3). OT binding sites in nCi/mg of tissue equivalent. 3 (N) mice and 6 (n) hippocampi have been analyzed for each group. Data represented in box and whisker-plots report the quantity of radiolabeling by hippocampus, with scattered plots that show individual data points. One-way ANOVA + Bonferroni *post hoc* test, **P<0.01, ****P<0.0001. Scale Bar: 3 mm.
Statistical analysis is reported in Table 5.

Figure 6: Quantification of somatostatin (SST) immunopositive cells in the anterior hippocampus region of *Magel2* KO adult mice having or not been treated by OT in the first week of life and compared with WT mice.

(**A-L**) Immunolabeling on coronal hippocampal sections at adulthood in WT (A,C,E) and *Magel2 KO* (B,D,F), and in WT (G,I,K) and *Magel2 KO*+OT (H,J,L) with a magnification in the aCA2/CA3d region (C,D,I,J) and in the DG region (E,F,K,L) in which the SST+ cells are counted. (**M-P**) Number of SST+ cells by section in both aCA2/CA3d (M,O) and aDG (N,P) and comparing WT (N=4, n= 48) with *Magel2* KO (N=4, n=48) animals (M,N) or WT (N=3, n=36) with *Magel2* OT+ (N=5, n=56) (O,P) mice. N: number of animals, n: number of sections/hippocampus. Data represented in whisker-plots report the number of SST+ cells by section with Q2(Q1, Q3), with scattered plots showing individual data points. Mann-Whitney Test **P<0.01, ***P<0.001. Scale bar (A-H): 500 µm; (C-L): 100 µm.
Statistical analysis is reported in Table 6.

Figure 6-figure supplement 1: Quantification of cFos/SST immunopositive cells and cFos/PV immunopositive cells in the anterior hippocampus region of adult WT mice following a social memory test (+SI).

(**A**) Immunolabelling on coronal hippocampal sections at adulthood in WT showing the cFos/SST+ cells or the cFos/PV+ cells (arrows) in the aCA2/CA3d and aDG regions. (**B**) Quantification of the cFos+ cells among the SST+ cells or PV+ cells in the aCA2/CA3d and aDG regions. Data in the histograms report the percent of cFos+ cells among the SST+ or PV + cells. Counting has been performed on 6 sections of 2 WT+SI mice.

Figure 6-figure supplement 2: Quantification of paravalbumin (PV) immunopositive cells in the anterior hippocampus region of *Magel2* KO adult mice compared with WT mice.

bioRxiv preprint doi: https://doi.org/10.1101/2020.09.21.306217; this version posted September 21, 2020. The copyright holder for this preprint (which was not certified by peer review) is the author/funder, who has granted bioRxiv a license to display the preprint in perpetuity. It is made available under aCC-BY-NC-ND 4.0 International license.

(**A-D**) PV immunolabeling on coronal hippocampal sections at the level of aCA2/CA3d and aDG regions in WT (A-C) and *Magel2 KO* (B-D). (**E-F**) Number of PV+ cells by section in both aCA2/CA3d (E) and aDG (F) and comparing WT (N=4) with *Magel2* KO (N=4) mice (M-N). Scale bar: 100µm. Data represented in whisker-plots report the number of PV+ cells by sections (8 sections/ hippocampus) with Q2(Q1, Q3) for each genotype and scattered plots showing individual data points. Mann-Whitney Test.

Figure 7: Spontaneous Glutamatergic and GABAergic synaptic activity of CA3 pyramidal neurons in the anterior hippocampus region of *Magel2* KO mice versus WT juvenile mice and having been OT-treated or vehicle-treated in neonates.

(**A**) Paradigm of the test. WT or *Magel2 KO* mice have been or not injected with OT in the first week of life then neurons are recorded in brain slices at P25. (**B**) Examples of whole cell recordings performed at a holding potential of -45 mV for each genotype or treatment. The glutamatergic synaptic currents are inwards and the GABAergic synaptic currents are outwards (**C-D**) Values in the different genotypes and treatment of the Glut-sPSCs frequency (C) and amplitude (D). (**E-F**) Values in the different genotypes and treatment of the GABA-sPSCs frequency (E) and amplitude (F). *Magel2* KO (N= 7, n=16), WT (N=7, n=15), *Magel2* KO+OT, (N=5, n=21) and WT+OT (N=4, n=15) have been analyzed, with N: number of mice and n: number of recorded cells. Data represented in whisker-plots report the different values of recorded cells with mean ±SEM, with scattered plots showing individual data points. One-way ANOVA + Tuckey *post hoc* test. *P<0.05, **P<0.01.
Statistical analysis is reported in Table 7.

Figure 7-figure supplement 1. Miniatures Glutamatergic and GABAergic synaptic activitiy of aCA3 pyramidale neurons in the anterior hippocampus region of *Magel2* KO juvenile mice compared with WT.

(**A)** Representative whole-cell recordings of miniature Glutamatergic (inward) and GABAergic (outward) currents (holding potential=-45mV) in juvenile WT and *Magel2* KO aCA3 pyramidal neurons. (**B-E**) The amplitudes (B and D) and frequencies (C and E) of the miniatures glutamatergic (B and C) and GABAergic (D and E) postsynaptic currents. GABAergic frequency (Hz) (WT n=16; *Magel2* KO n=17), GABAergic amplitude (pA) (WT n=16; *Magel2* KO n=17) and glutamatergic frequency (WT n=14; *Magel2* KO n=18) are similar but glutamatergic amplitude (pA) is significantly different. WT (N=5, n=14); *Magel2* KO (N=5, n=18). N: number of mice and n: number of recorded cells. Data represented in histograms are mean ± SEM. Mann Whitney test, ***P< 0.001.
Statistical analysis is reported in Table S7.

Figure 7-figure supplement 2. Morphology of aCA3 recorded pyramidal neurons in *Magel2* KO versus WT mice.

(**A**) Representative distribution of apical and (**B**) basal dendritic complexity obtained with Sholl analysis. (**C**) Quantification of total length of the apical and (**D**) basal dendrites. (**E**) Quantification of the mean number of bifurcations in apical and (**F**) basal dendrites. (**G**) Quantification of the mean number of total branches in apical and (**H**) basal dendrites following 3D reconstructions from CA3 pyramidal neurons recorded in previous experiments (Figure 6). (**I**) Representative WT and *Magel2* KO reconstructed CA3 pyramidal neurons. Histograms indicate Q2(Q1, Q3). Each dot represents a neuron (n). WT (N=3, n=7), *Magel2* KO (N=3, n=11). N: number of mice and n: number of recorded cells. Mann-Whitney test.
Statistical analysis is reported in Table S7.

bioRxiv preprint doi: https://doi.org/10.1101/2020.09.21.306217; this version posted September 21, 2020. The copyright holder for this preprint (which was not certified by peer review) is the author/funder, who has granted bioRxiv a license to display the preprint in perpetuity. It is made available under aCC-BY-NC-ND 4.0 International license.

Figure 8. The excitatory-to-inhibitory developmental GABA-shift in *Magel2* KO versus WT hippocampi and the effect on an OT-treatment.

(**A-B**) GABA-induced Ca^{2+} responses in *Magel2* KO developing hippocampal neuronal cultures versus WT. (**A**) Percentage of WT and *Magel2* KO E18 hippocampal neurons showing GABA-induced Ca^{2+} responses at selected in vitro days (DIV). (**B**) Representative traces of $[Ca^{2+}]i$ variations (delta F340/380) in DIV4 WT and *Magel2* KO neurons upon 100 µM GABA administration. Data are presented in histograms with mean ± SEM; unpaired t test with Welch's correction: ****P<0.0001.

(**C-D**) Average values of the driving force for GABA (DF_{GABA}) of aCA3 pyramidal neurons in *Magel2* KO versus WT mice (C) and, following an OT-treatment, with WT+OT and *Magel2* KO+OT compared with WT (D). (**C**) To reveal a delay of the GABA shift between *Magel2* KO versus WT mice, measures were performed at P1, P7 and P15 using cell-attached recordings of single $GABA_A$ channels. Data are presented in histograms with mean ± SEM; unpaired t test with Welch's correction: *P<0.05. (**D**) To assess the effect of an OT-treatment on the GABA-shift delay, measures were performed at P7. N: number of mice and n: number of recorded cells. One-way ANOVA + Dunnett's *post hoc* test: **P<0.01.:

Statistical analysis is reported in Table 8.

Figure 8-Supplement 1. **Parameters to validate the *in vitro* Calcium imaging analysis and the DF_{GABA} study in *Magel2* KO versus WT mice.**

(**A**) Amplitude of GABA-induced and (**B**) KCl-induced Ca^{2+} peaks in WT and *Magel2* KO E18 neurons at the different DIVs. Number of responsive cells is reported in the bars. Data are from two to five different preparations, 6-8 embryos each preparation (six to fifteen coverslips analyzed).

(**C-F**) Electrophysiological parameters of pyramidal cells (PCs) and interneurons (INs) recorded at P7 in *Magel2* KO versus WT CA3 region of hippocampus. (C) Driving force for GABA (DF_{GABA}) measured with single $GABA_A$ channels in cell-attached mode in INs and PCs. (D) Resting membrane potential (RMP) of INs and PCs measured in whole-cell current-clamp mode. (E) Cell capacitance of recorded neurons. (F) Conductance of the $GABA_A$ channels recorded in cell-attached mode (presented in Figure 8C). Histograms report mean ± SEM. Unpaired t test with Welch's correction: *P<0-05, **P<0.01, ****P<0.0,001.

Statistical analysis is reported in Table S8.

Figure 9. Abundance and phosphorylation state of KCC2 in WT and *Magel2* KO pups (P7).

(**A**) Immunoblot analysis of WT (N=5) and *Magel2* KO (N=6) hippocampi of P7 mice with pan-KCC2 antibody or phosphorylation site-specific antibodies recognizing P-Ser^{940} or P-Thr^{1007} of KCC2. An antibody recognizing neuron-specific ß3 tubulin was used to normalize the quantity of proteins. Numbers on the left indicate molecular weight. (**B**) Boxplots report band intensities from (A) as Q2(Q1,Q3), with scattered plot showing individual data points. Mann-Whitney test, *P<0.05. (**C**) A model of KCC2-dependent control of neuronal Cl^- in *Magel2* KO pups. At this stage of neuronal development, the surface expression of KCC2, that determines its ion-transport activity, depends on the ratio of reciprocal phosphorylation of its Ser^{940} and Thr^{1007} residues. The Ser^{940} phosphorylation increases KCC2's cell surface stability, whereas the Thr^{1007} phosphorylation exerts opposite to Ser^{940} effect and favors internalization (shown with brown arrows). Compared to WT, the CA3 neurons in hippocampi from *Magel2* KO mice are characterized by depolarizing action of GABA (e.g. activation of GABA generates Cl^- efflux) that reflects higher $[Cl^-]_i$. In *Magel2* KO hippocampi the amount of KCC2's Ser^{940}

bioRxiv preprint doi: https://doi.org/10.1101/2020.09.21.306217; this version posted September 21, 2020. The copyright holder for this preprint (which was not certified by peer review) is the author/funder, who has granted bioRxiv a license to display the preprint in perpetuity. It is made available under aCC-BY-NC-ND 4.0 International license.

phosphorylation is significantly lower as compared to WT hippocampi whereas the amount of phosphorylated Thr^{1007} remains unchanged. Respectively, the decreased $P\text{-}Ser^{940}/P\text{-}Thr^{1007}$ ratio results in predominance of KCC2 internalization over surface expression. As consequence of the decreased amount of surface expressed molecules, the Cl^- extrusion ability of KCC2 is decreased that causes increase of $[Cl^-]_i$ and depolarizing shift of GABA.

The model includes also important components that are known to control the level of Ser^{940} and Thr^{1007} phosphorylation. The Ser^{940} is directly phosphorylated by kinase C (pkC) and dephosphorylated under pathology conditions by protein phosphatase type 1 (PP1). The Thr^{1007} is directly phosphorylated by SPAK. It remains to be elucidated whether in *Magel2* KO mice the decreased level of Ser^{940} results from reduction of pkC activity or enhancement of PP1 action.

Statistical analysis is reported in Table 9.

bioRxiv preprint doi: https://doi.org/10.1101/2020.09.21.306217; this version posted September 21, 2020. The copyright holder for this preprint (which was not certified by peer review) is the author/funder, who has granted bioRxiv a license to display the preprint in perpetuity. It is made available under aCC-BY-NC-ND 4.0 International license.

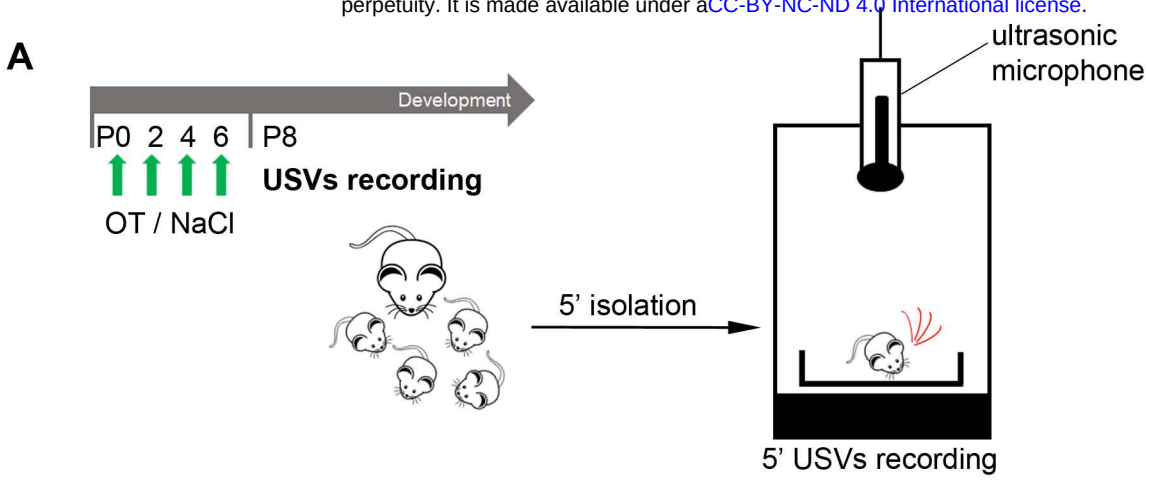

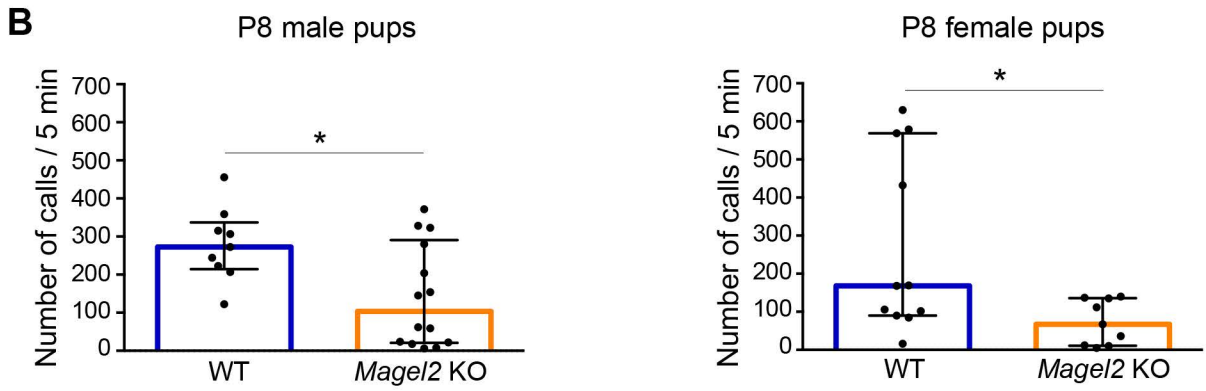

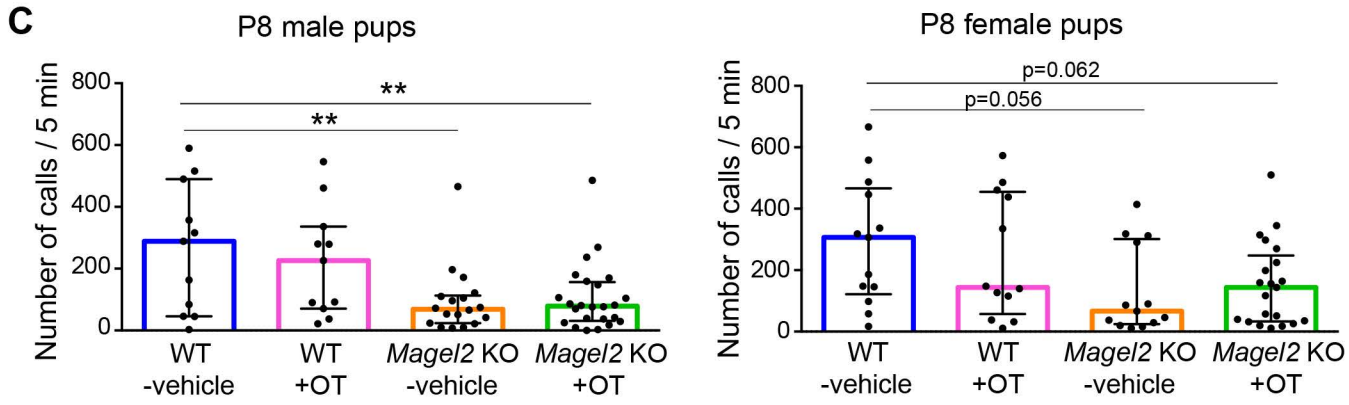

Figure 1.

bioRxiv preprint doi: https://doi.org/10.1101/2020.09.21.306217; this version posted September 21, 2020. The copyright holder for this preprint (which was not certified by peer review) is the author/funder, who has granted bioRxiv a license to display the preprint in perpetuity. It is made available under aCC-BY-NC-ND 4.0 International license.

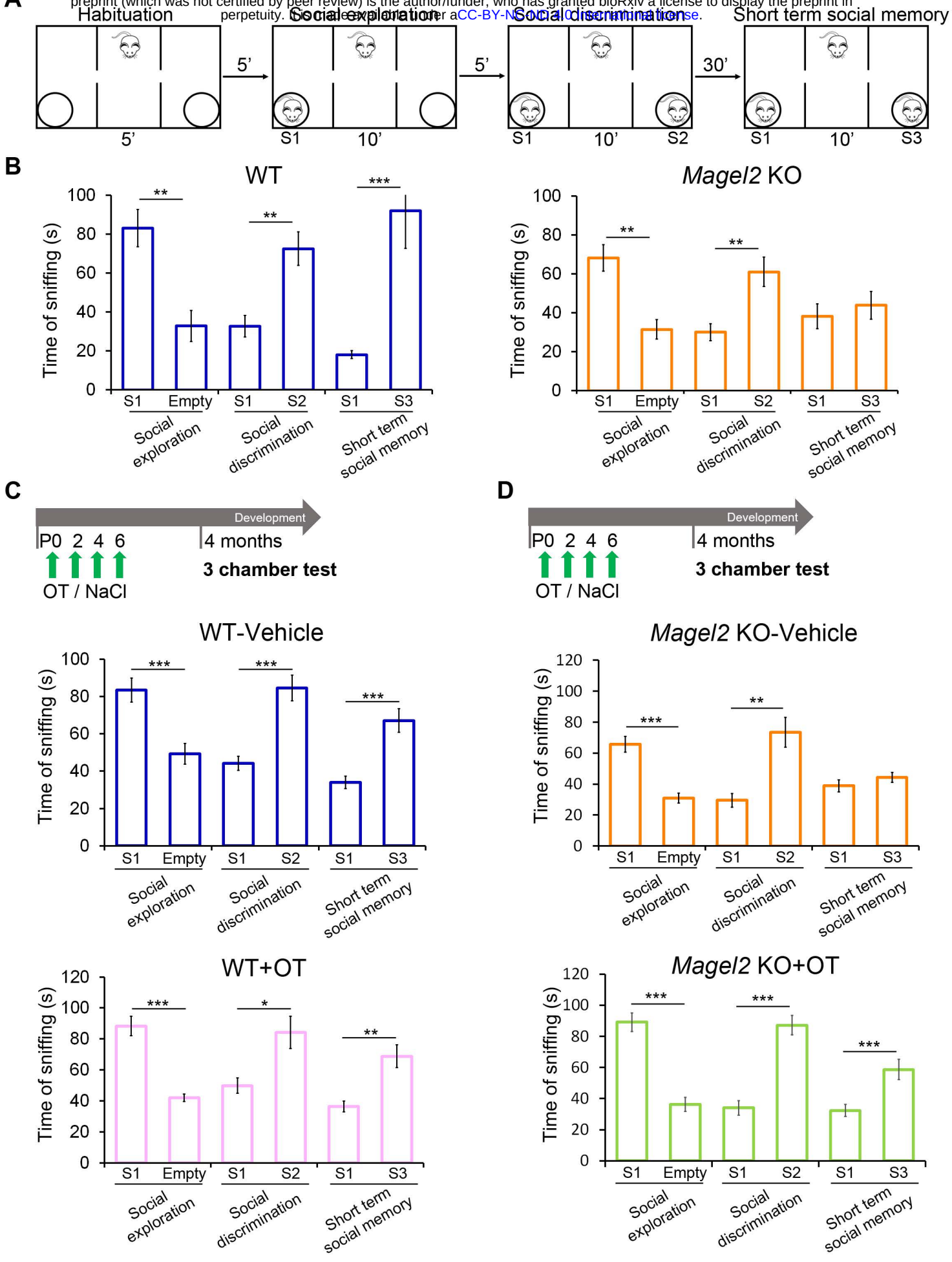

Figure 2.

bioRxiv preprint doi: https://doi.org/10.1101/2020.09.21.306217; this version posted September 21, 2020. The copyright holder for this preprint (which was not certified by peer review) is the author/funder, who has granted bioRxiv a license to display the preprint in perpetuity. It is made available under aCC-BY-NC-ND 4.0 International license.

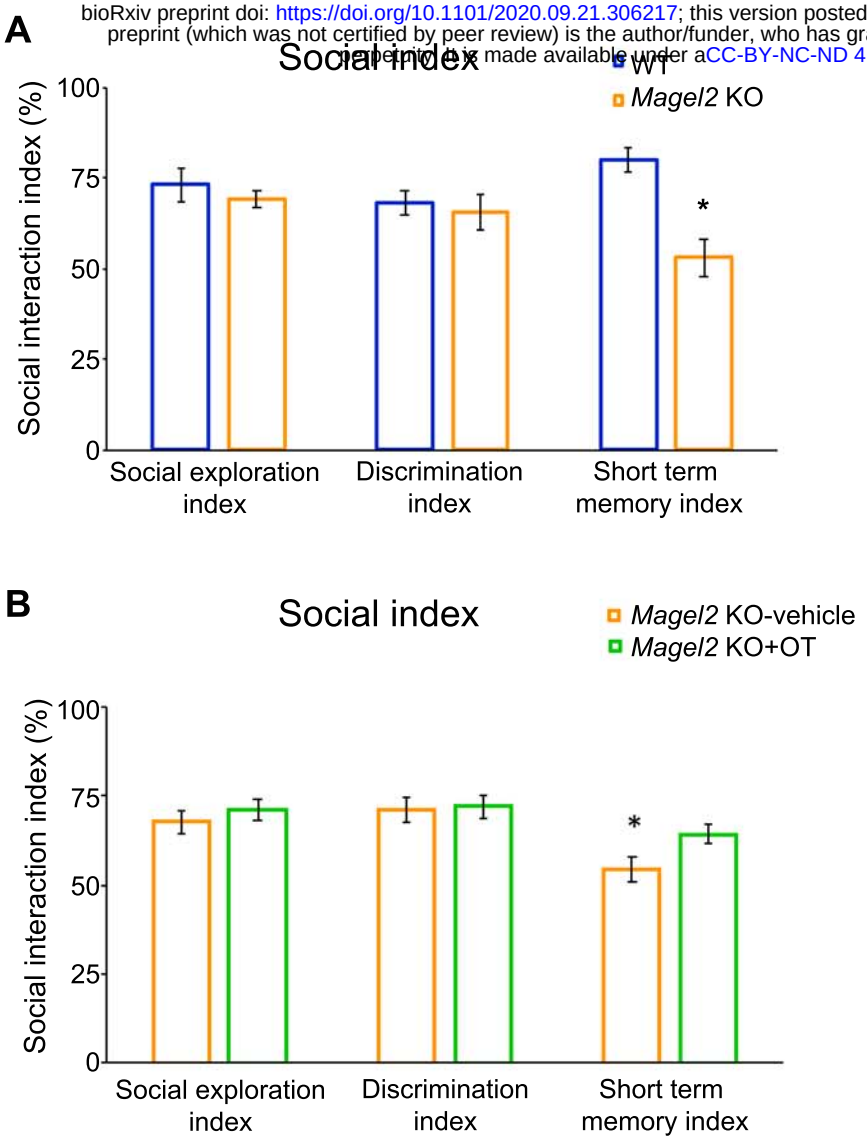

Figure 2 supplement 1.

bioRxiv preprint doi: https://doi.org/10.1101/2020.09.21.306217; this version posted September 21, 2020. The copyright holder for this preprint (which was not certified by peer review) is the author/funder, who has granted bioRxiv a license to display the preprint in perpetuity. It is made available under aCC-BY-NC-ND 4.0 International license.

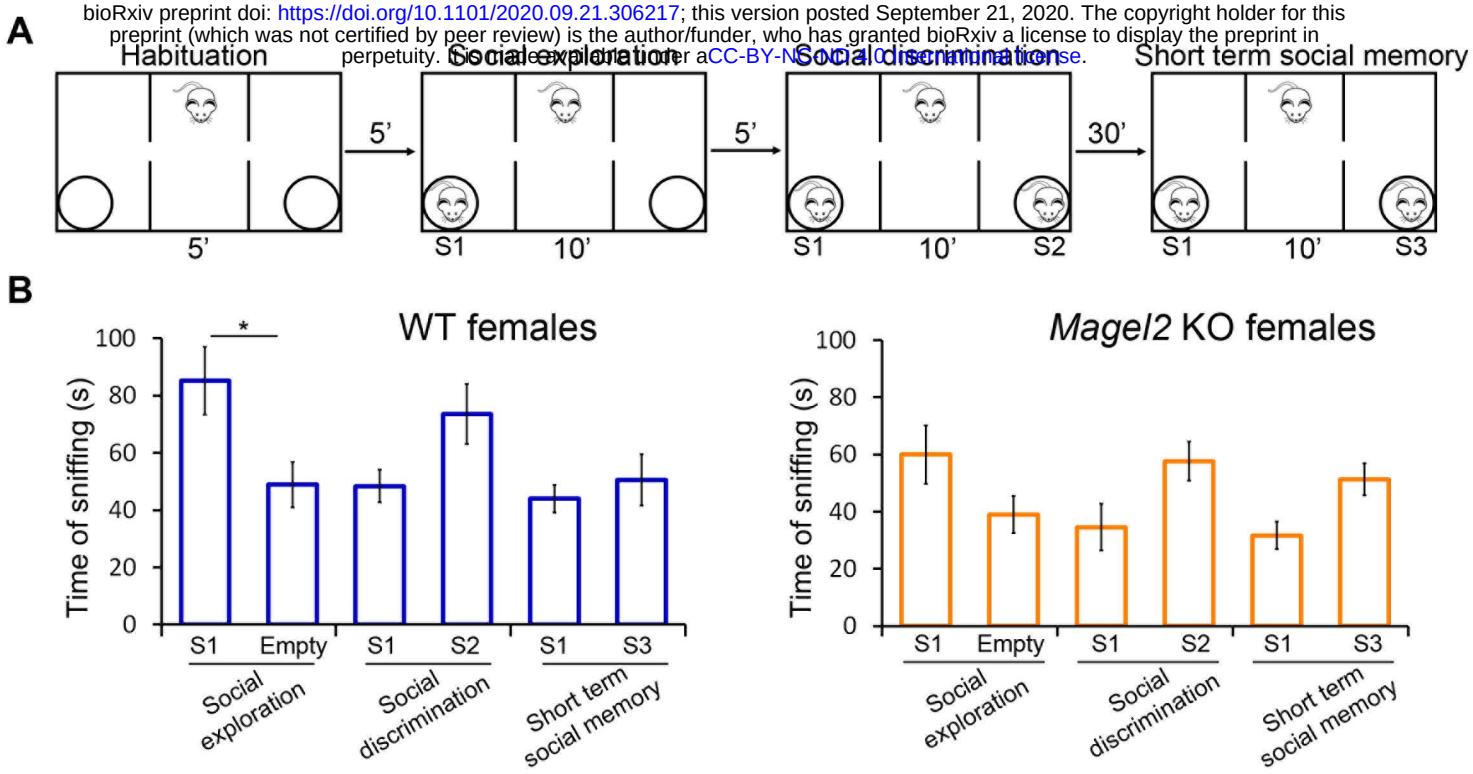

Figure 2 supplement 2.

bioRxiv preprint doi: https://doi.org/10.1101/2020.09.21.306217; this version posted September 21, 2020. The copyright holder for this preprint (which was not certified by peer review) is the author/funder, who has granted bioRxiv a license to display the preprint in perpetuity. It is made available under aCC-BY-NC-ND 4.0 International license.

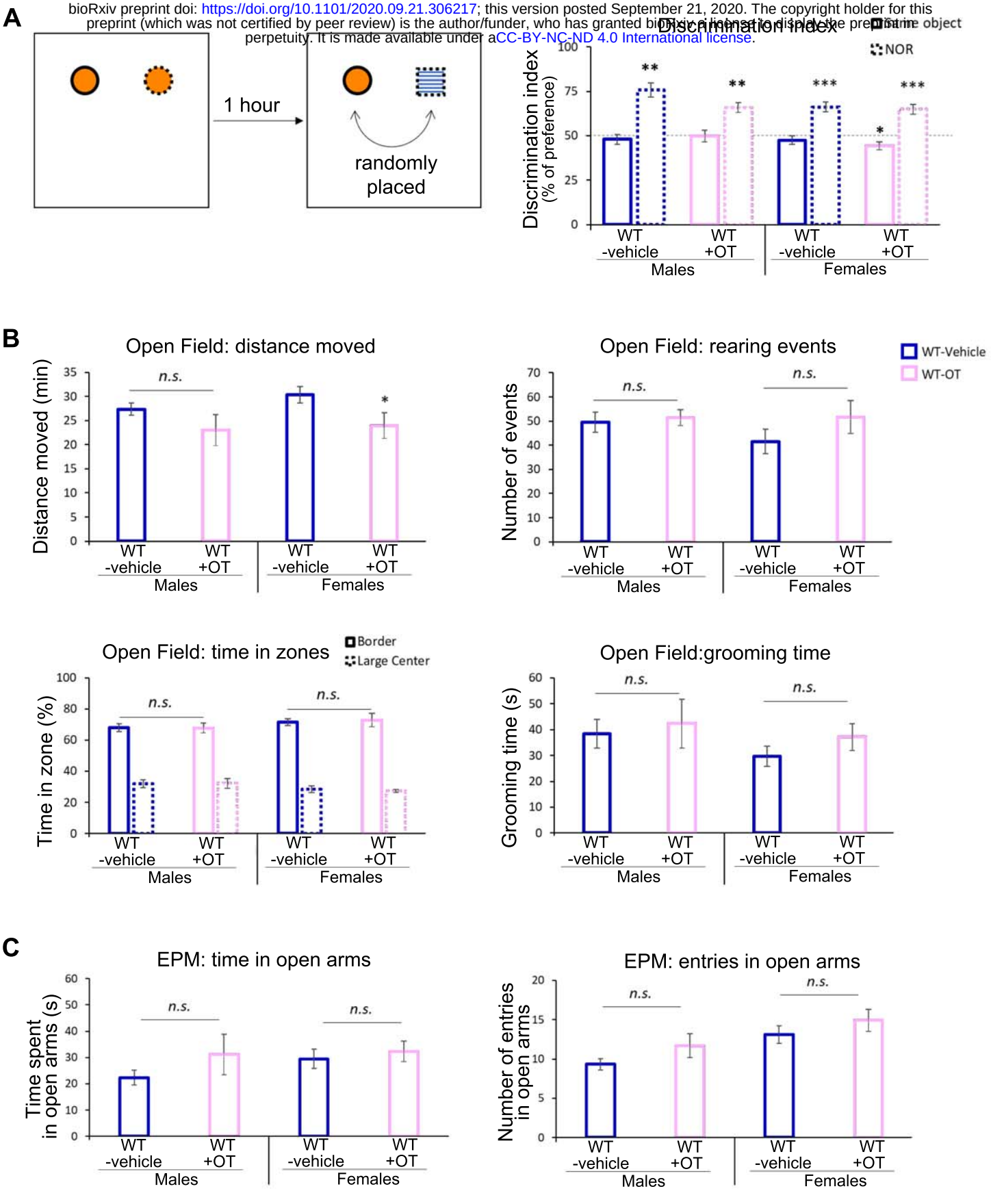

Figure 2 supplement 3.

bioRxiv preprint doi: https://doi.org/10.1101/2020.09.21.306217; this version posted September 21, 2020. The copyright holder for this preprint (which was not certified by peer review) is the author/funder, who has granted bioRxiv a license to display the preprint in perpetuity. It is made available under aCC-BY-NC-ND 4.0 International license.

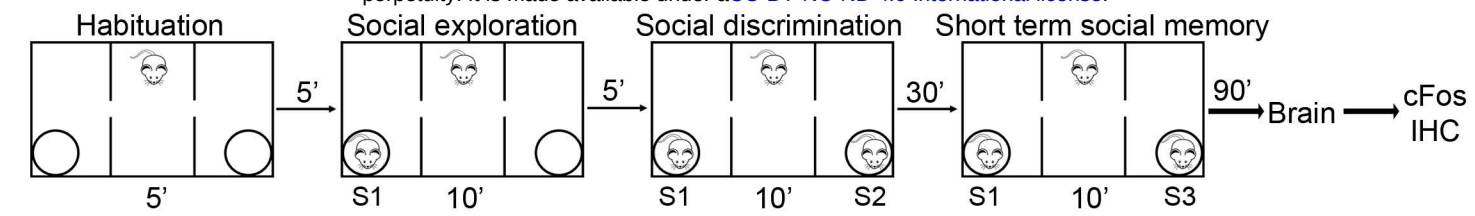

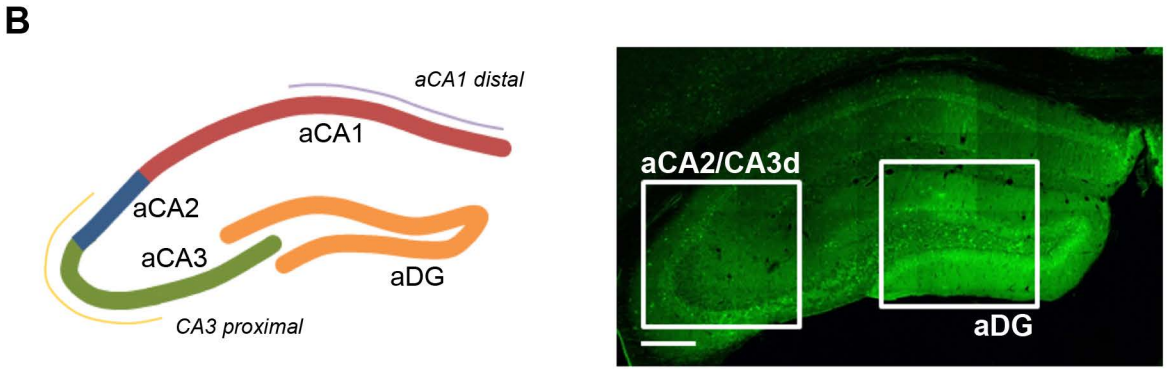

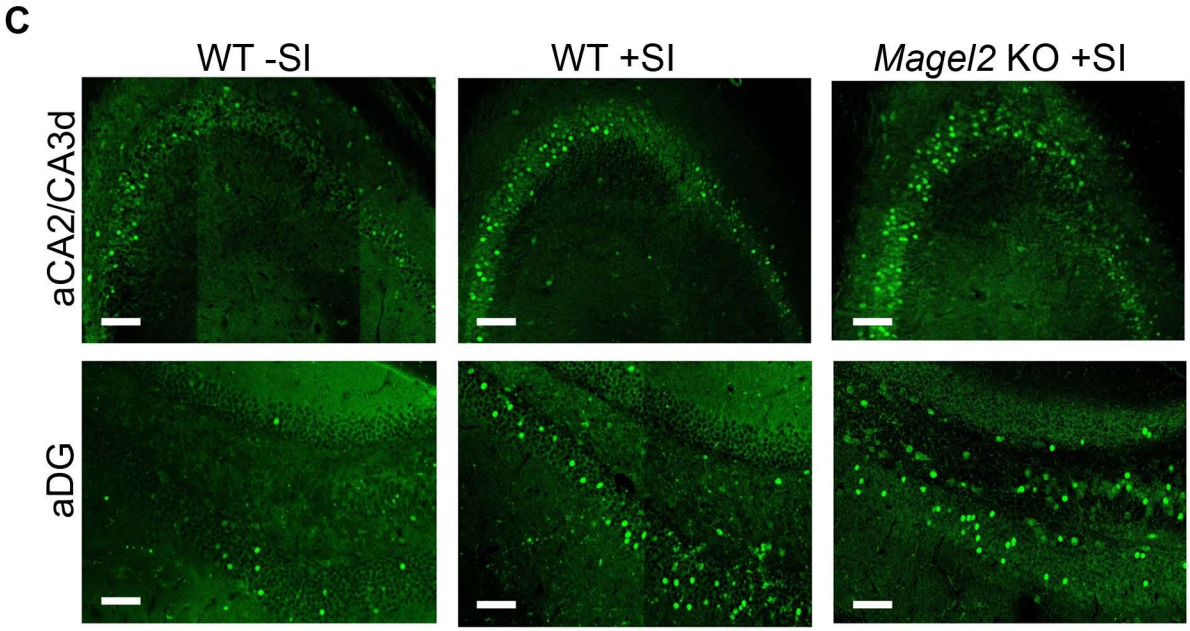

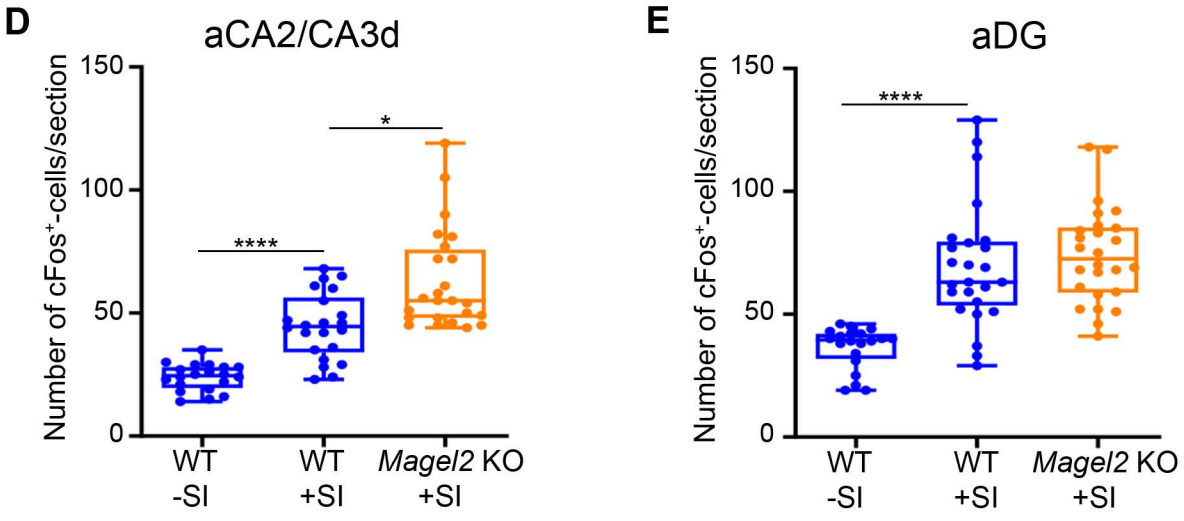

Figure 3.

bioRxiv preprint doi: https://doi.org/10.1101/2020.09.21.306217; this version posted September 21, 2020. The copyright holder for this preprint (which was not certified by peer review) is the author/funder, who has granted bioRxiv a license to display the preprint in perpetuity. It is made available under aCC-BY-NC-ND 4.0 International license.

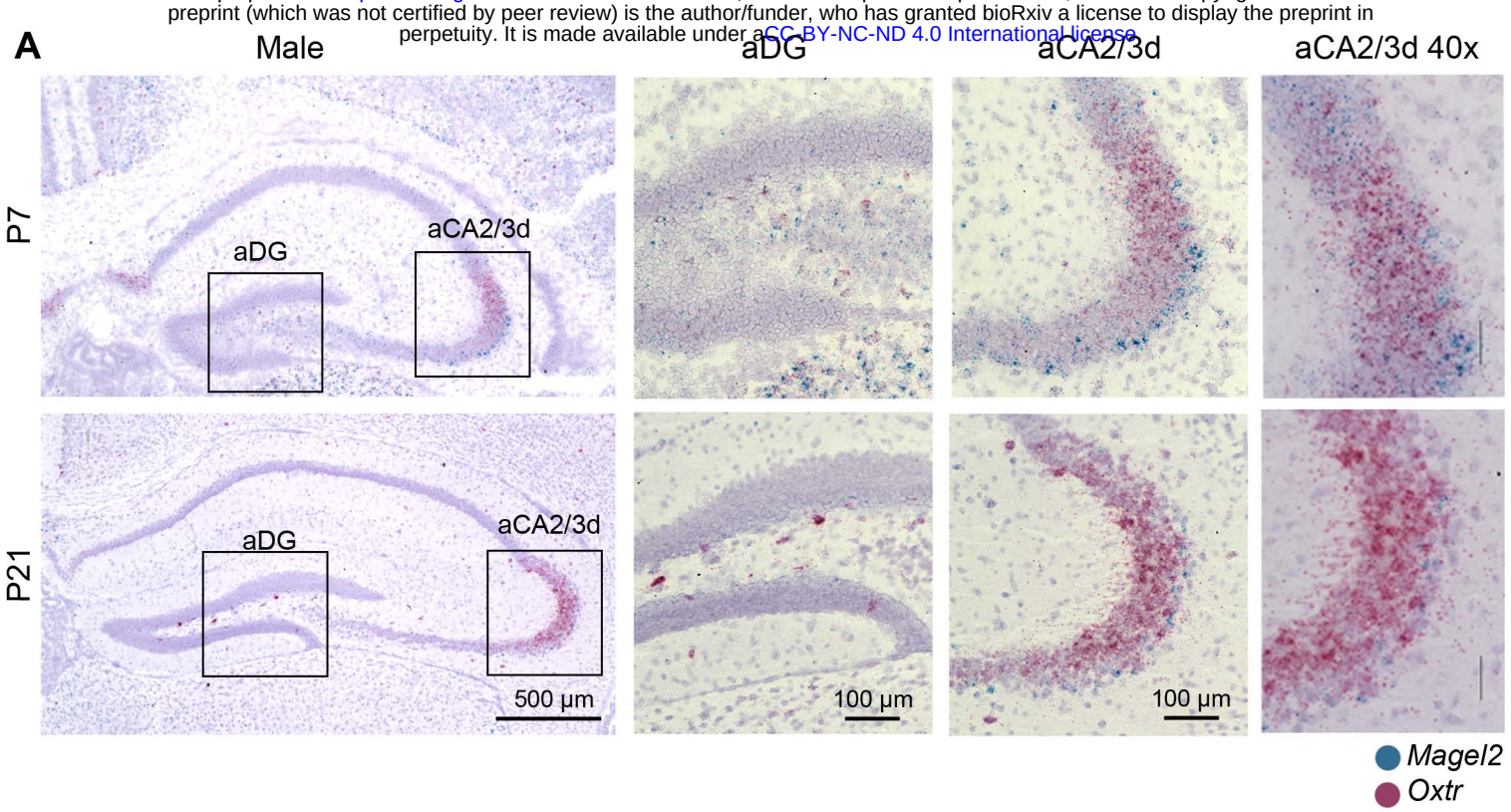

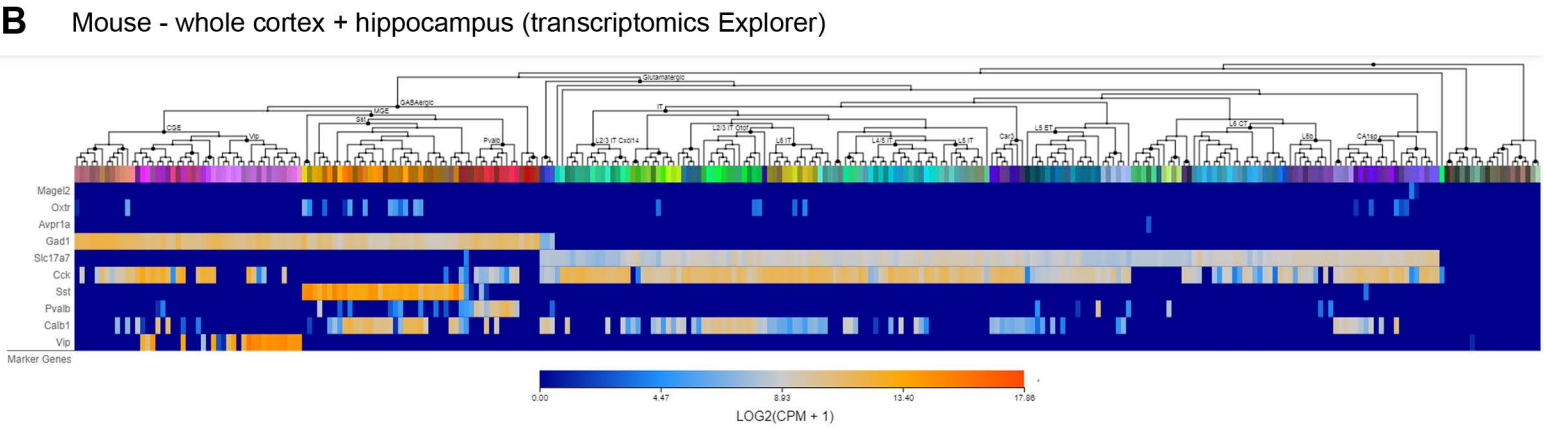

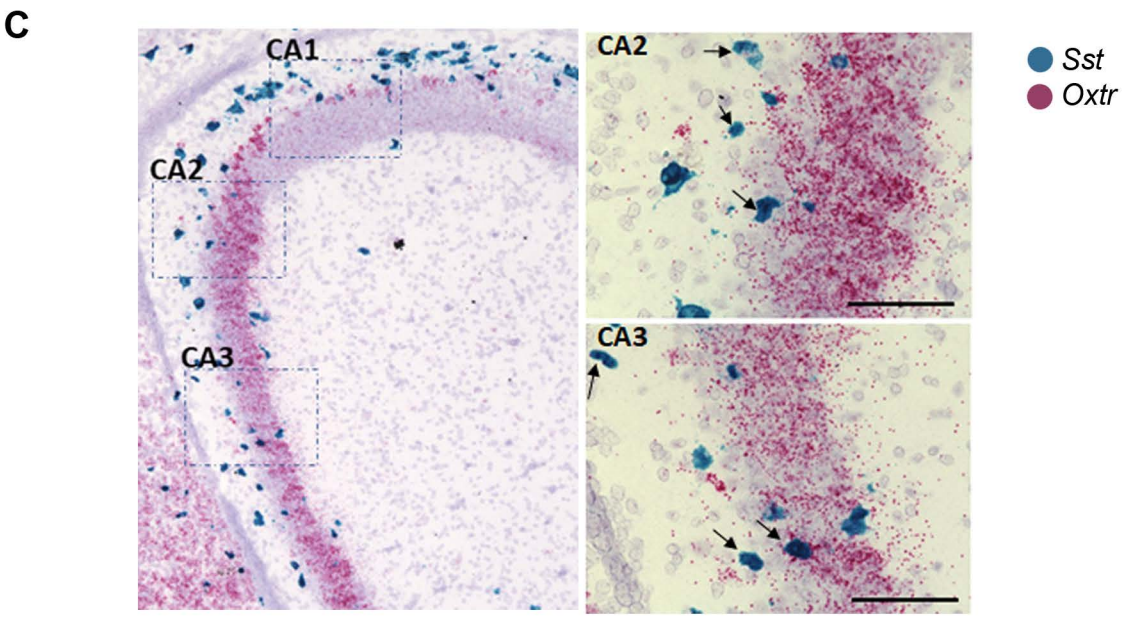

Figure 4.

bioRxiv preprint doi: https://doi.org/10.1101/2020.09.21.306217; this version posted September 21, 2020. The copyright holder for this preprint (which was not certified by peer review) is the author/funder, who has granted bioRxiv a license to display the preprint in perpetuity. It is made available under aCC-BY-NC-ND 4.0 International license.

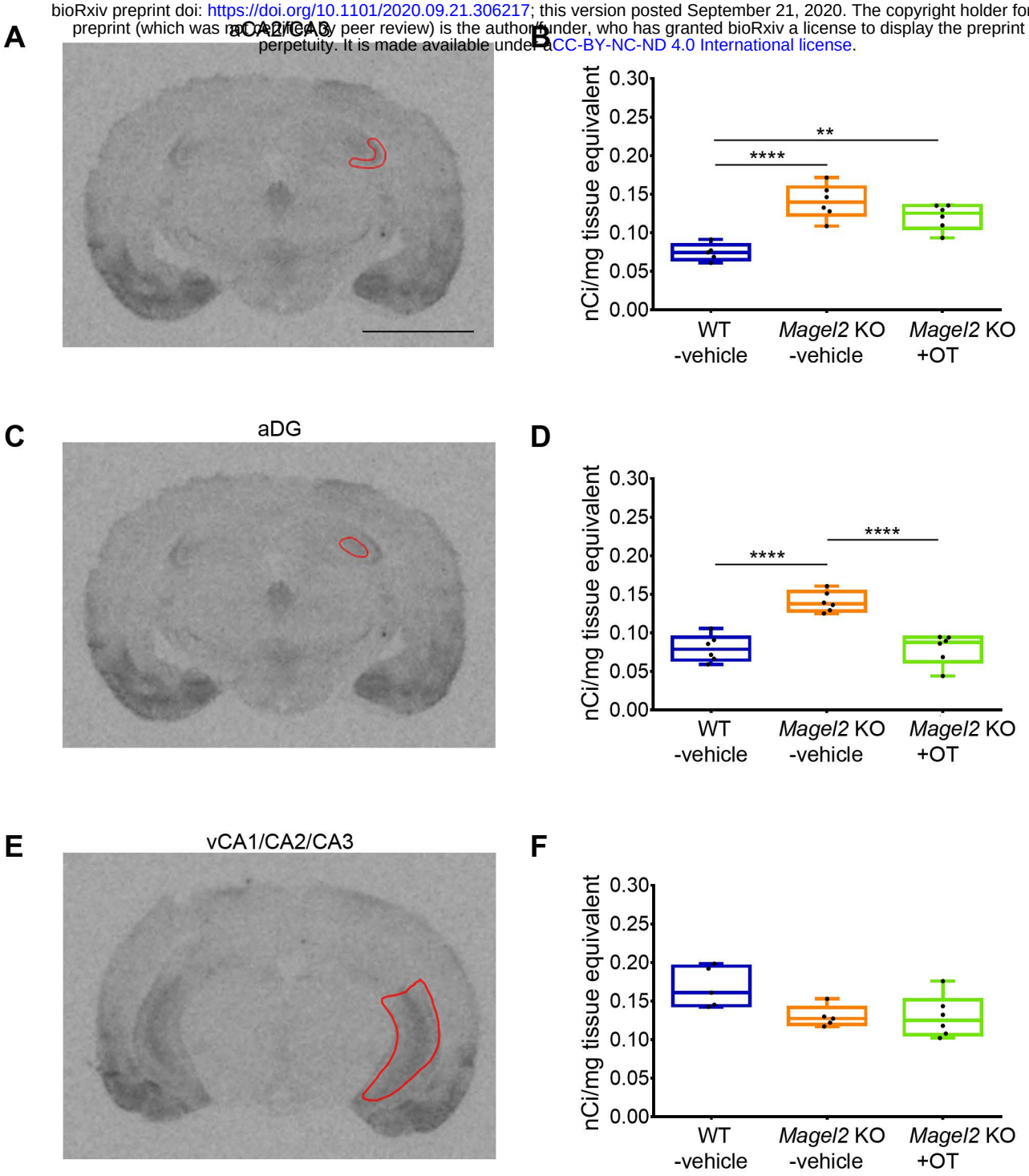

Figure 5.

bioRxiv preprint doi: https://doi.org/10.1101/2020.09.21.306217; this version posted September 21, 2020. The copyright holder for this preprint (which was not certified by peer review) is the author/funder, who has granted bioRxiv a license to display the preprint in perpetuity. It is made available under aCC-BY-NC-ND 4.0 International license.

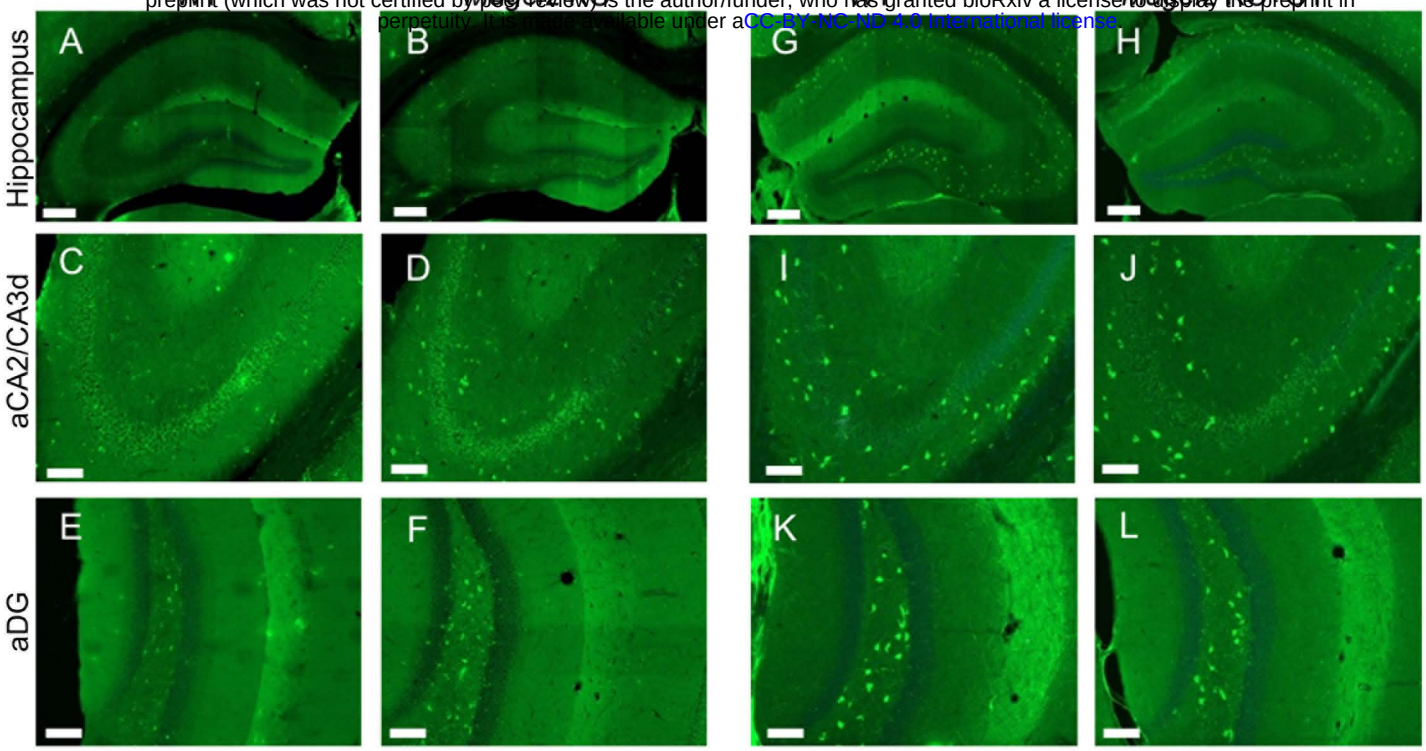

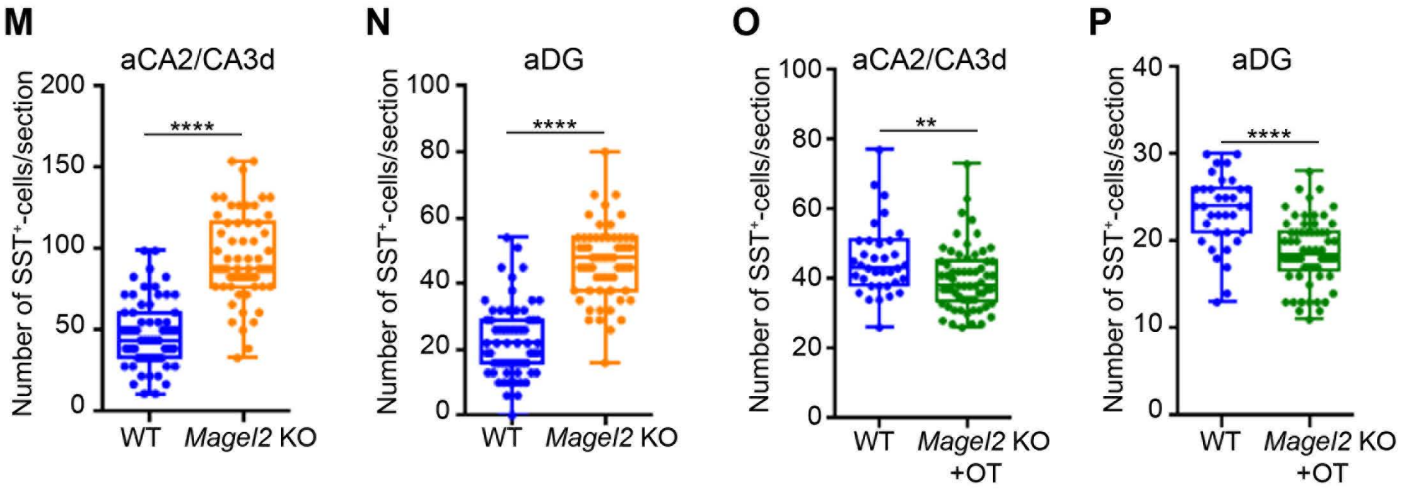

Figure 6.

bioRxiv preprint doi: https://doi.org/10.1101/2020.09.21.306217; this version posted September 21, 2020. The copyright holder for this preprint (which was not certified by peer review) is the author/funder, who has granted bioRxiv a license to display the preprint in perpetuity. It is made available under aCC-BY-NC-ND 4.0 International license.

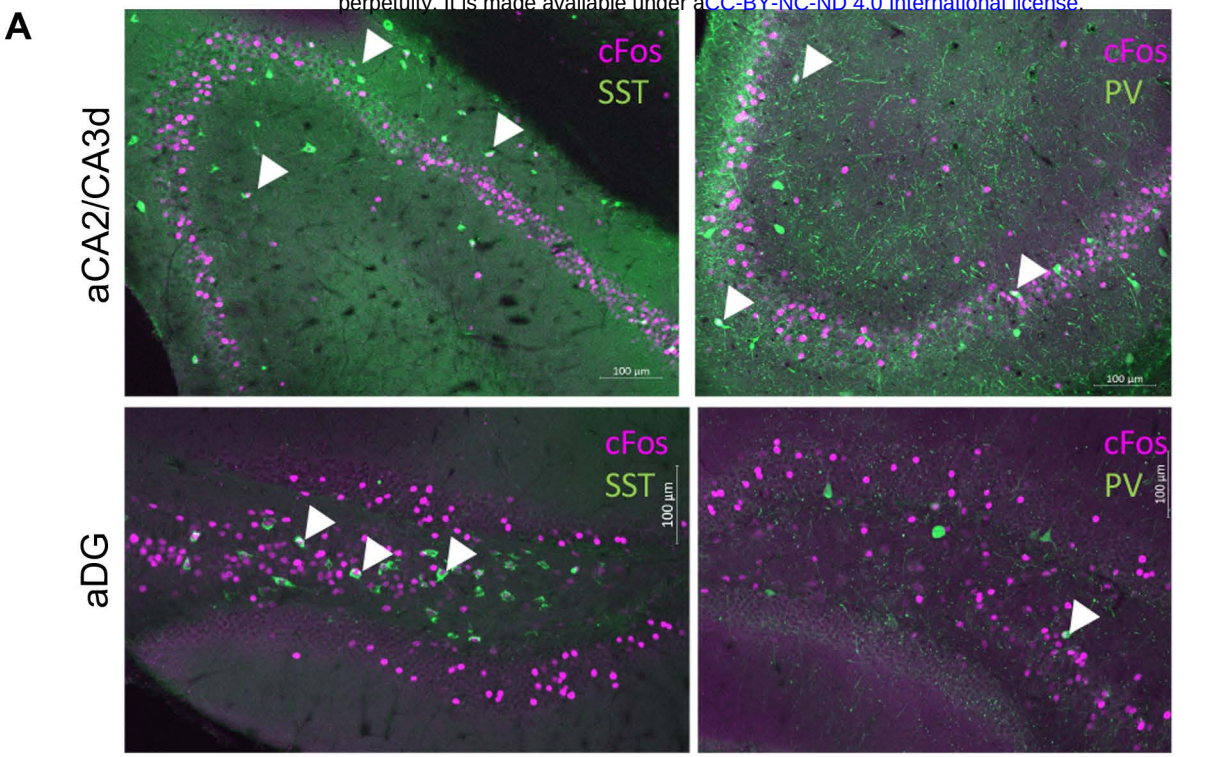

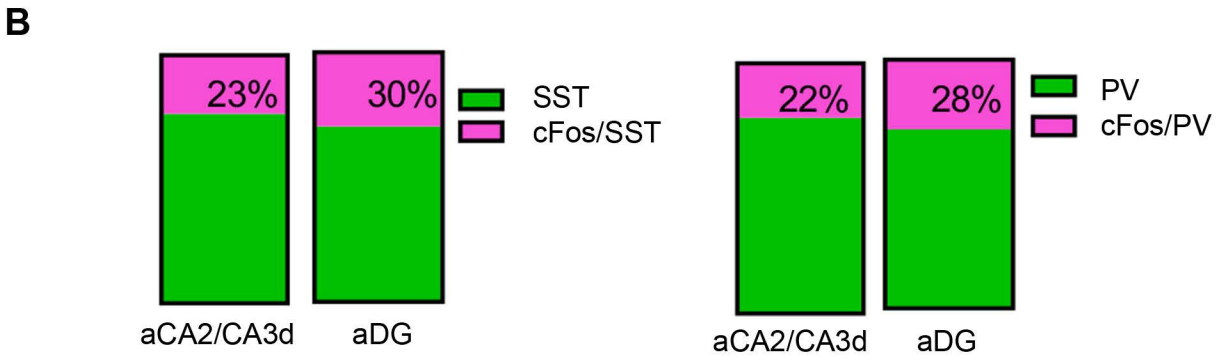

Figure 6 supplement 1.

bioRxiv preprint doi: https://doi.org/10.1101/2020.09.21.306217; this version posted September 21, 2020. The copyright holder for this preprint (which was not certified by peer review) is the author/funder, who has granted bioRxiv a license to display the preprint in perpetuity. It is made available under aCC-BY-NC-ND 4.0 International license.

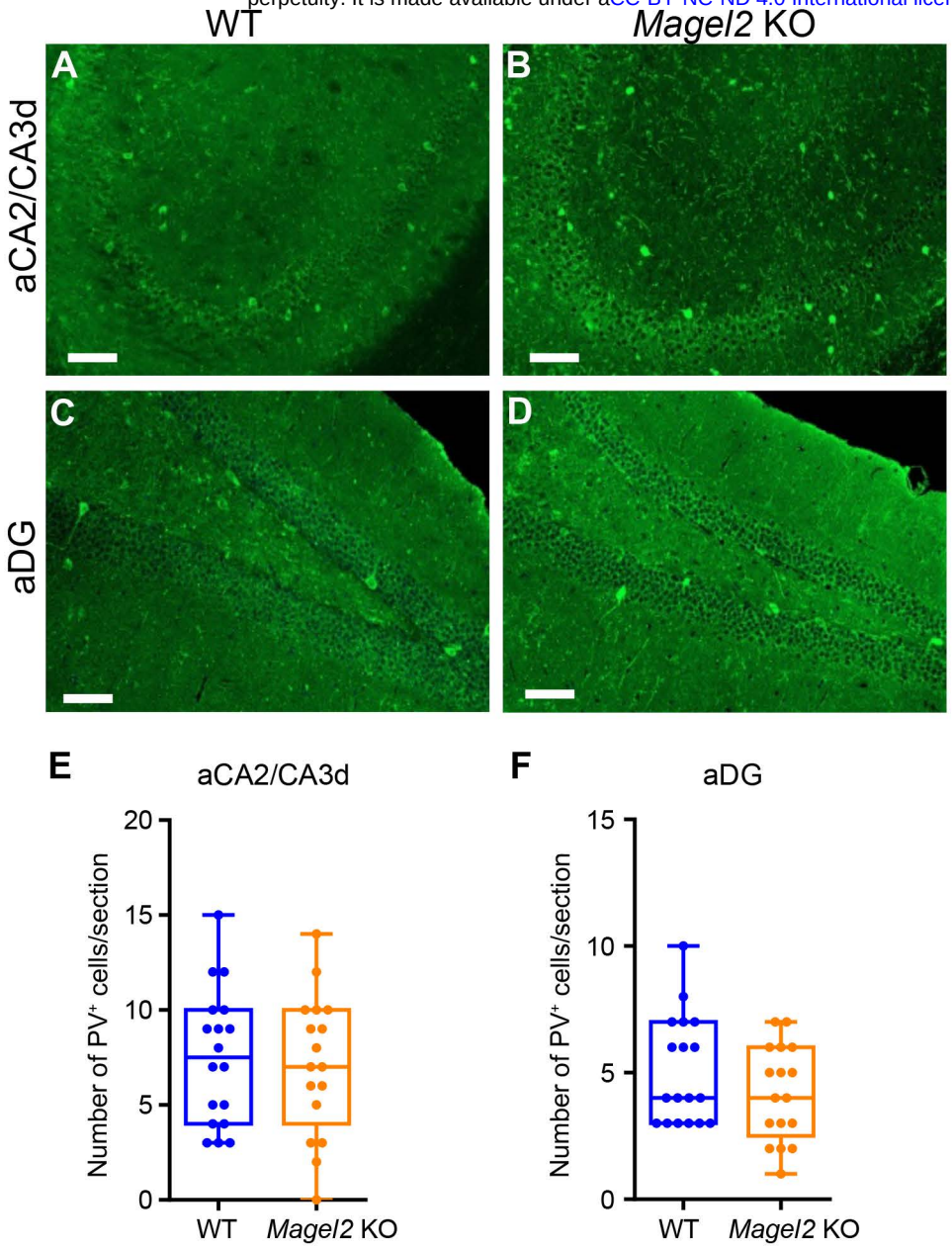

Figure 6 supplement 2.

bioRxiv preprint doi: https://doi.org/10.1101/2020.09.21.306217; this version posted September 21, 2020. The copyright holder for this preprint (which was not certified by peer review) is the author/funder, who has granted bioRxiv a license to display the preprint in perpetuity. It is made available under aCC-BY-NC-ND 4.0 International license.

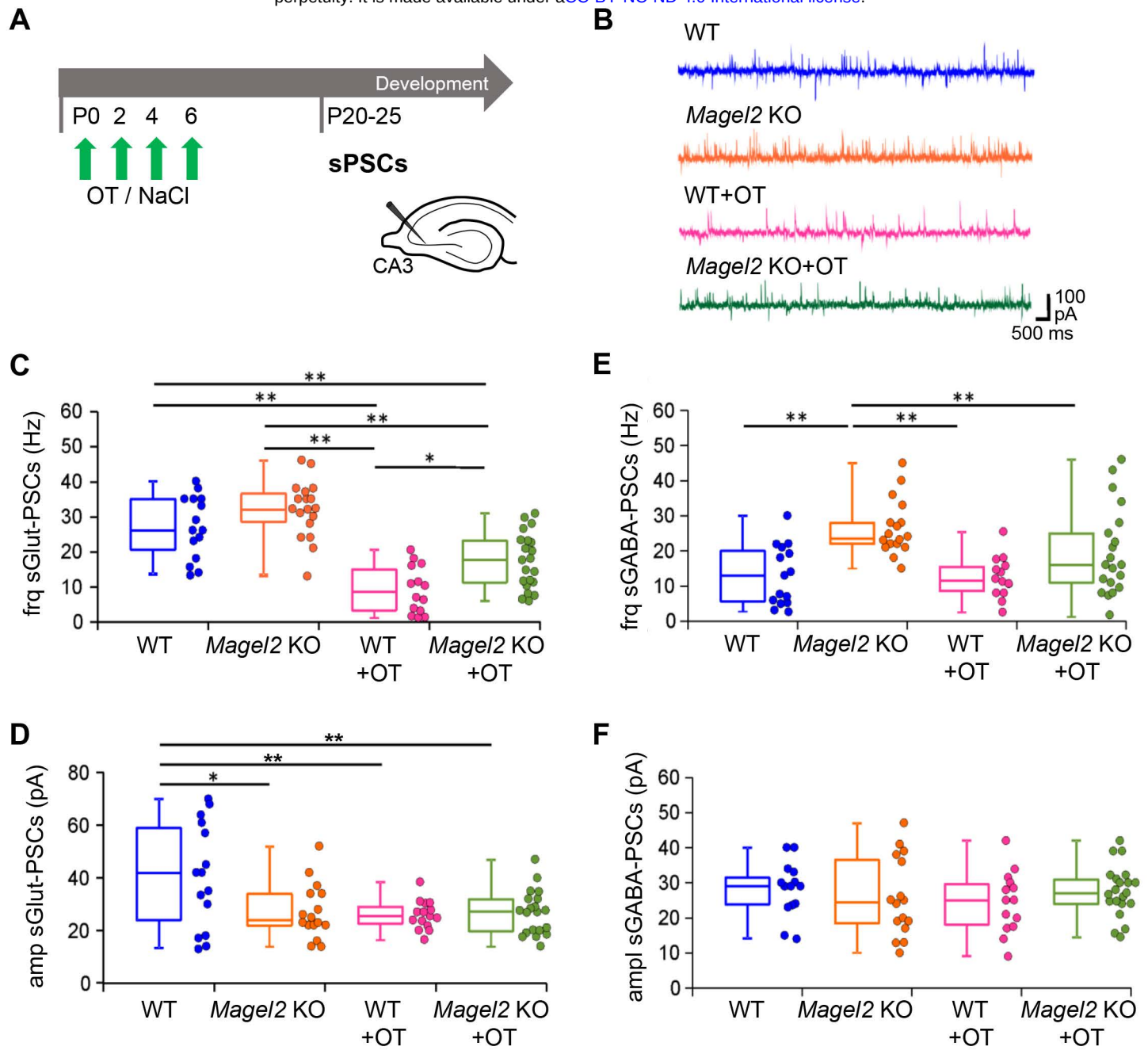

Figure 7.

bioRxiv preprint doi: https://doi.org/10.1101/2020.09.21.306217; this version posted September 21, 2020. The copyright holder for this preprint (which was not certified by peer review) is the author/funder, who has granted bioRxiv a license to display the preprint in perpetuity. It is made available under aCC-BY-NC-ND 4.0 International license.

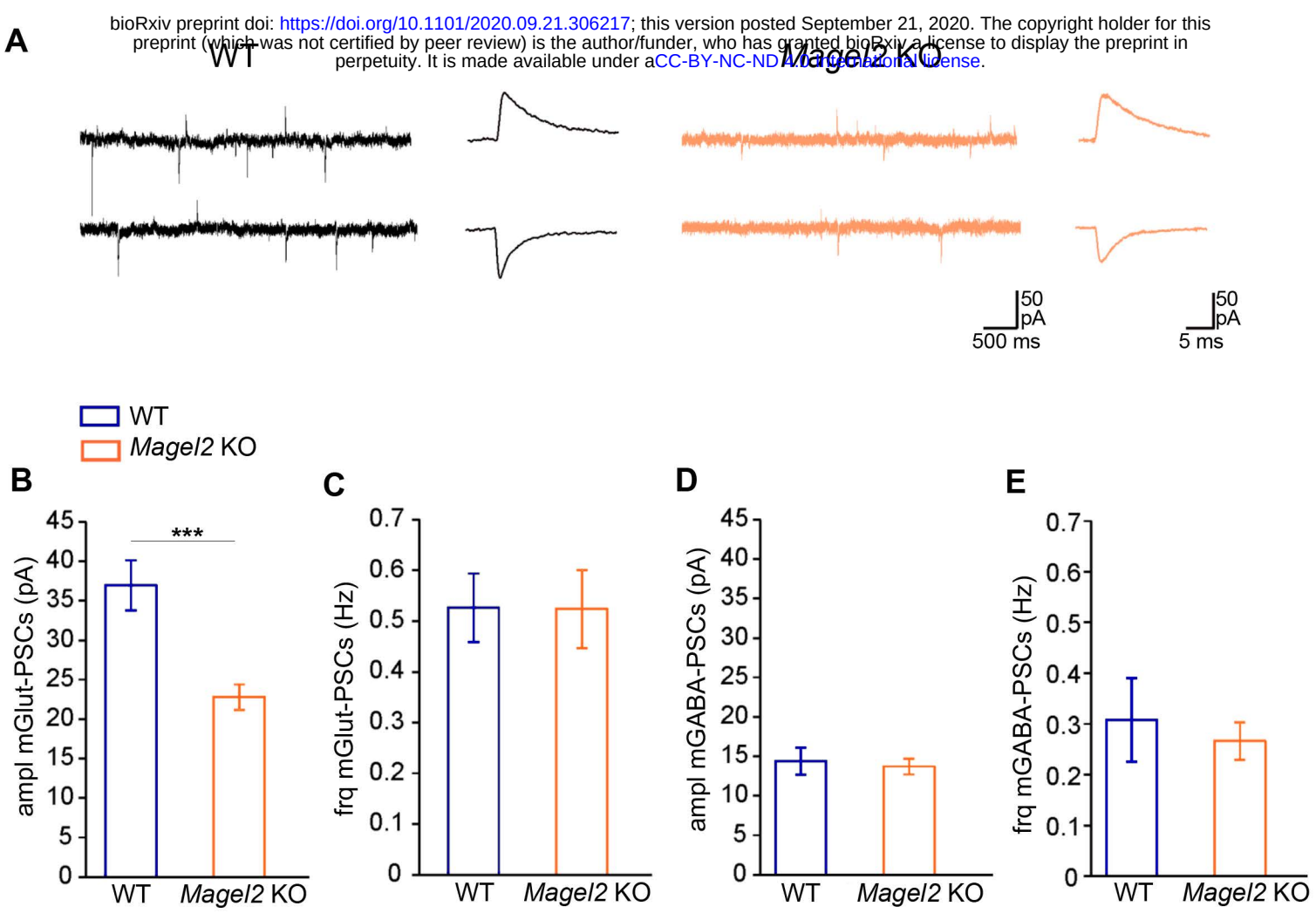

Figure 7 supplement 1.

bioRxiv preprint doi: https://doi.org/10.1101/2020.09.21.306217; this version posted September 21, 2020. The copyright holder for this preprint (which was not certified by peer review) is the author/funder, who has granted bioRxiv a license to display the preprint in perpetuity. It is made available under aCC-BY-NC-ND 4.0 International license.

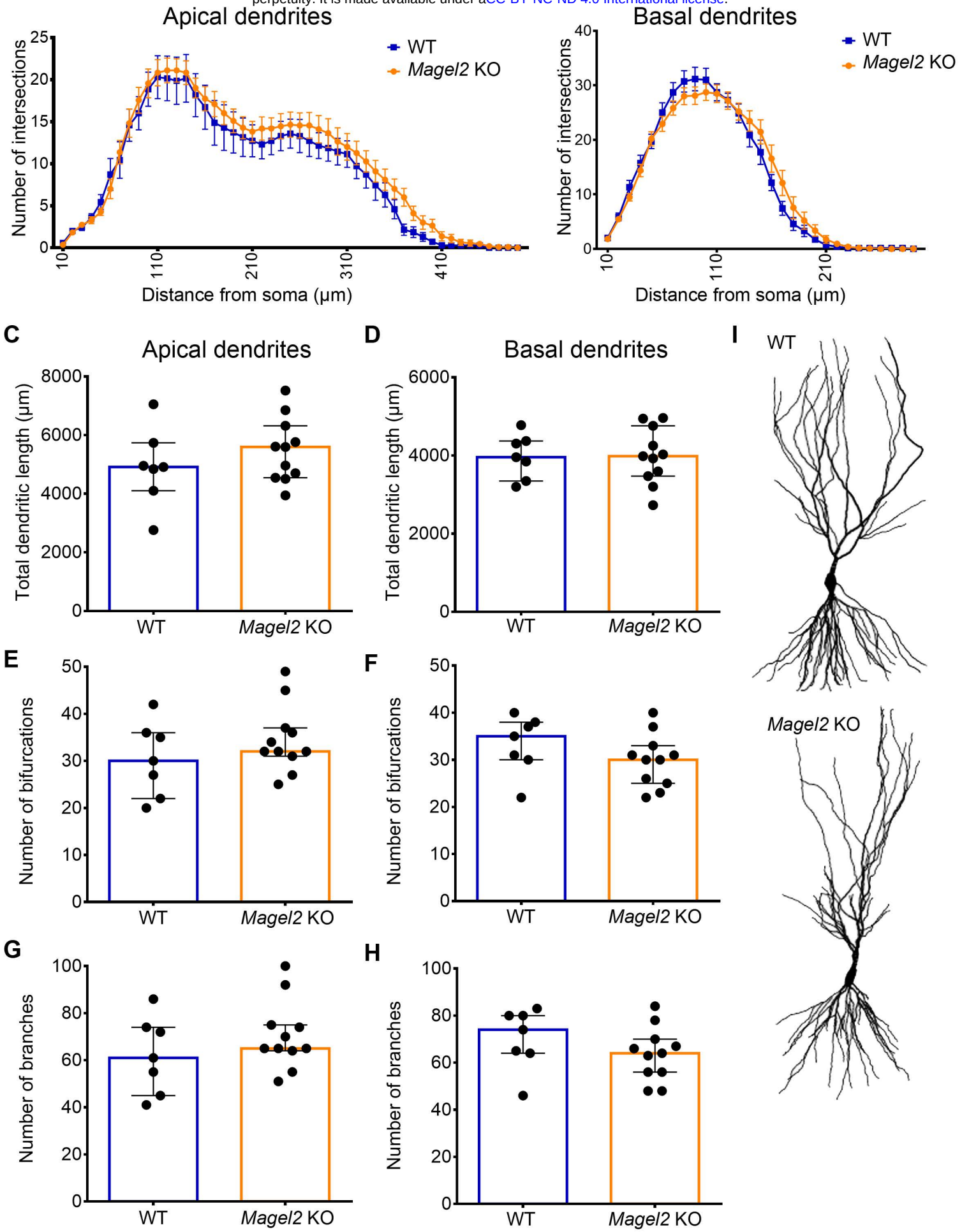

Figure 7 supplement 2.

bioRxiv preprint doi: https://doi.org/10.1101/2020.09.21.306217; this version posted September 21, 2020. The copyright holder for this preprint (which was not certified by peer review) is the author/funder, who has granted bioRxiv a license to display the preprint in perpetuity. It is made available under aCC-BY-NC-ND 4.0 International license.

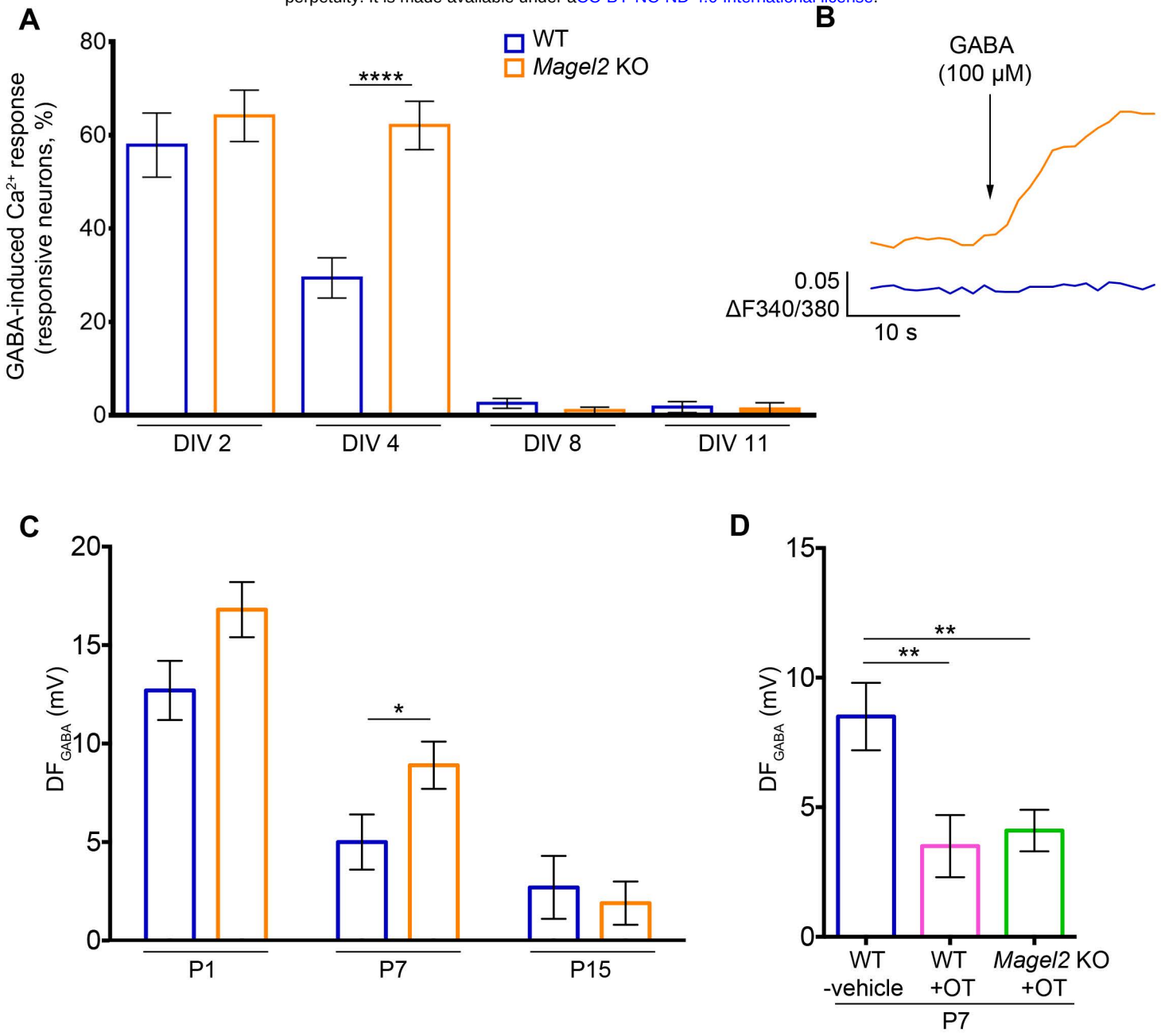

Figure 8.

bioRxiv preprint doi: https://doi.org/10.1101/2020.09.21.306217; this version posted September 21, 2020. The copyright holder for this preprint (which was not certified by peer review) is the author/funder, who has granted bioRxiv a license to display the preprint in perpetuity. It is made available under aCC-BY-NC-ND 4.0 International license.

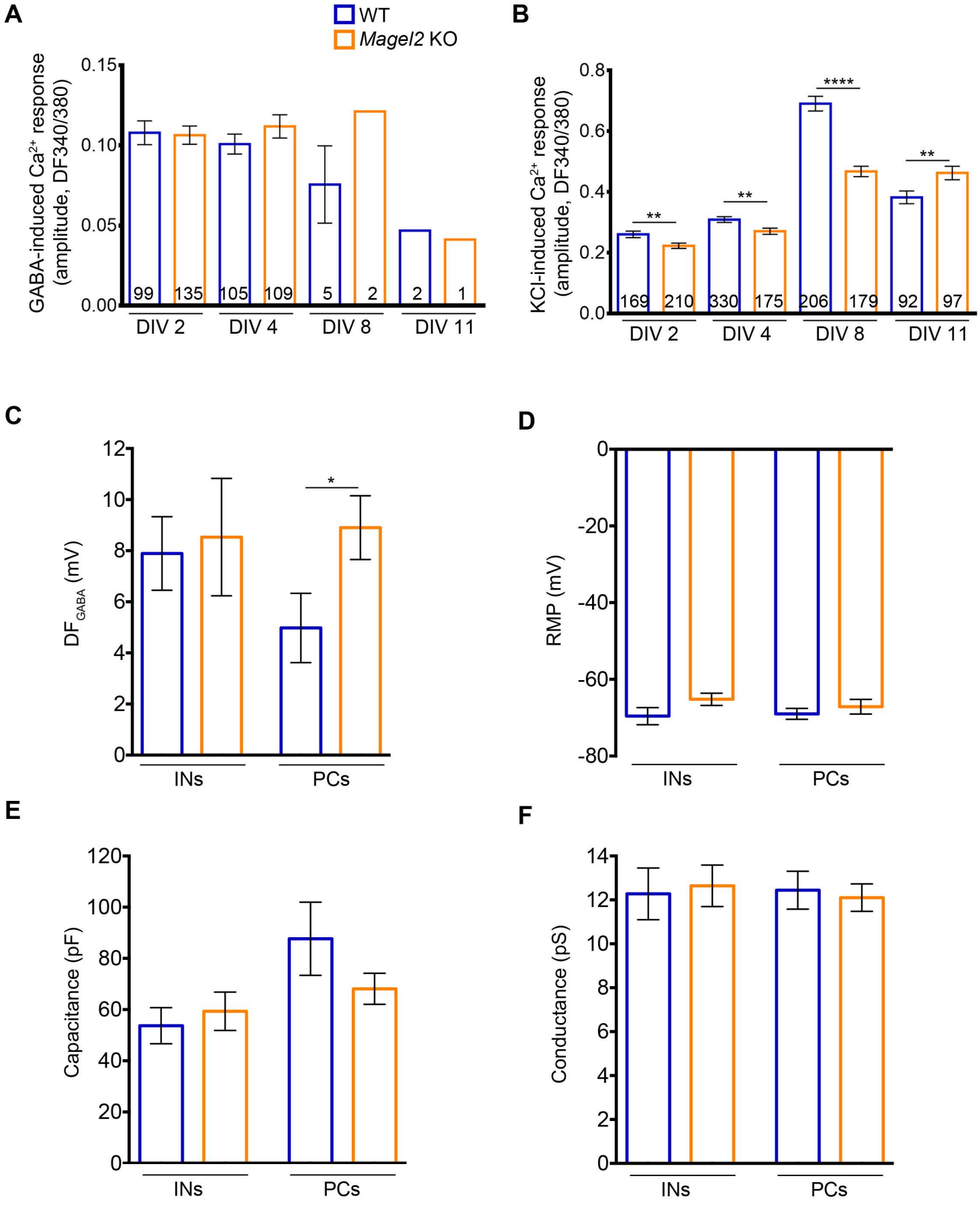

Figure 8 supplement 1.

bioRxiv preprint doi: https://doi.org/10.1101/2020.09.21.306217; this version posted September 21, 2020. The copyright holder for this preprint (which was not certified by peer review) is the author/funder, who has granted bioRxiv a license to display the preprint in perpetuity. It is made available under aCC-BY-NC-ND 4.0 International license.

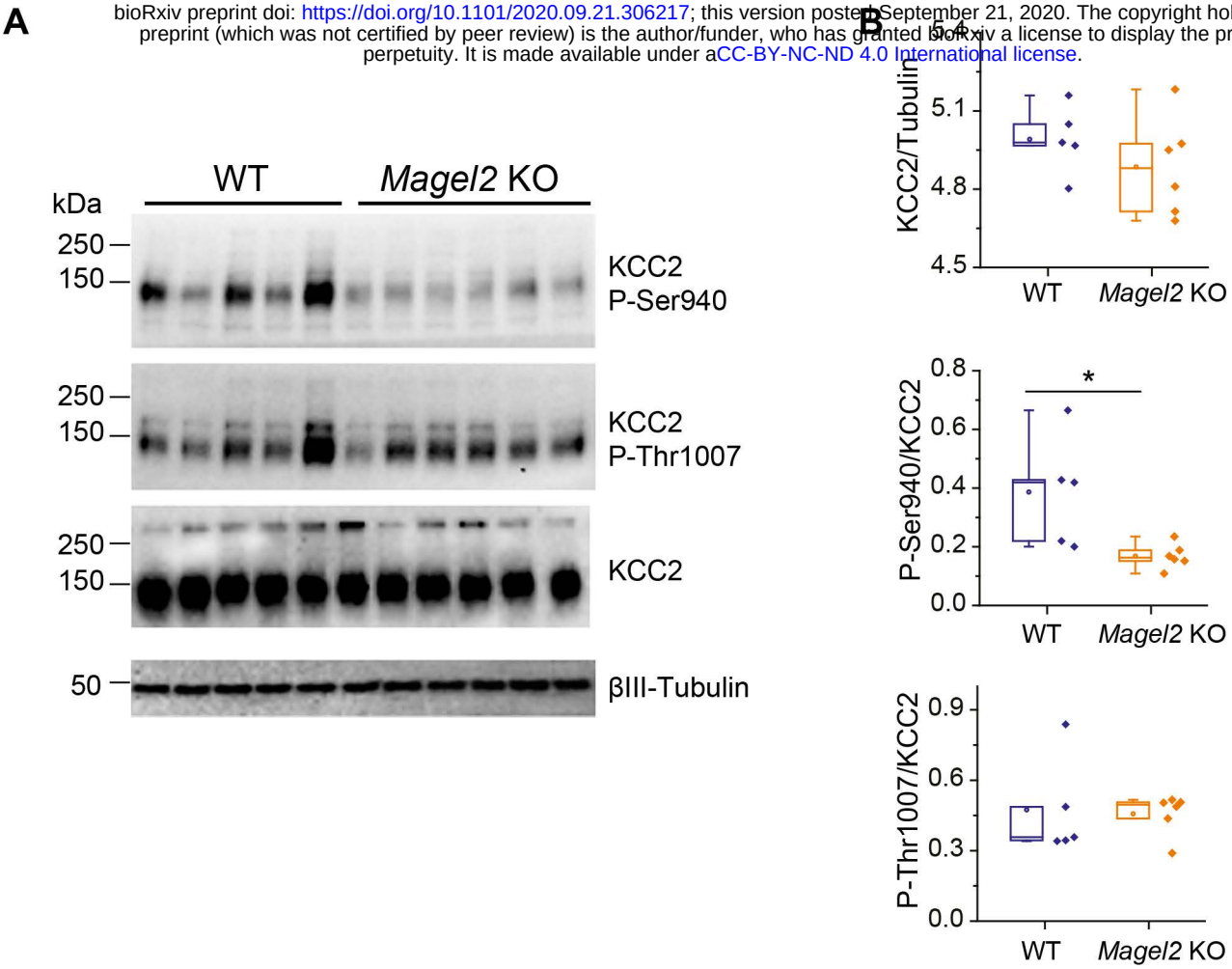

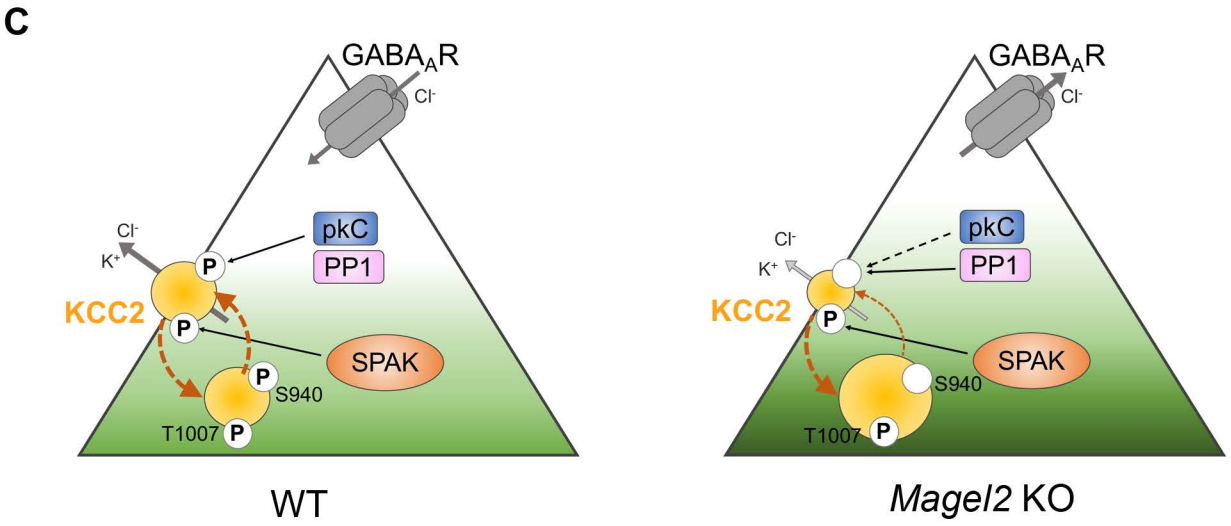

Figure 9.

Supplementary data: **Statistical file**

Table 1 : Figure 1

Table 2 : Figure 2

Table S2 : Figure 2-figure supplement 1; Figure 2-figure supplement 2; Figure 2-figure supplement 3

Table 3 : Figure 3

Table 5 : Figure 5

Table 6 : Figure 6

Table 7 : Figure 7

Table S7 : Figure 7-figure supplement 2

Table 8 : Figure 8

Table 9 : Figure 9

Table 1

Figure	Parameter	Genotype	Treatment	Gender	Number of individuals	Median (Q1,Q3)	Statistical test	p-value
1B	Total number of calls	WT	-	male	9	272 (214,336.5)	Mann-Whitney	**p=0.0387**
		Magel2 KO	-	male	14	103.5 (21,290.8)		
		WT	-	female	11	168 (90,569)		**p=0.0379**
		Magel2 KO	-	female	9	67 (11,136)		

1C	Total number of calls	WT	vehicle	male	11	289 (46,490)	one-way ANOVA, Dunnett's post-hoc test	
		WT	OT	male	11	226 (71,336)		WT-vehicle vs WT+OT, p=0.8329
		Magel2 KO	vehicle	male	18	69 (23.5,113)		**WT-vehicle vs *Magel2* KO-vehicle, p=0.0083**
		Magel2 KO	OT	male	24	79 (31,156.3)		**WT-vehicle vs *Magel2* KO+OT, p=0.0096**
		WT	vehicle	female	13	307 (122,466.5)		
		WT	OT	female	12	144 (57.5,455.3)		WT-vehicle vs WT+OT p=0,8177
		Magel2 KO	vehicle	female	13	67 (24.5,301.5)		**WT-vehicle vs *Magel2* KO-vehicle, p=0.056**
		Magel2 KO	OT	female	21	144 (33.5,247.5)		**WT-vehicle vs *Magel2* KO+OT, p=0.0622**

Table 2

Figure	Parameter	Test specifications		Genotype	Treatment	Sex	Number of individuals	Mean ± SEM	Statistical test	p-value	Median (Q1,Q3)	Statistical test	p-value
2B	Interaction time (sniffing in seconds)	Social exploration	S1	WT	-	male	**12**	**78.0 ± 7.7**	paired t-test	**p=0.00134**	73.48 (52.34, 100.58)	Wilcoxon Signed Rank Test	**p<0.001**
			Empty					**34.5 ± 6.6**			27.52 (16.72, 56.22)		
		Social discrimination	S1	WT	-	male		**33.7 ± 4.7**		**p=0.000129**	28.04 (21.00, 45.96)		**p<0.001**
			S2					**70.7 ± 7.4**			78.68 (53.50, 89.12)		
		Short-term social memory	S1	WT	-	male		**28.0 ± 6.0**		**p=0.0263**	21.08 (14.34, 33.84)		**p=0.042**
			S3					**77.2 ± 16.3**			60.28 (32.78, 109.96)		
		Social exploration	S1	*Magel2* KO	-	male	9	68.1 ± 6.8		**p=0.000133**	65.04 (51.80, 81.44)		**p=0.004**
			Empty					31.5 ± 5.0			24.64 (21.32, 44.88)		
		Social discrimination	S1	*Magel2* KO	-	male		30.0 ± 4.3		**p=0.0169**	25.92 (21.76, 43.56)		**p=0.012**
			S2					61.0 ± 7.6			65.92 (44.48, 71.60)		
		Short-term social memory	S1	*Magel2* KO	-	male		38.2 ± 6.4		**p=0.472**	37.68 (22.88, 47.20)		p=0.359
			S3					43.9 ± 7.1			46.16 (22.20, 55.56)		
2C	Interaction time (sniffing in seconds)	Social exploration	S1	WT	vehicle	male	18	83.5 ± 6.5	paired t-test	**p=0.00179**	79.48 (70.24, 95.40)	Wilcoxon Signed Rank Test	**p=0.001**
			Empty					49.2 ± 5.6			41.88 (33.00, 65.74)		
		Social discrimination	S1	WT	vehicle	male		44.2 ± 3.8		**p=0.000291**	45.96 (28.34, 53.86)		**p<0.001**
			S2					84.5 ± 6.9			79.16 (58.58, 107.38)		
		Short-term social memory	S1	WT	vehicle	male		34.0 ± 3.3		**p=0.000571**	31.60 (25.06, 39.00)		**p=0.001**
			S3					67.1 ± 6.4			67.44 (41.44, 97.10)		
		Social exploration	S1	WT	OT	male	10	88.3 ± 6.3		**p<0.0001**	83.68 (70.94, 98.44)		**p=0.002**
			Empty					42.0 ± 2.3			44.76 (33.98, 48.36)		
		Social discrimination	S1	WT	OT	male		49.9 ± 4.9		**p=0.00776**	49.64 (36.72, 63.86)		**p=0.010**
			S2					84.2 ± 10.5			71.84 (57.14, 103.48)		
		Short-term social memory	S1	WT	OT	male		36.4 ± 3.4		**p=0.00917**	35.08 (27.90, 47.72)		**p=0.020**
			S3					68.8 ± 7.4			71.84 (46.10, 86.92)		
2D	Interaction time (sniffing in seconds)	Social exploration	S1	*Magel2* KO	vehicle	male	19	65.8 ± 5.1	paired t-test	**p<0.0001**	69.44 (58.72, 79.04)	Wilcoxon Signed Rank Test	**p<0.001**
			Empty					31.0 ± 3.2			26.88 (22.80, 40.40)		
		Social discrimination	S1	*Magel2* KO	vehicle	male		29.5 ± 4.3		**p<0.0001**	26.80 (14.64, 36.96)		**p<0.001**
			S2					73.5 ± 7.0			74.64 (43.12, 92.64)		
		Short-term social memory	S1	*Magel2* KO	vehicle	male		38.8 ± 4.0		p=0.259	42.08 (25.36, 52.08)		p=0.374
			S3					44.2 ± 3.1			43.20 (37.52, 50.64)		
		Social exploration	S1	*Magel2* KO	OT	male	19	89.1 ± 6.0		**p<0.0001**	84.40 (68.24, 113.60)		**p<0.001**
			Empty					36.2 ± 4.5			34.56 (21.12, 50.96)		
		Social discrimination	S1	*Magel2* KO	OT	male		34.0 ± 4.7		**p<0.0001**	33.52 (17.44, 43.60)		**p<0.001**
			S2					87.2 ± 6.2			86.16 (75.12, 98.00)		
		Short-term social memory	S1	*Magel2* KO	OT	male		32.4 ± 3.8		**p=0.000702**	28.96 (22.40, 38.40)		**p<0.001**
			S3					58.6 ± 6.5			53.32 (43.76, 64.80)		

Table S2

Figure	Parameter	Test specifications		Genotype	Treatment	Sex	Number of individuals	Median (Q1,Q3)	Statistical test	p-value
2supl1 A	Social index	Social exploration index	S1/Empty	WT	-	male	9	69.129 (62.504,84.591)	Mann-Whitney	p=0.930
				Magel2 KO	-		9	70.387 (63.281,74.867)		
		Discrimination index	S2/S1	WT	-	male	9	69.399 (58.508,76.801)		p=0.596
				Magel2 KO	-		9	67.067 (51.376,76.300)		
		Short-term memory index	S3/S1	WT	-	male	9	80.484 (78.511,84.959)		**p=0.001**
				Magel2 KO	-		9	54.192 (44.777,64.752)		
2supl1 B	Social index	Social exploration index	S1/Empty	*Magel2* KO	vehicle	male	19	71.333 (65.560,75.758)	Mann-Whitney	p=0.484
				Magel2 KO	OT		19	75.079 (58.744,82.863)		
		Discrimination index	S2/S1	*Magel2* KO	vehicle	male	19	72.195 (61.802,83.006)		p=0.907
				Magel2 KO	OT		19	72.581 (60.550,81.239)		
		Short-term memory index	S3/S1	*Magel2* KO	vehicle	male	19	51.515 (45.474,60.818)		**p=0.021**
				Magel2 KO	OT		19	65.056 (55.882,72.986)		

Figure	Parameter	Test specifications		Genotype	Treatment	Sex	Number of individuals	Mean ± SEM	Statistical test	p-value	Median (Q1,Q3)	Statistical test	p-value
2supl2 B	Interaction time (sniffing in seconds)	Social exploration	S1	WT	-	female	11	85.18 ± 11.89	paired t-test	**p=0.0201**	89.04 (55.28, 104.48)	Wilcoxon Signed Rank Test	**p=0.019**
			Empty					48.85 ± 8.04			42.32 (28.40, 75.28)		
		Social discrimination	S1	WT	-	female		48.37 ± 5.71		**p=0.0329**	49.76 (31.52, 66.96)		p=0.054
			S2					73.49 ± 10.53			75.84 (41.52, 102.00)		
		Short-term social memory	S1	WT	-	female		43.99 ± 4.82		p=0.488	43.60 (33.28, 54.88)		p=0.898
			S3					50.54 ± 8.99			38.08 (29.28, 83.68)		
		Social exploration	S1	*Magel2* KO	-	female	9	59.93 ± 10.28		p=0.134	50.24 (39.36, 71.64)		p=0.250
			Empty					39.06 ± 6.55			42.56 (20.48, 55.48)		
		Social discrimination	S1	*Magel2* KO	-	female		34.57 ± 8.20		p=0.0719	28.80 (23.44, 35.40)		p=0.129
			S2					57.67 ± 6.86			56.08 (48.24, 66.04)		
		Short-term social memory	S1	*Magel2* KO	-	female		31.70 ± 4.87		**p=0.0308**	34.08 (16.72, 45.76)		**p=0.039**
			S3					51.33 ± 5.59			54.32 (34.96, 62.84)		

Figure	Parameter	Test specifications		Genotype	Treatment	Sex	Number of individuals	Median (Q1,Q3)	Statistical test	p-value
2supl3 A	NOR	Discrimination index (% of preference)	same object	WT	vehicle	male	10	46.822 (42.071,53.412)	One-Sample Singled Rank Test 50%	p=0.557
			new object				10	76.740 (64.570,83.103)		**p=0.002**
			same object	WT	OT	female	10	52.327 (39.516,59.132)		p=1.000
			new object				10	65.772 (59.652,73.432)		**p=0.002**
			same object	WT	vehicle	male	19	46.334 (41.667,55.738)		p=0.293
			new object				17	65.625 (57.805,69.979)		**p<0.001**
			same object	WT	OT	female	12	46.392 (38.371,48.776)		**p=0.034**
			new object				12	64.978 (56.382,74.646)		**p<0.001**
2supl3 B	Open Field	Distance mouved (in minutes)		WT	vehicle	male	18	26.517 (23.086,32.118)	Mann-Whitney	p=0.111
				WT	OT		11	21.989 (19.289,26.250)		
				WT	vehicle	female	16	31.654 (23.711,37.174)		**p=0.048**
				WT	OT		12	22.620 (15.569,32.495)		
		Rearing (number of events)		WT	vehicle	male	18	51.000 (36.000,62.000)		p=0.747
				WT	OT		11	52.000 (41.250,60.750)		
				WT	vehicle	female	16	41.000 (27.000,45.000)		p=0.185
				WT	OT		12	47.000 (38.000,60.000)		
		Grooming time (in seconds)		WT	vehicle	male	18	36.160 (25.120,47.280)		p=0.723
				WT	OT		11	45.680 (17.140,65.420)		
				WT	vehicle	female	16	25.600 (21.600,45.120)		p=0.299
				WT	OT		12	36.400 (21.080,53.600)		
		Time in zone		WT	vehicle	male	18	28.616 (26.283,38.172)		p=0.574
				WT	OT		11	31.249 (28.050,36.235)		
				WT	vehicle	female	16	27.970 (21.667,31.806)		p=0.676
				WT	OT		12	25.530 (12.785,42.204)		
2supl3 C	EPM	Time in open-arms		WT	vehicle	male	21	18.960 (14.680,30.320)	Mann-Whitney	p=0.342
				WT	OT		10	23.600 (17.440,40.840)		
				WT	vehicle	female	19	25.440 (16.720,44.800)		p=0.491
				WT	OT		12	31.720 (21.400,42.540)		
		Open-arms entries		WT	vehicle	male	21	10.000 (6.500,11.500)		p=0.149
				WT	OT		10	12.000 (7.000,14.250)		
				WT	vehicle	female	19	12.000 (11.000,15.000)		p=0.326
				WT	OT		12	14.000 (11.250,19.500)		

Table 3

Figure	Parameter	Brain region	Genotype	Behavioral test	Treatment	Gender	Number of individuals	Number of sections	Median (Q1,Q3)	Statistical test	p-value
3D	Number of cFos-positive cells	aCA2/CA3d	WT	-SI	-	male	3	18	24.5 (19.5,28)	one-way ANOVA, Dunnett's post-hoc test	
			WT	+SI	-	male	4	24	44.5 (34,56)		**WT-SI vs WT +SI, p<0.0001**
			Magel2 KO	+SI	-	male	4	24	55 (48,75)		**WT+SI vs *Magel2* KO+SI, p=0.03**
3E	Number of cFos-positive cells	aDG	WT	-SI	-	male	3	18	39.5 (31.7,42)	one-way ANOVA, Dunnett's post-hoc test	
			WT	+SI	-	male	4	24	63 (53.5,79.5)		**WT-SI vs WT+SI, p<0.0001**
			Magel2 KO	+SI	-	male	4	24	72.5 (58.7,85.2)		WT+SI vs *Magel2* KO+SI, n.s.

Table 5

Figure	Parameter	Brain region	Genotype	Treatment	Gender	Number of individuals	Number of sections	Median (Q1,Q3)	Statistical test	p-value
5B	nCi/mg of tissue equivalent	aCA2/CA3	WT	vehicle	male	3	24	0.07469 (0.06504,0.08431)	one-way ANOVA, Bonferroni's post-hoc test	**WT-vehicle vs *Magel2* KO-vehicle, p<0.0001**
			Magel2 KO	vehicle	male	3	24	0.1395 (0.1231,0.1593)		**WT-vehicle vs *Magel2* KO+OT, p=0.0021**
			Magel2 KO	OT	male	3	24	0.1254 (0.1057,0.1354)		*Magel2* KO-vehicle vs *Magel2* KO+OT, p=0.2232
5D	nCi/mg of tissue equivalent	vCA1/CA2/CA3	WT	vehicle	male	3	24	0.07877 (0.06478,0.09454)	one-way ANOVA, Bonferroni's post-hoc test	**WT-vehicle vs *Magel2* KO-vehicle, p<0.0001**
			Magel2 KO	vehicle	male	3	24	0.1378 (0.1284,0.1535)		WT-vehicle vs *Magel2* KO+OT, p>0.9999
			Magel2 KO	OT	male	3	24	0.08789 (0.06257,0.0942)		***Magel2* KO-vehicle vs *Magel2* KO+OT, p<0.0001**
5F	nCi/mg of tissue equivalent	aDG	WT	vehicle	male	3	24	0.1610 (0.1440,0.1953)	one-way ANOVA, Bonferroni's post-hoc test	WT-vehicle vs *Magel2* KO-vehicle, p=0.0722
			Magel2 KO	vehicle	male	3	24	0.1274 (0.1196,0.1415)		WT-vehicle vs *Magel2* KO+OT, p=0.0590
			Magel2 KO	OT	male	3	24	0.1252 (0.1066,0.1517)		*Magel2* KO-vehicle vs *Magel2* KO+OT, p>0.9999

Table 6

Figure	Parameter	Brain region	Genotype	Treatment	Gender	Number of individuals	Number of sections	Median (Q1,Q3)	Statistical test	p-value
6M	Number of SST-positive cells	aCA2/CA3d	WT	-	male	4	65	44 (33, 61)	Mann-Whitney	WT versus Magel2 KO p<0,0001
			Magel2 KO	-	male	4	62	88 (77, 116)		
6O			WT	-	male	3	35	43 (38, 51)		WT versus Magel2 KO+OT p<0,01
			Magel2 KO	OT	male	5	62	38 (34, 45)		
6N	Number of SST-positive cells	aDG	WT	-	male	4	48	22 (16, 29)	Mann-Whitney	WT versus Magel2 KO p<0,0001
			Magel2 KO	-	male	4	48	48 (38, 54)		
6P			WT	-	male	3	35	24 (21, 26)		WT versus Magel2 KO+OT p<0,0001
			Magel2 KO	OT	male	5	62	18.5 (16.7, 21)		

Table 7

Figure	Parameter	Genotype	Treatment	Gender	Number of individuals	Number of neurons	Median (Q1,Q3)	Statistical test	Comparison	P-value
7C	Glut frequency (Hz)	WT	-	male	7	15	26 (18, 35)	One way ANOVA + Tukey post-hoc test	WT vs *Magel2* KO	n.s.
		Magel2 KO	-	male	7	18	32 (27, 37.5)		*Magel2* KO vs KO+OT	p<0.01
		WT	OT	male	4	15	8.5 (2.7, 16.2)		WT vs WT+OT	p<0.01
		Magel2 KO	OT	male	5	21	11 (17.6, 23.2)		WT+OT vs KO+OT	p<0.01
7E	GABA frequency (Hz)	WT	-	male	7	15	13 (5.2, 21)	One way ANOVA + Tukey post-hoc test	WT vs *Magel2* KO	p<0.01
		Magel2 KO	-	male	7	18	23.5 (21.7, 29.2)		*Magel2* KO vs KO+OT	p<0.01
		WT	OT	male	4	14	11.5 (8, 16.2)		WT vs WT+OT	p<0.01
		Magel2 KO	OT	male	5	21	12.5 (10.5, 17.2)		WT+OT vs KO+OT	n.s.
7D	Glut amplitude (pA)	WT	-	male	7	15	42(18, 61)	One way ANOVA + Tukey post-hoc test	WT vs *Magel2* KO	p<0.05
		Magel2 KO	-	male	7	16	24 (22, 34)		*Magel2* KO vs KO+OT NS	
		WT	OT	male	4	15	25.5 (21.7, 34)		WT vs WT+OT	p<0.01
		Magel2 KO	OT	male	5	20	27.3 (19.3, 32)		WT+OT vs KO+OT	p<0.01
7F	GABA amplitude (pA)	WT	-	male	7	15	29 (23.6, 33)	One way ANOVA + Tukey post-hoc test	WT vs *Magel2* KO	n.s.
		Magel2 KO	-	male	7	16	24.5 (17.5, 37.5)		*Magel2* KO vs KO+OT	n.s.
		WT	OT	male	4	15	25 (17.4, 30.4)		WT vs WT+OT	n.s.
		Magel2 KO	OT	male	5	21	27.1 (24, 31.5)		WT+OT vs KO+OT	n.s.

Table 7-Supplementary 1

Figure	Parameter	Genotype	Treatment	Gender	Number of individuals	Number of neurons	Mean ± SEM	Statistical test	p-value
7supl1 C	Glut frequency (Hz)	WT	-	male	5	13	0.73 ± 0.2	Mann-Whitney	n.s.
		Magel2 KO	-	male	5	16	0.67 ± 0.14		
7supl1 E	GABA frequency (Hz)	WT	-	male	5	12	0.30 ± 0.08	Mann-Whitney	n.s.
		Magel2 KO	-	male	5	12	0.26 ± 0.03		
7supl1 B	Glut amplitude (pA)	WT	-	male	5	13	33.3 ± 3	Mann-Whitney	**p<0,01**
		Magel2 KO	-	male	5	14	23.8 ± 1.8		
7supl1 D	GABA amplitude (pA)	WT	-	male	5	13	17.6 ± 2.7	Mann-Whitney	n.s.
		Magel2 KO	-	male	5	11	13.5 ± 1		

Figure	Parameter	Genotype	Treatment	Gender	Number of individuals	Number of neurons	Median (Q1,Q3)	Statistical test	p-value
7supl2 C	Total length apical dendrites	WT	-	male	3	7	3957 (3349,4372)	Mann-Whitney	p=0.89
		Magel2 KO	-	male	3	11	3982 (3472,4760)		
7supl2 D	Total length basal dendrites	WT	-	male	3	7	4914 (4102,5739)	Mann-Whitney	p=0.46
		Magel2 KO	-	male	3	11	5596 (4546,6318)		
7supl2 E	Mean number of apical bifurcations	WT	-	male	3	7	30 (22,36)	Mann-Whitney	p=0.31
		Magel2 KO	-	male	3	11	32 (31,37)		
7supl2 F	Mean number of basal bifurcations	WT	-	male	3	7	35 (30,38)	Mann-Whitney	p=0.25
		Magel2 KO	-	male	3	11	30 (25,33)		
7supl2 G	Mean number of apical branches	WT	-	male	3	7	61 (45,74)	Mann-Whitney	p=0.31
		Magel2 KO	-	male	3	11	65 (64,75)		
7supl2 H	Mean number of basal branches	WT	-	male	3	7	74 (64,80)	Mann-Whitney	p=0.29
		Magel2 KO	-	male	3	11	64 (70,84)		

Table 8

Figure	Parameter	Days in vitro	Genotype	Treatment	Number of preparations	Number of neurons	Mean ± SEM	Statistical test	p-value
8A	Percentage of responsive neurons	DIV2	WT	-	3	169	57.88 ± 6.866	Unpaired t test with Wlech's correction	p=0.479
			Magel2 KO	-	4	210	64.15 ± 5.519		
		DIV4	WT	-	5	330	29.42 ± 4.315		**p<0.0001**
			Magel2 KO	-	3	175	62.09 ± 5.196		
		DIV8	WT	-	3	206	2.553 ± 1.052		p=0.233
			Magel2 KO	-	2	179	1.016 ± 0.709		
		DIV11	WT	-	2	92	1.759 ± 1.188		p=0.813
			Magel2 KO	-	2	97	1.333 ± 1.333		

Figure	Parameter	Age	Genotype	Treatment	Number of individuals	Number of neurons	Mean ± SEM	Statistical test	p-value
8C	Driving Force GABA (mV)	P1	WT	-	3	19	12.7 ± 1.5	Unpaired t test with Wlech's correction	p=0.0535
			Magel2 KO	-	3	20	16.8 ± 1.4		
		P7	WT	-	6	42	5.0 ± 1.4		**p=0.0358**
			Magel2 KO	-	7	56	8.9 ± 1.2		
		P15	WT	-	3	23	2.7 ± 1.6		p=0.6805
			Magel2 KO	-	4	29	1.9 ± 1.1		

8D	Driving Force GABA (mV)	P7	WT	vehicle	3	37	8.5 ± 1.3	one-way ANOVA, Dunnett's post-hoc test	
			WT	OT	3	37	3.5 ± 1.2		**WT-vehicle vs WT+OT, p=0.0041**
			Magel2 KO	OT	4	56	4.1 ± 0.8		**WT-vehicle vs *Magel2* KO+OT, p=0.0055**

Table 8-Supplementary 1

Figure	Parameter	Days in vitro	Genotype	Treatment	Number of preparations	Number of neurons	Mean ± SEM	Statistical test	p-value
8supl1 A	Amplitude of GABA-induced peaks	DIV2	WT	-	3	169	0.108 ± 0.007	Unpaired t test with Wlech's correction	p=0.873
			Magel2 KO	-	4	210	0.106 ± 0.006		
		DIV4	WT	-	5	330	0.101 ± 0.006		p=0.251
			Magel2 KO	-	3	175	0.112 ± 0.007		
		DIV8	WT	-	3	206	0.076 ± 0.024		p=0.53
			Magel2 KO	-	2	179	0.121 ± 0.051		
		DIV11	WT	-	2	92	0.047 ± 0.004		
			Magel2 KO	-	2	97	0.041		
8supl1 B	Amplitude of KCl-induced peaks	DIV2	WT	-	3	169	0.261 ± 0.011	Unpaired t test with Wlech's correction	**p=0.007**
			Magel2 KO	-	4	210	0.223 ± 0.009		
		DIV4	WT	-	5	330	0.309 ± 0.010		**p=0.0059**
			Magel2 KO	-	3	175	0.271 ± 0.010		
		DIV8	WT	-	3	206	0.691 ± 0.024		**p<0.0001**
			Magel2 KO	-	2	179	0.468 ± 0.017		
		DIV11	WT	-	2	92	0.382 ± 0.021		**p=0.009**
			Magel2 KO	-	2	97	0.463 ± 0.022		

Figure	Parameter	Age	Genotype	Treatment	Number of individuals	Number of neurons	Mean ± SEM	Statistical test	p-value
8supl1 C	Driving Force GABA	P7 - interneurons	WT	-	4	12	7.9 ± 1.4	Unpaired t test with Wlech's correction	p=0.8150
			Magel2 KO	-	4	17	8.5 ± 2.3		
		P7 - pyramidal cells	WT	-	6	42	5.0 ± 1.4		**p=0.0358**
			Magel2 KO	-	7	54	8.9 ± 1.2		
8supl1 D	Resting Membrane Potential	P7 - interneurons	WT	-	4	15	-69.6 ± 2.2	Unpaired t test with Wlech's correction	p=0.1198
			Magel2 KO	-	4	20	-65.2 ± 1.6		
		P7 - pyramidal cells	WT	-	4	22	-69.0 ± 1.4		p=0.4346
			Magel2 KO	-	4	24	-67.1 ± 1.9		
8supl1 E	Capacitance	P7 - interneurons	WT	-	4	7	53.7 ± 7.0	Unpaired t test with Wlech's correction	p=0.5908
			Magel2 KO	-	4	14	59.4 ± 7.5		
		P7 - pyramidal cells	WT	-	4	22	87.7 ± 14.3		p=0.2179
			Magel2 KO	-	4	25	68.1 ± 6.0		
8supl1 F	Conductance	P7 - interneurons	WT	-	4	12	12.3 ± 1.2	Unpaired t test with Wlech's correction	p=0.8115
			Magel2 KO	-	4	16	12.6 ± 0.9		
		P7 - pyramidal cells	WT	-	4	24	12.4 ± 0.9		p=0.7526
			Magel2 KO	-	4	30	12.1 ± 0.6		

Table 9

Ratio	Genotype	Traetment	Number of individuals (brains)	Median (Q1, Q3)	Statistical test	p-value
KCC2/tubulin	WT	-	5	5 (4.8, 5.1)	Mann Whitney	n.s.
	Magel2 KO	-	6	4.9(4.5, 5)		
P-Ser^{940}/KCC2	WT	-	5	0.42 (0.21, 0.54)		**p<0,05**
	Magel2 KO	-	6	0.16 (0.14, 0.20)		
P-Thr^{1007}/KCC2	WT	-	5	0.36 (0.34, 0.66)		n.s.
	Magel2 KO	-	6	0.49 (0.40, 0.50)		